Contribution of Noise to the Variance of Integrating Detectors

A Thesis Submitted to the

College of Graduate Studies and Research

in Partial Fulfillment of the Requirements

for the degree of Master of Science

in the Department of Electrical Engineering

University of Saskatchewan

Saskatoon

By

Thomas Johan Meyer

Permission to Use

In presenting this thesis in partial fulfilment of the requirements for a Postgraduate degree from the University of Saskatchewan, I agree that the Libraries of this University may make it freely available for inspection. I further agree that permission for copying of this thesis in any manner, in whole or in part, for scholarly purposes may be granted by the professor or professors who supervised my thesis work or, in their absence, by the Head of the Department or the Dean of the College in which my thesis work was done. It is understood that any copying or publication or use of this thesis or parts thereof for financial gain shall not be allowed without my written permission. It is also understood that due recognition shall be given to me and to the University of Saskatchewan in any scholarly use which may be made of any material in my thesis.

Requests for permission to copy or to make other use of material in this thesis in whole or part should be addressed to:

Head of the Department of Electrical and Computer Engineering
Engineering Building
57 Campus Drive
University of Saskatchewan
Saskatoon, Saskatchewan
Canada
S7N 5A9

Abstract

X-ray medical imaging provides invaluable medical information, while subjecting patients to hazardous ionizing radiation. The dosage that the patient is exposed to may be reduced, at the cost of image resolution. A technology that promises lower dosage for a given resolution is direct conversion digital imaging, typically based on amorphous Selenium semiconductor. Sufficient exposure should be used for the first exposure to avoid subsequent exposures; a challenge is then to reduce the necessary exposure for a suitable image. To quantify how little radiation the detector can reliably discriminate, one needs an analysis of the variance that $1/f$ and white noise contribute to the signal of such detectors. An important consideration is that the dark current, which varies with time, is subtracted from the photocurrent, to reduce the spurious spatial variance in the image. In this thesis, the variance that $1/f$ noise contributes to integrating detectors is analysed, for a very general integrating detector. Experiments were performed to verify the theoretical results obtained for the $1/f$ noise variance contribution.

Acknowledgements

I wish to thank my parents for their support and encouragement in the years devoted to this project, and before that.

I wish to thank my supervisors, Drs Robert Johanson and Safa Kasap for their guidance, and Dr Kasap for his financial support during this project.

I wish to thank Helen Tilanus for introducing me to schooling, while encouraging my desire to learn - a truly rare achievement.

I wish to thank Shihan Christopher Thomson for teaching me to pursue my goals doggedly, and for respecting my dignity while doing so.

I wish to thank the late Dr Edwin Arinze for teaching me to analyze complicated problems methodically, yet keeping an eye open for unexpected relationships. I also wish to extend my condolences to his family with his recent passing.

I wish to thank Drs Belev and Majid for many interesting and helpful discussions.

Finally, I wish to thank the members of my committee, Drs Chen, Degenstein and Dinh, for their efforts.

Contents

List of Figures

Chapter 1

Introduction to X-ray Detection

This research is motivated by a problem in electronic x-ray imaging. X-ray imaging exposes patients to hazardous radiation. By obtaining a sufficient exposure in an initial imaging, subsequent exposures may be avoided. Certain technologies promise a lower minimum exposure for reliable imaging than others. The problem that this thesis considers, is how to calculate the uncertainty contribution that $1/f$ noise adds to the total uncertainty of a detector, which may be used with other parameters and considerations, to calculate a minimum exposure for reliable imaging.

The results of this research are however applicable to a broad range of integrating detectors. This also research sheds light on the statistical time-evolution of $1/f$ noise. Previous workers had achieved somewhat similar results for model $1/f$ noise signals as is achieved in this research for general $1/f$ noise, and thus there was always a question as to whether these results are generally applicable to $1/f$ noise, or just to the model signals used in previous work. The previous results were also less precise. My research shows that the results are generally applicable to the broad category of so-called 'second-order stationary' $1/f$ noise, which is defined in chapter 2. Before this variance can be discussed, the context and thus the motivation of this research is necessary; this is discussed next.

1.1 X-ray Imaging Detection—Motivation for Research

X-ray medical imaging is integral to modern medicine. It yields a detailed image of bone (or other tissue [1, 2]) without an overtly invasive procedure - a photographic plate is exposed to x-radiation through a patient, with said patient's bone, or contrast media in other organs, casting a partial shadow on the plate, thus yielding a detail rich image. Diagnostically valuable features, such as cracks and other abnormalities, may be visible

in the image obtained.

Yet this procedure is covertly invasive. The patient is exposed to x-rays, which are photons with energies between 1 keV and 100 keV; depending on the material irradiated, the minimum energy required for ionization is typically between 1 and 10 eV, and as such, x-rays are ionizing radiation [3]. Early x-ray workers had noticed skin burns and cancers in themselves and their patients, arising from exposure to x-rays [4, 5]. Ionizing radiation tracks, which are long, narrow regions of radiation-induced ionization, e.g. from x-rays, may damage proteins and DNA, leading to birth defects and the above–mentioned cancers; there is no dose that is 'safe' in the sense of being free of additional cancer risk [6]. Cells can often, but not always, repair genetic damage, and induced damage to genetic structures from a single ionization track are often irreparable [7]. Gofman and O'Connor catalogued a cancer-risk-multiplier effect from radiation exposure [8]. It is consequently desirable to reduce the average exposure of the general population, so as to reduce the number of cancers per generation, as well as to increase the average age of cancer induction [8]. It has been noted that acceptable per image and cumulative dosage drops with time [9].

An x-ray tube emits a spectrum of x-rays, from the lowest energies to the tube potential; lower energy photons more readily interact with soft tissues, and could supply detail of blood vessels and the like (e.g. [10]). Usually, such detail is not of interest, or may be obtained via contrast media (e.g. [11, 12]), and the low energy photons, which tend to burn the skin, may be filtered out ([13, 14]). Beyond filtration, there are several methods to reduce radiation exposure for an x-ray image, but almost without exception, they involve loss of diagnostically valuable detail. The detail lost includes resolution, i.e. the smallest detectable feature size grows, and distinction of density, i.e. the brightness difference that may reliably be discriminated between neighboring regions is reduced [15]. The light-sensitive portions of x-ray films are not very dense, and are consequently not very sensitive to x-rays; to make the films more sensitive to x-rays, they are placed between image intensifying phosphor screens, which emit visible light—to which the film is more sensitive—upon being struck by x-rays; about 98% of a typical x-ray image's density is due to the screens' action [16]. The phosphor screens tend to reduce the resolution with the minimum radiation requirement, and tend to require finer control of radiation

exposure[17]. Higher resolution screens are available, but require more exposure than low exposure, or 'fast' screens, though less than raw film [18]. Unnecessary detail may thus be sacrificed to reduce patient exposure.

Yet it would be useful to reduce the necessary exposure for a given amount of detail. One technology that promises this is 'direct conversion' digital radiation detection. It has high x-ray sensitivity at rather high resolutions [19]. This technology also has other advantages over film, such as not requiring chemical development. The chemical developers used for film present a disposal problem, and dumping the chemicals may lead to environmental problems, e.g. the development of fungi that is resistant to the fungicide in the developer, as may occur due to the reduced concentration of the fungicide when dumped. For a list of typical developer ingredients, see [20]. In order to use 'direct conversion' detectors with confidence, it is necessary to determine how little radiation the detectors can discriminate reliably.

Several random electronic phenomena, or noise, occur in electronic equipment; an analysis is needed to quantify how noise affects how little radiation a digital radiography detector can discriminate reliably. The standard measures of these random phenomena are general per unit of temporal frequency energy or power densities, rather than the contribution they make to a detector's uncertainty. One must relate these standard measures to the extent of uncertainty that these random phenomenon produces in the detected quantity of radiation. Most of the standard measures have somewhat engineerable magnitudes, and are hence subject to manipulation. These random electronic phenomena are known as noise.

Semiconductors are quite commonly used to detect and image infra-red, visible and ultra-violet radiation, as one may readily divide the detection surface into small cells that detect radiation independently of each other, when they are made of semiconductor materials. These cells typically have a square surface for detecting incident radiation, and are called picture elements (*pixels*). Various semiconductors are used to detect x-radiation; all have *Johnson noise*, which is a voltage or current that arises from the resistance of the cell, *shot noise*, which arises from individual electron motion, e.g. over a PN junction in the cell or a non-Ohmic contact on the cell, $1/f$ noise, which is a poorly understood variation in the resistance of the cell, and *mains interference*, from which the equipment is

generally shielded. The noise analyses of the Johnson and shot noise contributions to the detector variance are rather uncontroversial, and a somewhat accepted $1/f$ noise analysis exists [21, 22]. Mains or electro-magnetic interference (EMI) was only considered in the research reported in this thesis to the extent that it corrupted other noise measurements, and aside from simple precautions taken to avoid EMI in experimental work, EMI was ignored. All of the above interference and noise types are present in the electronics that develop the incoming radiation into a readable electrical quantity, adding to the random uncertainty in the detected photon count.

The above noise analyses are notable in two respects. Firstly, they are strictly inconsistent - Johnson and shot noise are analyzed in a different manner than $1/f$ noise is. However, analyzing Johnson and shot noise in the manner that $1/f$ noise is analyzed would not provide a grossly different result than what is obtained for these noise types with the standard analysis. Secondly, these analyses ignore measures taken in practical detectors for eliminating temperature related and other undesireable effects, specifically the subtraction of 'dark-current' (the spurious background measure) from the exposure 'photo-current' measure. In chapter 3, I consider the effect of this subtraction on these noise types. I also extend this noise analysis to sampling systems that sample non-high-pass filtered signals (unlike audio, which is bandlimited to about 20Hz-20KHz). Experiments were performed to test the noise analysis developed in chapter 3; they are reported in chapter four.

1.2 Imaging Technologies

In medical x-ray imaging, a portion of a patient's body is irradiated from some direction, by an x-ray source that is ideally a distant, uniform point source, typically achieved to approximation by putting the anode face of an x-ray tube at a small angle relative to the cathode [23]. The 'anode' is the electrode that absorbs the electrons emitted by the 'cathode,' and from whose surface the x-rays are emitted. Putting the anode at a small angle relative to the cathode yields a smaller source surface area for the radiation, thus making the image sharper. A detector is placed opposite the part of the body to be imaged, relative to the radiation source; said part of the body casts an x-ray shadow on

the detector. This setup imposes a minimum mottle, or spurious variation in the detected picel-to-pixel density (image brightness) difference, beyond any mottle caused by random variation in the detection technology, or by systematic irregularities in the x-ray source [24].

Mottle may mask real features on an x-ray image, by adding a general haziness to the image. X-ray imaging is used to study bone, or with contrast media, other organs; fairly subtle features often distinguish separate pathologies, and entire textbooks (e.g. [25, 26, 27]) are devoted to their interpretation. Stress fractures are particularly subtle [28], and are as such one would expect them to be more subject to being obscured by mottle.

I first explain this inherent (quantum) mottle, then the mottle or spurious variance of specific detection technologies, ending with the mottle that is the focus of this research.

1.2.1 Inherent Photon Count Variation (Quantum Mottle)

To properly image a patient, said patient must be uniformly irradiated over the imaging area, or corrections must be performed for systematically non-uniform exposure, but the exposure is expected to be randomly non-uniform, as is shown below. Consider the irradiated detector without the patient. Let some area of the detector be uniformly exposed, i.e. over time, the same average photon arrival rate is effective over the pixels in that area.

Photon emission, and hence arrival from the source, is a random process in a x-ray tube. Over a long period of irradiation, two pixels in this area accumulate x-ray photons at statistically identical rates, but over a short period of exposure, their photon counts may differ substantially, relative to their average photon count. A standard approach is that of Poisson [29] - let the arrival time of the nth photon at some pixel be t_n. The difference in the arrival times of two consecutive photons is τ_n, which is an exponentially distributed random variable,

$$\tau_n = t_{n+1} - t_n \tag{1.1}$$

$$\forall n \{ f(\tau_n) = e^{-\lambda \tau_n} \} \tag{1.2}$$

and the arrival time difference of any one pair of photons is statistically independent of the arrival time difference of any other photon pair.

The variance of the photon count of such an arrival behavior has been shown to be [30]

$$\sigma^2_{Poisson} = \lambda T \tag{1.3}$$

where λ is the average arrival rate, and T is the observation period. The expected number of photons that arrive is by definition

$$\mu = \lambda T \tag{1.4}$$

where λ is the photon arrival rate. The variance of the difference in photon count between two on-average equally yet statistically independently exposed pixels is

$$\sigma^2_{2 \text{ pixels}} = 2\lambda T \tag{1.5}$$

Thus two pixels subject to the same irradiation are expected to differ in photon count. The significance of the difference is expressed by the signal-to-noise ratio (SNR). The SNR is usually defined as the ration of the power of the signal or measured quantity to the variance of said measured quantity. A higher SNR indicates lower importance of uncertainty, and is thus a measure of the effect of mottle. For the two pixels,

$$SNR = \frac{\mu^2}{\sigma^2} = \frac{\lambda T}{2} \tag{1.6}$$

This result shows that a higher quality image can be achieved with greater exposure - a problem of course for the patient. A tradeoff is needed between patient exposure and safety on the one hand, and image quality on the other. This SNR is for an ideal detector, that gives perfectly accurate and precise photon counts; actual detectors will miscount photons, adding to the denominator of the SNR, and systematically undercount photons, scaling down the numerator. Some practical detectors are next considered in their technological imperfection.

1.2.2 Geiger Counter

A Geiger-Mueller tube is a radiation detector that produces a consistent pulse of current for each ionizing radiation that is absorbed to produce at least one ion pair inside the tube, if the absorbed radiation is suitably separated temporally from the previous and

next absorbed radiation [31]. Due to its size and complexity, it is not generally suitable for imaging. The sensor is typically in the shape of a circular-cylindrical tube, with the cylindrical wall being conductive, and concentric about an inner conductor[32]. The volume of the sensor is filled with a non-electron-affine gas, e.g. a mixture of argon and neon, and a slight quantity of halogen, e.g. bromide, as explained below[33]. Non-electron-affine gasses gain energy when ionized, whereas electron-affine gasses, e.g. halogens, lose energy with their first electron gain.

The tube may be operated in three modes, depending on the applied voltage[34]:

1. Ionization chamber mode. Each ionizing particle produces one or more ion pairs; the integrated current is less than or equal to the number of ions produced, depending on whether any recombinations occur. This mode occurs at the lowest applied voltages.

2. Proportional counter. Due to the shape of the sensor, the electric field strength is highest near the central conductor. As the applied voltage is increased, an operating region is reached where an electron gains such energy from the field as to release a second electron upon impact with a gaseous atom, hence leading to a current avalanche. The current avalanche ceases as space charge density, in the form of positive ions, build up around the anode. No new pulse can form until the ions have drifted to the cathode to a sufficient extent to restore the field around the central conductor - this period is called the *dead time*; After the dead time, the pulses have not regained their full height; it takes the *recovery time* for the pulses to regain their full height[35]. The avalanche process multiplies the photocurrent.

3. Geiger-Mueller (GM). Raising the potential beyond the propotional counter mode causes GM operation. Not only is the current multiplied, but the gaseous ions enter excited states to an extent much greater than under the proportional counter mode. If a photon is emitted in the course of deexcitation, it may be absorbed further from the central conductor than it was emitted, and the resulting photoelectron is earlier in the photomultiplication process than the ion-absorbed electron was, hence causing further current multiplication. A space-charge layer again builds up, but such as to cause each separate primary-ionization-induced pulse to have approximately the same shape and charge.

A post-pulse deionization/deexcitation may lead to a secondary pulse without an additional absorption, leading to a spurious absorption count. These spurious pulses are 'quenched' by two methods, often applied sumultaneously: A halogen is added to the tube to absorb and 'degrade' the energy level of a deexcitation photon, to prevent further ionization upon emission, and a quenching circuit is added to suppress current spikes until the ions have had time to recombine and drift away from the anode, to remove the space-charge layer.

One might assume that the number of pulses registered be necessarily equal to the number of x-ray photons striking the tube, but many x-ray photons may pass through the tube unabsorbed. One photon might arrive and be absorbed during the discharge or dead time of another photon, in which case no new pulse will be formed or counted. Background gamma radiation may also cause discharges, irrespective of the x-ray source. Failure to absorb the photons reduces the photon count in a systematic way, scaling down the measure of radiation, but also adds a variance to the detected photon count, as the failure to absorb a photon is random. Absorption of irrelevant photons also increases the uncertainty in the total photon count, but increases the total detected quantity. The Geiger photon count thus has systematic errors, for which one may correct, and random errors, which add to the true uncertainty; both reduce SNR.

1.2.3 Film

Film is the traditional imaging detector. X-ray photons are absorbed by light sensitive salts in the film, and the film is chemically developed to produce a visible image. X-ray photons may pass through the film unabsorbed, or be absorbed in the filler material of the film; this reduces the detected photon count, as may be measured by separated light-sensitive salts. A light-sensitive salt may with some finite probability absorb an x-ray photon, without being separated (false negative), e.g. due to already having been separated by a previous x-ray photon, or by chance not entering the (statistically favoured) separated state. Similarly, a thermal variation or scattered x-ray photon may separate a light-sensitive salt that does not correspond to a feature inside the patient (false positive). These false readings add to the uncertainty in the detected photon count. Both the

systematic failure to detect photons, and the spurious (mis)activations reduce the SNR of the image.

The x-ray photons have extremely short wavelengths, leading to very high probability of non-interaction with the light-sensitive molecules; a standard solution is to have a fluorescent sheet next to the film, thus absorbing the short wavelength x-ray photons, and emitting visible photons, that are more readily absorbed by the film, by virtue of their longer wavelengths. Fluoresced photons have somewhat random directions; this reduces the effective resolution of a film (or other imaging detector) as photons aimed at one pixel give rise to photons striking other pixels, although the loss of resolution may be minimized by bringing the film closer to the fluorescent screen, or by making the screen thinner [17].

1.2.4 Digital Radiography

Two major types of electronic imagers or detectors exist, namely direct and indirect conversion types. In indirect conversion detectors, x-ray photons are absorbed by phosphors to emit visible photons, that can be detected by a less dense, and hence less x-ray sensitive, regular semiconductor detector pixel array. In direct detection detectors, the x-ray photons are detected by a pixel array with the detection elements consisting of semiconductor material that is more sensitive to x-rays.

Once the incoming photon, scintillated or x-ray, is absorbed by the pixel detection element, it produces one or more electron-hole pairs, thus increasing the conductivity of the detection element. This increase in conductivity gives rise to a photo-current which is an increase over the pre-absorbtion dark-current. This photocurrent is initially roughly proportional to the number of absorbed photons, and then decays back to the dark current after the exposure ends. In many practical systems, the photocurrent is very small, and is accumulated for detection; the accumulation of the photocurrent affects the uncertainty contribution from electronic noise sources. The accumulation of photocurrent is usually, to excellent approximation, time integration. Thermal, random generation of electron-hole pairs spuriously adds to the photocurrent, and recombination of electron-hole pairs subtracts; together they add a variance to the detected photon count, hence reducing SNR. Noise processes that add to the variance of the photocurrent include the diffusion of

carriers across carrier-depleted boundaries (shot noise), thermal resistance noise (Johnson noise), and slowly but randomly changing resistance ($1/f$ noise).

1.3 The Standard Approach to Noise Analysis

The focus of this thesis is the contribution that $1/f$ noise makes to the uncertainty in the photon count of an electronic radiation detector - uncertainty is understood here as the variance in the measured photon count *arising purely from material behavior inside the detector* rather than variance in the actual number of absorbed photons - hence some introduction to electronic noise processes is needed. Dark current subtraction is excluded here, and is considered in chapter three.

Noise sources are characterized by their variance contribution per unit frequency, or power-spectral density (PSD). The PSD is usually represented as S, and is a function of frequency,

$$S = S(f) \tag{1.7}$$

An important discrimination of noise sources, which has determined the method in which the detector variance contribution is calculated, is the 'shape' of the PSD. For material-determined random electronic continuous time (noise) signals, three shapes represent almost all unmodified noise sources; they are

1. White noise, which has constant PSD. Examples of white noise include a. *shot noise* [36], e.g. the arrival of individual x-ray photons in the previous section, and electrons individually diffusing over a barrier,

$$S = Ie \tag{1.8}$$

   where I is the current and e is the fundamental charge, b. *Johnson noise* [36], which arises from the thermal interactions of charge carriers (electrons and holes) with resistive materials; the PSDs of the Johnson noise in the voltage and current are

$$S_V = 4KTR \tag{1.9}$$

$$S_I = 4KTG \tag{1.10}$$

and c. *excess avalanche noise*, which occurs in e.g. reverse-biased 'PIN' (P-type, Intrinsic, N-type) multiplier photo-detection diodes, when the field is sufficiently strong to cause temporary current avalanches [37],

$$S_I = M^2 Ie \tag{1.11}$$

where M^2 is the noise multiplier.

2. Telegraph-type noise or burst noise[38], where a (typically resistive [39]) system switches between (typically two) states somewhat haphazardly, albeit with an expected switching time τ. The PSD of telegraph noise is Lorentzian [40],

$$S(\omega) \propto \frac{S_0 \tau}{1 + \omega^2 \tau^2} \tag{1.12}$$

where S_0 is a constant. Other, non-telegraph type noises also have this PSD shape, e.g. Brownian motion [41], and 'white' noise sources usually have some maximum (if very high) frequency, beyond which their PSDs also roll off as $1/\omega^2$.

3. $1/f$ noise, so called because the PSD has the form

$$S(f) = \frac{S_0}{f} \tag{1.13}$$

$1/f$ noise is generally understood as resistive variation, with the PSD of the resistance noise characterized by a Hooge relation [42],

$$S_R(f) = \frac{R^2 \alpha_H}{N \cdot f} \tag{1.14}$$

where

$$N = n \cdot vol \tag{1.15}$$

N is the number of carriers in the sample of interest, vol is the volume of the sample, n is the carrier concentration of the sample, R is the sample's 'average' resistance (a problematic usage, as Keshner [21] pointed out, leading to changing α_H), and α_H is the Hooge coefficient of the sample.

Other statements of the Hooge model exist, e.g. conductance flutuations have PSD such that

$$\frac{S_G(f)}{G^2} = \frac{S_R(f)}{R^2} \tag{1.16}$$

and under the application of constant current or voltage, the resulting voltage or current noise is $S_V(f)$ or $S_I(f)$, such that

$$\frac{S_V(f)}{V^2} = \frac{S_I(f)}{I^2} = \frac{S_R(f)}{R^2} \tag{1.17}$$

The frequency exponent of the PSD is not exactly one for all samples, so that

$$S(f) = \frac{S_0}{f^\alpha} \tag{1.18}$$

with $0.6 \leq \alpha \leq 1.4$ (depending on the sample and its temperature, [43]) is also considered $1/f$ noise. S_0 may again depend on V, I, R etc.

Non-Hooge models exist, especially for active devices - transistor noise also contribute to uncertainty - and these models are quite successful for MOSFETs [44]. The origins of $1/f$ noise are poorly understood, and some notable theoretical treatments are mentioned in chapter 2.

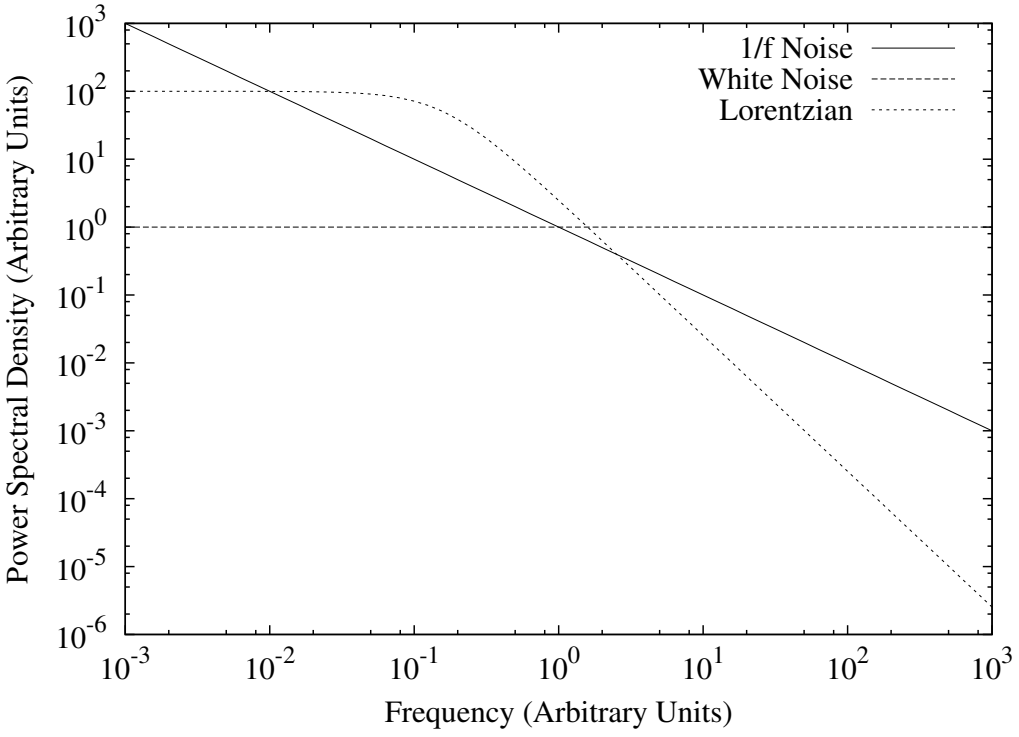

Figure 1.1: Different Power Spectral Density shapes

The PSD shapes of these types of noise are plotted in figure 1.1.

1.3.1 Total Noise Variance

The variance of a noise process is related to the bilateral PSD, as is shown below, by

$$\sigma^2 = \int_{-\infty}^{\infty} S(f)df \tag{1.19}$$

but for real noise sources, $S(f)$ is real, even and positive, hence the variance may be defined as

$$\sigma^2 = 2\int_{0}^{\infty} S(f)df \tag{1.20}$$

As defined, $S(f)$ is called the bilateral PSD, although a unilateral PSD can be defined, such that

$$\sigma^2 = \int_{0}^{\infty} S_{mono}(f)df \tag{1.21}$$

For ideal white noise, these integrals diverges linearly in f as $f \to \infty$, and for $1/f$ noise, they diverge logarithmically both as $f \to 0^{\pm}$ and $f \to \pm\infty$ - only for telegraph-type noise PSDs does the integral converge, as may be expected from the time domain behavior of telegraph noise. In practice, there will be some maximum frequency above which both $1/f$ and white noise sources will drop asymptotically as $1/\omega^2$, due to some maximum speed that characterises the process that gives rise to the noise signal. For $1/f$ noise, the lower limit poses a challenge, namely that no lower cut-off is imposed by any obvious physical considerations - and none have been found - measurements have been performed down to 10^{-8}Hz [45], without any deviations from $1/f$ detected, on one source. Should a lower cut-off exist, it might be material, preparation, operation and temperature dependent.

In practical radiation detectors, the signal is often small, and is hence collected, e.g. on a capacitor, so as to develop a measurable quantity. The collection, or time integration, strongly affects the variance contribution of the noise. Below, I show the standard calculation of the variance of integrated noise for different noise types.

1.3.2 Accounting for Integration

In the previous section, I showed the standard incoherent x-ray photon variance result, namely that the variance in the number of photons that arrive at a statistically constant rate, over some arbitrary period T, is equal to the expected number of photons, as in

equation 1.3, hence giving the (power) SNR as

$$\sigma^2 = SNR = \lambda T = \overline{n} \tag{1.22}$$

The difference from equation 1.5 is due to the fact that no pixels are being compared here - this is the per-pixel SNR, rather than the mottle. One may interpret this result as the variance in and SNR of the integrated photon flux. Shot noise, like incoherent photon arrival (e.g. medical x-rays), is also due to approximately Poisson-distributed events, in particular the arrival of individual electrons by diffusion, or by electrons individually arriving at an anode. One may thus expect that the SNR of a signal with shot-noise calculated on the basis of PSD, will also produce equation 1.3. I next show that it does, and use it as a foil to introduce necessary noise-related concepts and theorems, before calculating the variance of $1/f$ noise.

For individual arrival, or Poisson-like processes, the arrival of a particle, e.g. an electron or a photon, causes a reaction in the system into which it arrives. This reaction is the relaxation of the system to the disturbance of the impulse-like arrival of a particle. It is stereotypically an additive shift in the output, e.g. if the reaction to an arrival at time 0 is $h(t)$, then if two arrivals occur, one at time t_0 and the other at time t_1, then the response of the system to the two arrivals is

$$y(t) = h(t - t_0) + h(t - t_1) \tag{1.23}$$

Such a system is said to be linear time-invariant (LTI). This reaction function, $h(t)$, is called the 'impulse response'. A closely related entity is the transfer function, $H(f)$, which is the Fourier transform of the impulse response,

$$h(t) = \mathfrak{F}^{-1}\{H(f)\} \tag{1.24}$$

The transfer function relates the magnitude and phase of the Fourier transform of the output at some sinusoidal frequency to the magnitude and phase of the Fourier transform of the input at the same sinusoidal frequency.

A standard result for Poisson distributed disturbance-relaxation systems, such as those that produce shot noise, is Carson's theorem [46],

$$S(f) = \lambda\overline{a^2}|H(f)|^2 \tag{1.25}$$

where the PSD is $S(f)$, the occurance rate is λ, the mean-squared magnitude is $\overline{a^2}$ and the disturbance-relaxation transfer function is $H(f)$. Each electron arrival is roughly an impulse of current; the response of the system is dependent on the system's structure. To make the calculation independent of the structure of the system, one may treat the system as an all-pass system, such that the impulse response is an impulse, or Dirac delta function. One treats the arrivals as impulses, so that the system reaction can be calculated on the basis of spectral methods described below. With these considerations, one has

$$h(t) \simeq \delta(t) \tag{1.26}$$

which is the Dirac delta function,

$$H(f) \simeq 1 \tag{1.27}$$

$$\overline{a^2} = e^2 \tag{1.28}$$

The average electron arrival rate is simply the DC current divided by the fundmental charge, or

$$\lambda = I/e \tag{1.29}$$

Thus by Carson's theorem, the shot noise PSD is simply

$$S(f) \simeq Ie \tag{1.30}$$

Already, the PSD is proportional to the current, but integrating the PSD yields infinite variance (see equation 1.19) or zero SNR. While the average pulse width has been ignored, and hence the high-frequency roll-off, also accounting for it would still yield much less than the expected SNR. Time integration of the shot noise in the current must be accounted for, and will provide a stronger limitation on the variance than the that provided by the high-frequency roll-off.

Let the time length that a detector integrates for a detection be T. One may use a mathematical device, namely a moving integrator, to represent the effect of time integration. The moving integrator takes some input signal, $x(t)$, and creates an output, $y(t)$, which is an integral of $x(t)$ over a period T, e.g.

$$y(t) = \int_{t-T}^{t} x(t')dt' \tag{1.31}$$

Thus an integration from time $t_0 - T$ to t_0 is $y(t_0)$. The integrator is a linear time-invariant (LTI) filter, with impulse response

$$h(t) = u(t) - u(t - T) \tag{1.32}$$

where $u(t)$ is the unit step function. This may be seen by convoluting the input signal with the impulse response,

$$y(t) = x(t) * h(t) = \int_{-\infty}^{\infty} x(t - \tau) \cdot h(\tau)\, d\tau \tag{1.33}$$

which simplifies to equation 1.31. The transfer function of the moving integrator is

$$H(\omega) = e^{-j\omega T/2} T \mathrm{sinc} \frac{\omega T}{2} \tag{1.34}$$

If the input of this device is the signal with shot-noise in a detector, and the detector takes an image from time $t_0 - T$ to time t_0, then $y(t_0)$ is the accumulated signal after detection. This shot noise variance is what one would measure in the relevant electronics. Of course, one does not know before-hand what will be measured, and in taking an image, one does not know what portion of the photo-current is spurious, as noise is random.

In general, noise arises from statistical mechanics; an infinite number of noise signal progressions can be defined, each of which accord with the statistical mechanics that give rise to the noise. Each of these possible noise progression signals is a member of the *ensemble* that defines the noise source. In connection to noise ensembles, it should be noted that the Poisson arrival time approach is a mathematical model based - however roughly - on a consequence of the statistical mechanics of that system; it is not derived here from statistical mechanics.

One may mathematically define two major classes of noise on the basis of their ensemble progressions, namely those that tend toward statistically identical behavior in the future as in the past, and those that undergo gross structural or causal shifts in the course of the noise progression, hence continuously or regularly diverging from previous behavior. To illustrate, consider a white noise source. For some ensemble member, $x_i(t)$, defined up to some time t_0, an *infinite* number of sub-ensemble members can be defined, such that they are identical with $x_i(t)$ up to t_0, but have some probability distribution for their value at $t_0 + dt$, for infintesimal dt - such a noise process *would* be considered unchanging, if the

variance of the distribution remains constant with time, but not if it changes with time. Power spectral densities are better defined for processes that do not undergo such gross changes.

A consequence of unchanging mechanics is that an ensemble member function, defined up to some point, e.g. t_0 above, with *statistically uncharacteristic behavior* for some period up to t_0, will tend with high probability to statistically more representative behavior after t_0. Processes with unchanging mechanics (or statistics [47]) are called stationary; if a process's first and second order statistics are stationary, then said process is said to be wide-sense stationary (WSS).

The correlation of a noise process with a delayed version of itself, may be shown to be related directly to the variance in question. The correlation may be calculated in two ways ([48, 49]). The first, known as autocovariance, is the ensemble expectation of the product of a noise signal at some specific time t_1, with the same noise signal at some other time $t_1 + \tau$,

$$\Phi_x(t_1, t_1 + \tau) = E\{x_i(t_1) \cdot x_i(t_1 + \tau)\} \tag{1.35}$$

where E denotes averaging over the ensemble of possible outcomes $x_i(t)$. If the noise process is WSS, the autocovariance is only a function of the time difference τ. The second type of computation, autocorrelation, is on the ensemble member that one happens to measure,

$$R_x(\tau; T_1, T_2) = \frac{1}{T_2 - T_1} \int_{T_1}^{T_2} x(t) \cdot x(t + \tau)\, dt \tag{1.36}$$

If $T_2 - T_1$ is sufficiently large as to be representative of the given WSS process, the resulting autocorrelation is said to be ergodic; for a WSS process, an ergodic autocorrelation is equal to the process's autocovariance [49]. For a zero-mean WSS process, $\Phi(0)$ is the variance of the process [50]. For WSS noise, the autocovariance is the inverse Fourier transform of the PSD, by the Wiener-Khintchine theorem [51],

$$\Phi(\tau) = \frac{1}{2\pi} \int_{-\infty}^{\infty} e^{j\omega\tau} S(\omega)\, d\omega \tag{1.37}$$

One may create a new noise process by filtering an existing noise process. If the PSD of the existing noise process is $S_{in}(f)$, and the filter is LTI with transfer function $H(f)$, then one may show, using the Wiener-Khintchine theroem, that the new noise process,

that appears at the output of the filter, has the PSD S_{new} [52]

$$S_{new}(f) = S_{in}(f) \cdot |H(f)|^2 \tag{1.38}$$

which is shown in outline in chapter 3. This relation allows one to calculate the PSD of $y(t)$ in equation 1.31,

$$S_y(f) = S_x(f) \cdot T^2 \text{sinc}^2 \pi T f \tag{1.39}$$

The ensemble variance of y(t) for all time, and hence of the integration detector shot noise, is

$$\sigma_I^2 = 2 \int_0^\infty S_y(f) df \tag{1.40}$$

$$= S_0 T \tag{1.41}$$

$$= IeT \tag{1.42}$$

The variance of the integrated shot noise per electron is

$$\sigma_n^2 = IT/e = \lambda T \tag{1.43}$$

as per equation 1.22.

One may wish to perform the same operation for $1/f$ noise, so as to calculate the variance contribution that $1/f$ noise makes,

$$\sigma_{1/f}^2 = 2 \int_0^\infty \frac{S_0}{f} T^2 \text{sinc}^2(\pi T f) df \tag{1.44}$$

however this integral diverges logarithmically in the low frequency limit. Although experiments have failed to detect a lower cut-off, experimental possibilty precludes the detection of a sufficiently low lower cut-off, as thermal variations over the time-scale needed to measure that low ($\tau \sim 1/f_0$) would obscure such a lower cut-off.. A lower cut-off will be assumed here for convergence; the PSD is

$$S(f) = \frac{2\pi S_0}{\sqrt{\omega^2 + \omega_0^2}} \tag{1.45}$$

The integration transfer function $H_{int}\omega$ may also be represented by

$$H_{int}(\omega) = T^2 \text{sinc}^2(\omega T/2) = 2 \int_0^T (T - t) \cos(\omega t)\, dt \tag{1.46}$$

The variance is then

$$\sigma_{1/f}^2 = \frac{2}{2\pi}\int_0^\infty \frac{2\pi S_0 T^2 \mathrm{sinc}^2(\omega T/2)}{\sqrt{\omega^2+\omega_0^2}} \tag{1.47}$$

By substituting equation 1.46 and reversing the order of integations, one obtains

$$\sigma_{1/f}^2 = 4\int_0^T (T-t)\int_0^T S_0 \frac{\cos(\omega t)}{\sqrt{\omega^2+\omega_0^2}}\,d\omega\,dt \tag{1.48}$$

$$= 4S_0\int_0^T (T-t)K_0(\omega_0 t)\,dt \tag{1.49}$$

Substituting the approximation,

$$K_0(x) = -C - \ln(x/2)... \tag{1.50}$$

one obtains for the variance,

$$\sigma_{1/f}^2 \simeq 2S_0(3/2 - C - \ln \pi T f_0) \tag{1.51}$$

The above variance calculation is somewhat naive, as any measurement performed in a detector will be with respect to some datum, e.g. dark current a minute before the measurement, irrespective of whether or not said datum is explicitly subtracted. If the datum is not subtracted, the pixel photon count is simply displaced from the true detected photon count of said pixel, over the longer term, and no variance is introduced due to this displacement; the displacement is then a different kind of uncertainty, and will thus still give rise to mottle. In practice, the subtraction of the individual pixel datum is preferable, as pixels may have gross diferences in their data, thus introducing consistent mottle. Moreover, the individual pixel datum may shift over time, e.g. due to thermal drifts, or $1/f$ noise. One may take a datum reading before or after an exposure, or use the average of before and after, to correct pixel photon counts. After correction for displacement, e.g. as caused by $1/f$ noise, second order uncertainty (variance) remains; this variance is considered in chapter 3.

Other workers made accounts of this variance, especially as it relates to $1/f$ noise.

Without explicitly considering correction, and outside the context of detectors, Keshner [21] investigated the variance *that would be experienced as variance rather than as an average* over the course of a finite length observation of $1/f$ noise *in the absense of a lower cut-off*. Keshner's total variance still diverges, but an infinite observation time is needed

to observe this infinite variance, and it diverges logarithmically with observation time. Keshner found the variance to depend logarithmically on the length of the observation window.

McDowell [22] et al. extended Keshner's method to the case where the frequency exponent is not exactly one, and the noise bearing signal is integrated, with specific application to x-ray detectors. An implicit calibration is also present in their work, as they simply give the variance contribution from $1/f$ noise as a function of 'observation time,' which they state is on the order of the time length that the equipment might ever be used.

In another paper, McDowell [53] et al. considered the difference between two equal length, unseparated integrations of the signal from an x-ray detector, but did not consider this as a general method to limit the variance of the noise, but rather as a kind of noise floor. While the methods in chapter 3 are on the surface comparable to their method, it arises from a different understanding of the noise contribution. The methods in chapter 3 are also more general.

In chapter 3, I derive the transfer functions of various correction regimes, e.g. using one or two dark-current data for subtraction from the photocurrent, and the variance contribution of various noise types under said regimes. In the next chapter, I recount some of the advances that have been made in the understanding of $1/f$ noise. Other groups did consider subtraction; in the literature, it is sometimes called "Correlated Double Sampling." Several groups use transfer functions to represent subtraction [54, 55, 56, 57]. Chapter 3 is effectively an algebraic generalization and extension of their methods, as numerical methods have been used in previous work [58], although one author has considered a CDS circuit as a low-pass filter to obtain algebraic results [59]—in chapter 3, CDS is considered as an integration, and very general results are obtained.

Chapter 2

Literature Review

The intent of this research is to understand the contribution $1/f$ noise makes to the variance in the quantity detected by an integrating detector. Such a project has two components: firstly, to understand how a given noise frequency exponent (α in equation 1.18) and reference-frequency, spectral-density magnitude (S_0 in equation 1.18) contribute to said variance, and secondly, what determines said spectral density exponent and reference frequency magnitude. The first component is presented in chapter 3. The second component requires an understanding of how $1/f$ noise arises; such understanding as it exists, is highly incomplete. This chapter serves to introduce what is understood about how $1/f$ noise arises and gains its magnitude and exponent. However, no general theory for the noise magnitude or exponent hase been developed - most 1/f noise sources are without an adequate model. This chapter serves to discuss the science of 1/f noise, and to critique a few papers. It may be skipped without any loss of continuity.

This chapter will discuss two types of $1/f$ noise studies, namely theoretical discussions of how $1/f$ noise may arise from understood phenomena, i.e. models, and experiments to see which phenomena might affect $1/f$ noise. Investigations have been made on the dependence of $1/f$ noise on sample size, carrier concentrations, relation to temperature and applied potentials, material type, and so forth.

2.1 Models

Lorentzian (equation 1.12) fluctuations, unlike $1/f$ noise, can readily be described theoretically; for an overview, see [60] and references therein. Subject to the constraint that $1/f$ noise is a fluctuation in resistance, a natural approach is to show that resistive Lorentzians acting together give rise to a $1/f$ spectrum.

One conceptually simple model is a sum over a distribution of statistically independent Lorentzian fluctuators, where the distribution declines in density as the inverse of the characteristic times, τ, of the fluctuators, as per Surdin, cited in [61]. Their cumulative PSD will be

$$S(\omega) \propto \int_0^\infty \frac{K}{\tau} \frac{\tau d\tau}{1+\omega^2\tau^2} = \frac{\pi K}{2\omega} \tag{2.1}$$

The resulting PSD is $1/f$, but it requires τ to range from 0 to ∞ which is unphysical. In practice, only a finite range of characteristic times is expected, which give rise to deviations from $1/f$, e.g.

$$S(\tau_{min}, \tau_{max}; \omega) \propto \int_{\tau_{min}}^{\tau_{max}} \frac{K}{\tau} \frac{\tau d\tau}{1+\omega^2\tau^2} = \frac{K}{\omega}[\arctan \omega\tau_{max} - \arctan \omega\tau_{min}] \tag{2.2}$$

This is illustrated in figure 2.1, for $\tau_{min} = 10^{-3}$s and $\tau_{max} = 1$s. The frequency span over the PSD reasonably approximates $1/f$ noise, may be calculated as per equation 2.11 below. The resulting frequency span, where the local slope lies between 0.8 and 1.2, limits asymptotically to

$$\mathrm{d}_f = \mathrm{d}_\tau - 1.11 \tag{2.3}$$

where d_f is the number of decades of frequency span where the local slope is $1/f$ and d_τ is the number of decades separation between τ_{min} and τ_{max},

$$\mathrm{d}_\tau = \log_{10}\left(\frac{\tau_{max}}{\tau_{min}}\right) \tag{2.4}$$

The relationship between d_f and d_τ is illustrated in figure 2.2. Of course, Lorentzians would be summed, not integrated; for an integral approximation to work, the characteristic times must be closely spaced, over a range that corresponds to the frequencies over which we observe $1/f$ noise.

An early model for $1/f$ noise in MOSFETs, which is a basis for subsequent models, is that of McWhorter. McWhorter's model explains $1/f$ noise as fluctuations in resistance due to the trapping of charge carriers from the valence or conduction bands into localized states, and detrapping or return of the carriers to transport states. The traps are assumed to be distributed uniformly over distance into the oxide that separates the gate from the channel. This energy barrier between a trap and the channel is a type of activation barrier, which causes the switching, or trapping/detrapping time to be thermally activated, i.e.

$$\tau = \tau_0 e^{\mathrm{E_a}/k_B T} \tag{2.5}$$

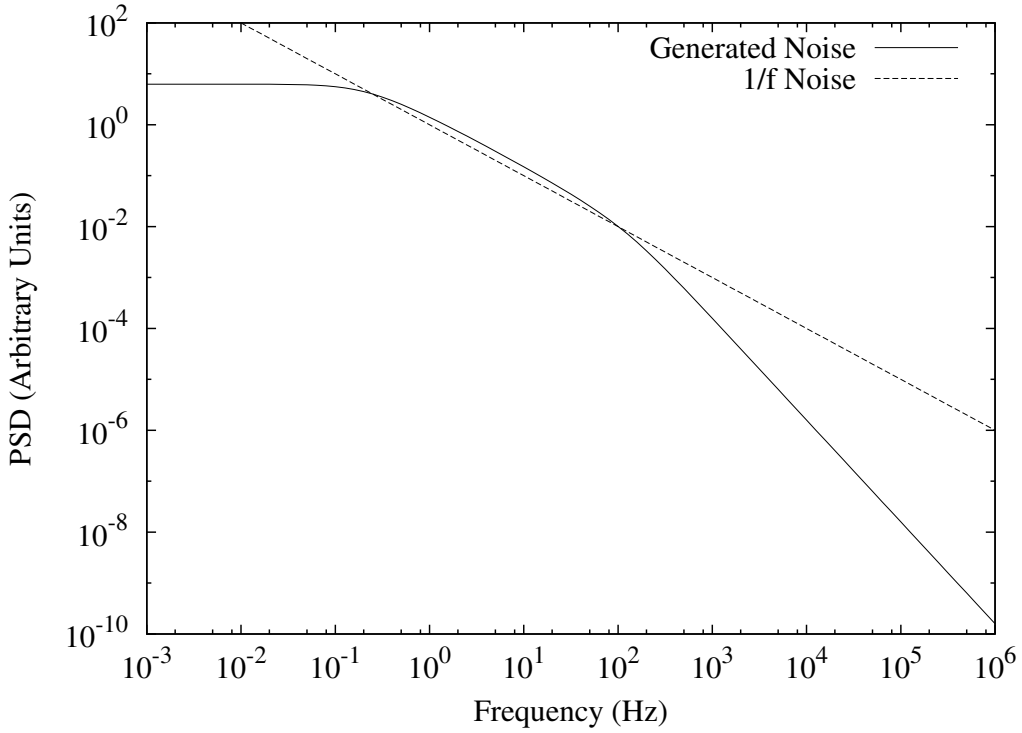

Figure 2.1: The noise produced by a Surdin distribution, i.e. $\propto 1/\tau$, with $\tau_{min} = 10^{-3}$s, $\tau_{max} = 1$s is 1/f only over a small range.

where τ_0 is the (very small compared to the Lorentzian characteristic times) characteristic attempt-to-escape time. As such, one may sum the resulting noise over the (flat) distribution in energy if the individual traps fluctuate independently of one another. Then

$$S(\omega) \propto \int_0^\infty \frac{\tau_0 e^{E_a/k_BT}\, dE_a}{1+\omega^2\tau_0^2 e^{2E_a/k_BT}} = \frac{k_BT}{\omega}(\pi/2 - \arctan\omega\tau_0) \tag{2.6}$$

in the approximation of an infinitely wide distribution. This flat distribution of activation energies of fluctuators is a more probable and intuitive explanation of $1/f$ noise than an inversely proportional distribution of characteristic times.

2.1.1 Dutta, Dimon and Horn

One interesting extension of McWhorter's approach is that of Dutta et al.[62], who use a non-flat distribution of activation energies that results in a PSD that varies in magnitude and exponent with temperature, in agreement with experiments, on 800Å thick Silver films. Their work contains a rather surprising conclusion, namely a very broad $1/f$ noise spectrum (60 decades, for one sample), which does not appear to be supported by the

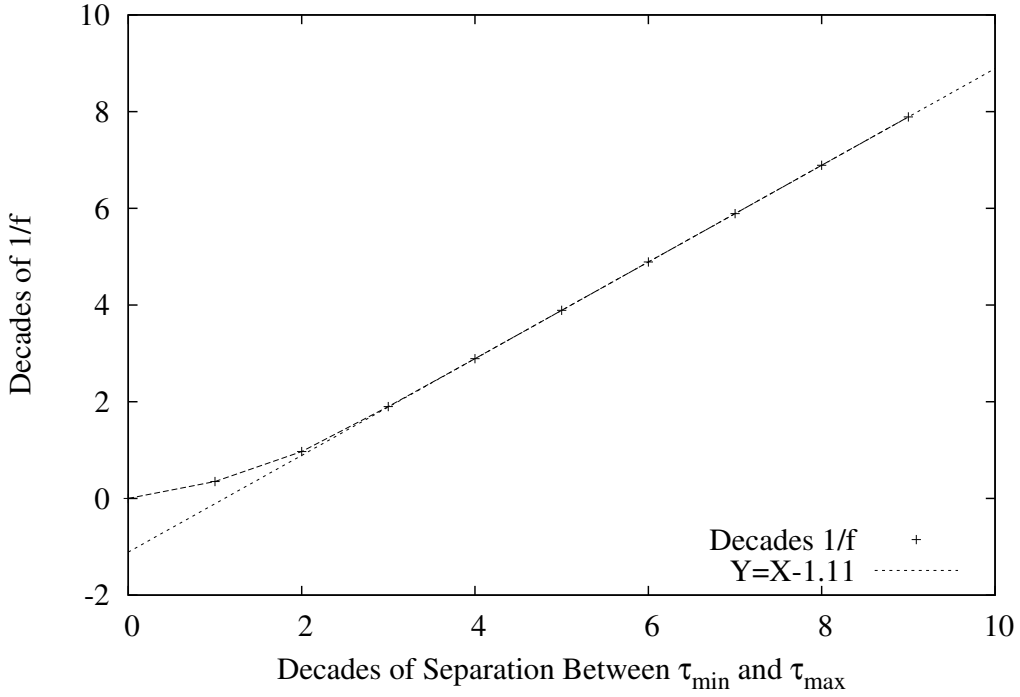

Figure 2.2: The decades separation between τ_{min} and τ_{max} versus the resulting number of decades of 1/f noise from a Surdin distribution of fluctuators, where $0.8 < \alpha < 1.2$, with the asymptotic tendency

theory that they present.

Their equation 1 has a typographical error - they give the PSD of a thermally activated Lorentzian as

$$S(\omega) \propto \frac{\tau_0 e^{\mathrm{E_a}/k_B T}}{1 + \omega^2 \tau_0^2 e^{\mathrm{E_a}/k_B T}} \tag{2.7}$$

instead of as

$$S(\omega) \propto \frac{\tau_0 e^{\mathrm{E_a}/k_B T}}{1 + \omega^2 \tau_0^2 e^{2\mathrm{E_a}/k_B T}} \tag{2.8}$$

It is not obvious whether their summation in their equation 2 is based on their erroneous equation 1. They approximate the integral of equation 2.7 or equation 2.8 as (their equation 3)

$$S_V(\omega, T) \propto \frac{k_B T}{\omega} D(\tilde{E}) \tag{2.9}$$

where $D(E)$ is the distribution of fluctuators with activation energy

$$\tilde{E} = -k_B T \ln \omega\tau_0 \tag{2.10}$$

τ_0 is the characteristic attempt rate, and α is the frequency exponent of the PSD,

$$\alpha = -\frac{\partial \ln S_V(\omega, T)}{\partial \ln \omega\tau_0} \tag{2.11}$$

Using their definition of α and their equation 3, they obtain their equation 4,

$$\alpha(\omega, T) = 1 - \frac{1}{\ln \omega\tau_0}\left[\frac{\partial \ln S_V(\omega, T)}{\partial lnT} - 1\right] \tag{2.12}$$

It is worth pointing out that in equation 2.9,

$$\alpha \simeq 1 + \frac{\partial D(\tilde{E})}{\partial \tilde{E}}\frac{k_B T}{D(\tilde{E})} \tag{2.13}$$

For a flat but limited distribution of activation energies $D(E)$, one obtains one additional decade of $1/f$ noise for every additional $2.3k_BT$ of width in $D(E)$. For a non-flat distribution, $|D'(E)k_BT/D(E)|$ must remain close to zero for the noise to remain close to $1/f$. Their distribution is sufficiently sharp, as per equation 2.13, yet narrow as to give only 5-10 decades of $1/f$ noise, their claim of 60 decades notwithstanding.

Dutta et al. claim, "Finally, we note that the observed scale invariance of the noise spectrum is reproduced in our model as an artifact: For $\omega \ll 1/\tau_0$, $\tilde{E}$ is extremely insensitive to changes in ω." This argument is faulty. Scale-invariance refers to noise having equal power in arbitrarily separated (or overlapping) decades of frequency span, or other frequency spans where the span is specified as a ratio between the maximum and minimum frequencies, and thus requires $\alpha \simeq 1$ over a large span of frequencies. Their claim rests on $\tilde{E}$ in equation 2.10 not changing much as ω becomes small. To test their claim, we may specify ω as being x decades below τ_0^{-1},

$$\omega = \tau_0^{-1} 10^{-x} \tag{2.14}$$

$$\tilde{E} = 2.3 k_B T x \tag{2.15}$$

Going 60 decades down in frequency at 300K implies going 3.6eV up in $\tilde{E}$; their $D(E)$ is about 0.6eV wide. $\tilde{E}$ is linear in terms of decades down in ω. In fact, $\tilde{E}$ has a logarithmic dependence on ω, and thus becomes more sensitive to ω as ω goes down, not less,

$$\frac{\partial \tilde{E}}{\partial \omega} \propto \frac{-1}{\omega} \tag{2.16}$$

A Gaussian-like distribution of fluctuator activation energies, such as that used by Dutta et al., will not tend to generate generally scale-invariant noise. This may be seen by substituting a Gaussian distribution into equation 2.13,

$$\alpha \simeq 1 - k_B T \frac{\tilde{E} - \mu}{\sigma^2} \tag{2.17}$$

This approximation suggests that α will tend toward positive or negative infinity - in practice, it will tend to 0 in the low frequency limit, and toward 2 in the high frequency limit; either way, it will not generate scale-invariance over any large frequency range. However, a fat-tailed distribution, e.g. that of Cauchy, will tend to generate a nearly scale-invariant 1/f noise down to very low frequencies, with the noise having features in $\alpha(\omega)$ around the frequency corresponding to the peak of the distribution of activation energies. This may be seen by substituting a Cauchy-shaped distribution of fluctuator activation energies into equation 2.13,

$$\alpha \simeq 1 - k_B T \frac{2a(\tilde{E} - E_0)}{(\tilde{E} - E_0)^2 + a^2} \tag{2.18}$$

which clearly tends to 1 as the energy $\tilde{E}$ tends above or below E_0. E_0 and a are parameters of the Cauchy distribution; the peak of the distribution is at E_0.

Fleetwood and Giordano in their 1985 paper [63] tested the predictions of Dutta et al., using noise measurements on a very narrow (530Å diameter) $Au_{60}Pd_{40}$ wire, over a wide range of temperatures (77K-430K). They use the interpretation that defects and their motion constitute the Lorentzian fluctuators, and thus interpret the change in noise densities at different frequencies in terms of the concentration of defects as defects being annealed away. They found Dutta's (et al.) model very successful, including its predictions of how the noise exponent would change with the noise density at a particular frequency. It is worth noting that Dutta's (et al.) prediction suggests that at $\tilde{E}(\omega) = 0.6\text{eV}$, $\alpha \simeq 1.75$.

It may be useful to measure α at a variety of frequencies at each temperature, to obtain a best-fit distribution of fluctuators and test the distribution of independent fluctuators formalism, as both Dutta et al. and Fleetwoord and Giordano measure α at one frequency over multiple temperatures.

2.1.2 Other Models

Hooge [61] presented a detailed analysis to show that the strict McWhorter model for MOSFETs predicts a noise level as a function of the Fermi level; this noise level agrees with experiment only over a narrow range of Fermi levels. Other models also exist to describe how a $1/f$ spectrum may arise.

Borovitskaya and Shur [64] published a model of $1/f$ noise inolving tail states of the band edges of semiconductors, i.e. those states most close to the band gap, when the Fermi-level is close to the band edge; their proposal produces $1/f$ if the tail states density exponentially decays into the band-gap. Pfeiffer [65] provides a quantum-physical $1/f$ noise model for crystalline intrinsic semiconductors, that ties the noise to lattice vibrations in one-dimensional semiconductors, through the exchange of energy between lattice vibrations and carrier motion. A Hamiltonian, which is the quantum operator equivalent to the energy of a system, was devised for this model system of one-dimensional lattice vibrations with carriers, that included the effect of the field on both the charge carriers and the lattice ions. Using this Hamiltonian, noise was derived with a PSD that was $1/f$ below a critical frequency, and $1/f^2$ above. Shklovskii [66] derived a variable range hopping conduction model of $1/f$ noise, for amorphous semiconductors. Germanium and n-type Gallium Arsenide are mentioned as materials to which his model may apply. The model predicts a resistive noise PSD magnitude that drops exponentially as the cube of the absolute temperature, and gives a moderate range of $1/f$ noise (2.5 – 7 decades are mentioned).

Kaulakys et al. [67, 68] use 'point process' non-linear stochastic differential equations

$$\frac{\mathrm{d}x}{\mathrm{d}t_s} = \Gamma x^{2\eta-1} + x^{\eta}\xi(t_s) \tag{2.19}$$

to produce $1/f$ noise; t_s is a normalized time, Γ and η are parameters of the differential equation, and $\xi(t)$ is a Gaussian white noise signal. The frequency exponent is

$$\alpha = 2 - \frac{2\Gamma + 1}{2\eta - 2} \tag{2.20}$$

and the resulting noise signal has a probability density function with the dependence

$$p(x) \sim x^{-\lambda} \tag{2.21}$$

$$\lambda = 2(\eta - \Gamma) \tag{2.22}$$

with different possible exponents. No materials are specified, to which this model may apply.

Alternatives are thus available to potentially explain $1/f$ noise where McWhorter or Dutta et al. cannot.

After the publication of the paper of Dutta et al., obvious questions were empirical proof of the existence of the individual Lorentzians, possible Lorentzian sources, and their nature. Possibilities for nature of the Lorentzians included defect motions in the case of metals, and carrier number and mobility fluctuations for semiconductors. Several theoretical and experimental papers were published on these questions; several experimental papers are discussed next.

2.2 Experimental Studies

A consequence of models like those of McWhorter and Dutta et al. is that a large set of Lorentzian fluctuators, with a high degree of statistical independence, and with an appropriate distribution of characteristic times, will yield $1/f$ type noise. Several experimental studies attempt to isolate fluctuators.

In parameter of $1/f$ noise that is indirectly of great significance to chapter 3, is the 'second spectra,' or the 'noise of the noise'. This is measured by taking say $k \cdot N$ samples, where k and N are integers, and N samples are necessary to estimate the power of noise in a given decade of interest at the sampling rate used. One then calculates the power in the decade of interest, for samples 1 to N, say using a Fourier sequence, and makes that power result the first point in a data sequence. This operation is then repeated for samples 2 to $N + 1$ to generate the second point of the data sequence, and so forth, to sample subset $[(k-1)N + 1]$ to kN. A PSD is then calculated for the resulting set of power points; this PSD is the second spectrum. The derivation of chapter 3 relies on the second spectrum being 'white' or constant, but will not be greatly modified for $\alpha < 1$. Kogan ascribes to

Weissman the position that non-flat second spectra indicates a divergence from Gaussian behavior, although both by definition and as is implied by Kogan, a non-white second spectrum must be second-order non-stationary [69]. A result of my work in chapter 3 is that a second-spectrum with $\alpha < 1$ is second-order stationary.

Garfunkel et al. [70] studied small numbers of fluctuators in very small (nanometer-scale), very cold (4K-30K) C-Cu and Si-Au amorphous conductor samples, as the cold slows down the fluctuators, making individual fluctuators easier to identify. They found both tunneling-type (two-level system) and thermally activated-type fluctuators. The density of fluctuators based on noise measurements at 4K accounted for the deviation of the heat capacity of the amorphous samples from expected trends. They found that TLS fluctuators often were not entirely statistically independent, and proposed that the fluctuators interacted. They found that anneals of 100K randomized spectral features, in particular the average power in a given continuous decade of frequency. They also measured second spectra over several octaves of first spectra; high frequency noise was found to have $1/f$ second spectra tendencies.

Black et al. [71] studied the cross-correlation of $1/f$ noise on two closely spaced current paths in metal films, to see if thermal fluctuations, which would quickly spread over a small distance, cause $1/f$ noise. They found no correlations, and conclude that the noise is produced very locally, and not due to resistivity increases from thermal fluctuations.

Bora and Raychaudhuri [72] studied the noise of metal films under electromigration (EM) stressing, which is the drift or diffusion of impurities and defects in a film under very high current densities and electric fields. They found a $1/f^{3/2}$ noise that grew in magnitude as the EM stressing persisted. Their system had both $1/f$ and $1/f^{3/2}$ noise, as schematically illustrated in figure 2.3. In their figure8a, they give the ratio of the $1/f$ S_0 to the $1/f^{3/2}$ S_0 at 1Hz as 2, whereas in their figure 13, they give the same ratio as 10. It appears that the incomplete understanding is both in the $1/f$ and EM stressing noise: both the $1/f$ and EM simulation S_0 disagree with the experimental results.

For their 1983 paper [73], Fleetwood and Giordano measured noise in unstressed and stressed films. They found that stressing a film tended to *decrease* the 10Hz noise magnitude, while increasing the spectral exponent. The effects were reduced over time as the strains inside the films relaxed, suggesting to the authors that $1/f$ noise results from strain

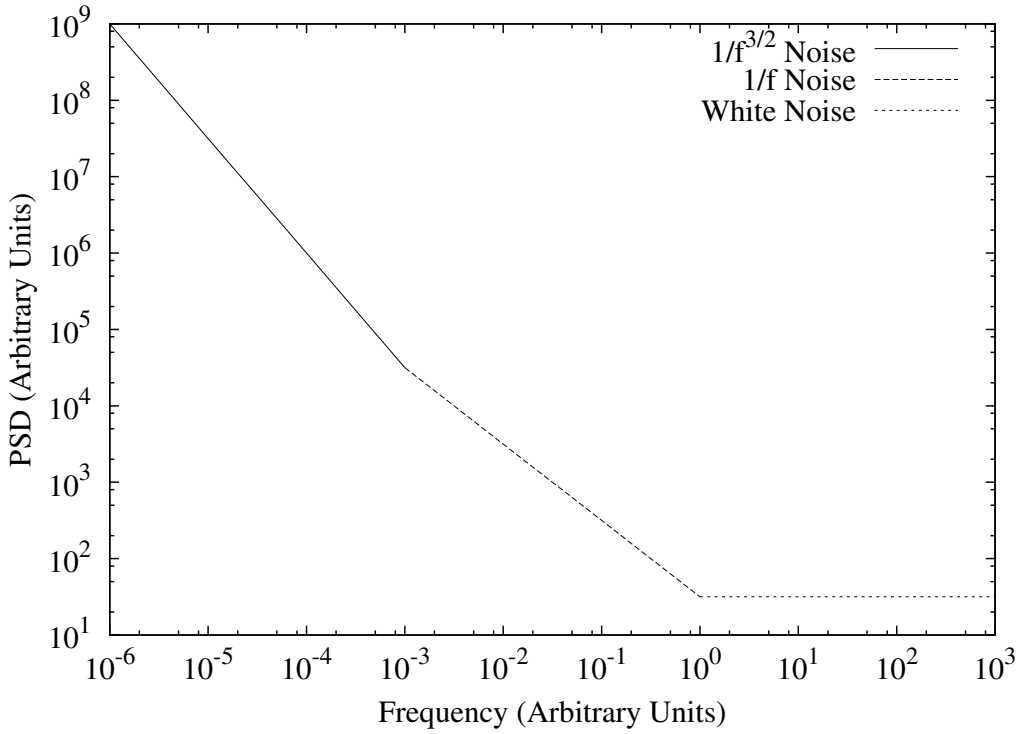

Figure 2.3: At the lower frequencies, the EM-stress induced $1/f^{3/2}$ noise is dominant; at higher frequencies, $1/f$ noise takes over, and finally, white noise becomes dominant at the highest frequencies.

relaxation; in light of the work of Bora and Raychaudhuri above, one might well ask if that is not a separate process of $1/f$ noise, or at least a separate mode of the process that gives rise to $1/f$ noise in metal films.

Pelz and Clarke [74] irradiated polycrystalline Cu films with 500keV electrons to investigate the effect of the irradiation on the $1/f$ noise of the samples; the samples were held at 90K. They expected spatially uncorrelated Frenkel defects, or pairs of vacancies with atoms in interstitial (off-lattice) positions. They found that annealing reduced the additional $1/f$ noise more rapidly that it did the additional resistivity, and anneals at temperatures as low as 108K would reduce the noise magnitude substantially. It appears that this irradiation does not affect the exponent of the noise process.

Parman et al. [75] studied the second spectra of current $1/f$ noise in hydrogenated amorphous silicon (a-Si:H), and found them to have a strong $1/f$ component. This they suggest is indicative that some traps modulate others, and hence invalidates the assumption of independent fluctuators. Bakker [76] suggests that $1/f$ noise in a–Si:H arises from

both the disorder, and from a random, randomly varying 'potential landscape,' or non-linear spatial variation in carrier potential. The 'potential landscape' due to amphoteric deep traps, i.e. traps that can capture both electrons and holes, also known as charged deep defects contribute to the noise. The random 'potential landscape' and fluctuations in potential tend to localize electrons.

Fantini et al. [77] investigated the noise dependence of chalcogenide-based (GST is $Ge_2Sb_2Te_5$) phase-change memories, both at low forward bias and at avalanche-inducing reverse bias. They found the current at low forward bias to be very much resistive, but becoming more exponentially dependent at higher biases. For the amorphous phase, the noise magnitude was slightly more than two orders of magnitude higher than for the device-polycrystalline phase. They found that both the white and $1/f$ noise in the avalanche mode had an effective multiplier M^2, i.e.

$$S_I = S_{I_0}(f)M^2 + 2qIM^2 \tag{2.23}$$

where the first term on the right is the $1/f$ term.

2.2.1 MOSFETs

Vandamme et al. [44] suggest that for n-channel MOSFETs, the noise arises from carrier concentration fluctuations, whereas for p–channel MOSFETs, mobility fluctuations make the dominant noise contributions. They state that for carrier concentration fluctuations, a Hooge parameter dependence

$$\alpha_H \propto \frac{1}{V_{GS} - V_{th}} \tag{2.24}$$

is expected, but that the same dependence is expected for carrier mobility fluctuations when there are impurity-produced cavities in the inversion layer. They further give as evidence that for p–channel MOSFETs,

$$S_{V_{eq}} = S_{I_{sat}}/g_m^2 \propto V_{GS} - V_{th} \tag{2.25}$$

which suggests that α_H is independent of $V_{GS} - V_{th}$. Their suggestions are interesting, as both mobility and number fluctuations may give rise to $1/f$ noise in crystalline semiconductor devices, alongside other mechanisms. The number fluctuations they attribute to the

capture of carriers near the gate (by diffused oxygen traps). Vandamme and Vandamme [78] found that physical models with very separate algebraic dependences are needed to account for $1/f$ noise in p and n–channel MOSFETS.

Aoki and Kato [79] performed noise measurements on 10keV x-ray irradiated and hot carrier injected MOSFETs. They found that hot-hole injection and irradiation much more quickly increased device noise than hot-electron injection. It is known (e.g. from [44] and references therein) that increases in sample or device noise indicates poor crystal quality, and is an indication of impeding failure.

As can be seen from the above overview, the $1/f$ understanding of MOSFETs is quite sophisticated, if still in many physical respects incomplete.

2.3 Tensor Noise Models

As the Lorentzians that give rise to $1/f$ noise in passive devices may be defects or other irregularities, it is plausible that the resistivity noise may be anisotropic, including in isotropic media. I next critique two papers on such proposals for 1/f noise.

2.3.1 Tensors: Kogan and Nagaev

Kogan and Nagaev's paper [80] shows how defects, whose resistivity is anisotropic, and whose movement constitutes internal friction, may give rise to $1/f$ noise. The fluctuator distribution is mainly flat, presumably in activation energy. They claim that a certain degree of anisotropy is necessary to achieve $1/f$ noise. They produce a similar result for so-called 'two-level' systems, where an electron may be somewhat trapped in one of two spatially and energetically seperated traps, and may transition or tunnel between the two levels or traps. Two-level systems are typically evident in very cold ($T < 1$K) samples. They state that the state of the electron would alter the local resistivity.

Some notable features of their defect (internal friction) model include:

1. They give the $1/f$ noise due to internal friction as

$$S(f) \simeq n(\tilde{E})[l\sigma_s(\tilde{E})]^2 \frac{k_B T}{Vf} \tag{2.26}$$

where $\tilde{E}$ is as per Dutta et al. above, l is the electron free path length, V is the volume of the sample, and $n(\tilde{E})$ is the defect concentration. The background internal friction is

$$Q_{BG} \simeq \frac{\pi}{2} n(\tilde{E}) B(\tilde{E}) \sim 10^{-4} \quad 10^{-3} \tag{2.27}$$

for metals, and $B(\tilde{E})$ is on the order of the elastic modulus times the 'atomic volume' squared. It is not clear whether this atomic volume' is that of a unit cell, or some more nebulous 'atomic volume'.

2. A given defect will have one of S orientations, where the physical meaning of s given that $1 \leq s \leq S$, is dependent on the crystal structure. The concentration of defects of orientation s in some volume is n_s, and the total concentration of defects is

$$n_d = \sum_{s=1}^{S} n_s \tag{2.28}$$

3. The defects are assumed to be distributed rather diffusely, so as to determine the average resistivity tensor by the concentration of the defects. In this manner, it becomes meaningful to speak of terms like $\partial \rho_{ij} / \partial n_s$.

4. They give a relationship that implies that one consequence of their model is

$$\forall s (1 \leq s \leq S) \implies \sum_{i=1}^{3} \left[\frac{\partial \rho_{ii}}{\partial n_s} - \frac{1}{S} \sum_{z=1}^{S} \frac{\partial \rho_{ii}}{\partial n_z} \right] = \text{ Constant} \tag{2.29}$$

This is a necessary consequence of their unnumbered equation

$$\mathrm{Tr}\{\delta P\} = 0 \tag{2.30}$$

given their condition in the text that defects fluctuate by changing orientation, without changing the total number of defects. They state this condition (equation 2.30)as obvious, but supply no justification.

2.3.2 Tensors: Weissman, Black and Snow

For materials that are on average isotropic in resistivity, the fluctuations in resistivity through the material need not be isotropic; Weissman et al. devised a statistical anisotropy parameter S (not to be confused with the S above) , that describes the statistical properties

of the resistivity noise tensor, for different types of aniostropic fluctuations[81]. They then relate this paramter to the noise on the orthogonal-to-current arm of a Maltese–cross–shaped sample [82]. Their derivation allows for a frequency-dependent statistical anisotropy parameter.

Resistivity fluctuation is understood to arise from defects and number or mobility fluctuations; their orientations may be random, or may be determined by the orientations of the crystal in which they occur, e.g. point defects (see [80] above); the individual fluctuations are expected to have Lorentzian spectra. The orientation of a fluctuation is its primary axes, along which one may directly calculate the electric field vector from the current density vector. To calculate e.g. the electric field vector arising from the current density at a given point, one needs all the components of the current density along the axes of the fluctuation tensor; one obtains then the electric field components along the same axes. One seeks however the fluctuation of the electric field due to the current density, along the axes of the sample.

To calculate the electric field vector from the current density along the sample axes, one must rotate the tensor to the axes of interest, by taking components of the electric field and current density along the tensor axes, as shown below. A uniform distribution of fluctuation axis orientations is expected; in order to rotate the tensor, the rotations of the axes to obtain all possible orientations must be defined. Allowing the coordinate system to remain right handed, any orientation of the axes can be described uniquely as three rotations, thereby avoiding explicit reference to the sample axes. The fluctuation tensor axes are the set x_n: firstly, one may define an x'_n set of axes, where $\hat{x}'_1$ and $\hat{x}'_2$ lie in the plane of $\hat{x}_1$ and $\hat{x}_2$, rotated by some angle ϕ, and $\hat{x}'_3 = \hat{x}_3$. Secondly, one may define an x''_n set of axes, where $\hat{x}''_1$ and $\hat{x}''_3$ lie in the plane of $\hat{x}'_1$ and $\hat{x}'_3$, rotated by an angle $\theta - \pi/2$. This angle is chosen so that $\pi/2$ corresponds to the unrotated case, and to let θ vary from 0 to π; $\hat{x}''_2 = \hat{x}'_2$. Finally, one may rotate $\hat{x}''_2$ and $\hat{x}''_3$ in their plane, by some angle ψ, to obtain the x'''_n axes.

Relevant variances and correlations may be calculated by averaging over time, solid

angle of x_1''' axis rotation, and angle of x_2'''–x_3''' rotation,

$$\langle ab\rangle_{t,\phi,\theta,\psi} = \lim_{T\to\infty}\frac{1}{T}\int_{-T/2}^{T/2}\frac{1}{2\pi}\int_0^{2\pi}\frac{1}{2}\int_0^{\pi}\frac{1}{2\pi}\int_0^{2\pi} a(t,\phi,\theta,\psi)\, b(t,\phi,\theta,\psi)\, d\psi\, sin\theta\, d\theta\, d\phi\, dt \tag{2.31}$$

In the following, let the vectors be column vectors, so that row vectors are achieved by transposition. The tensor rotation may be understood as follows. Let the resistivity tensor in the axes that define its orientation be

$$\delta P = \begin{pmatrix} \delta\rho_{11} & \delta\rho_{12} & \delta\rho_{13} \\ \delta\rho_{21} & \delta\rho_{22} & \delta\rho_{23} \\ \delta\rho_{31} & \delta\rho_{32} & \delta\rho_{33} \end{pmatrix} \tag{2.32}$$

Then

$$\delta\vec{E} = \delta P\,\vec{J} + P\,\delta\vec{J} \tag{2.33}$$

where Weissman et al. [81] consider the second term on the right to be zero, as the current is held constant. To find the tensor along the x_n' axes, we may use

$$\vec{x}_n' = R_\phi\,\vec{x}_n \tag{2.34}$$

where

$$R_\phi = \begin{pmatrix} \cos\phi & \sin\phi & 0 \\ -\sin\phi & \cos\phi & 0 \\ 0 & 0 & 1 \end{pmatrix} \tag{2.35}$$

and

$$R_\phi^{-1} = R_{-\phi} \tag{2.36}$$

Then

$$\delta\vec{E}' = R_\phi\,\delta\vec{E} = R_\phi\,\delta P\,\vec{J} \tag{2.37}$$

however

$$\vec{J} = R_\phi^{-1}\,\vec{J}' \tag{2.38}$$

so

$$\delta\vec{E}' = R_\phi\,\delta P\,R_\phi^{-1}\,\vec{J}' \tag{2.39}$$

Using the associative property of matrix multiplication, one may identify the rotated tensor as

$$\delta P' = R_\phi\,\delta P\,R_\phi^{-1} \tag{2.40}$$

Next, one seeks the tensor after the $\theta - \pi/2$ rotation,

$$R_\theta = \begin{pmatrix} \sin\theta & 0 & \cos\theta \\ 0 & 1 & 0 \\ -\cos\theta & 0 & \sin\theta \end{pmatrix} \tag{2.41}$$

$$R_\theta^{-1} = \begin{pmatrix} \sin\theta & 0 & -\cos\theta \\ 0 & 1 & 0 \\ \cos\theta & 0 & \sin\theta \end{pmatrix} \tag{2.42}$$

$$\delta P'' = R_\theta \, \delta P' \, R_\theta^{-1} \tag{2.43}$$

All orientations of x_1 have been accounted for, but x_2 and x_3 must still be rotated,

$$R_\psi = \begin{pmatrix} 1 & 0 & 0 \\ 0 & \cos\psi & \sin\psi \\ 0 & -\sin\psi & \cos\psi \end{pmatrix} \tag{2.44}$$

$$R_\psi^{-1} = R_{-\psi} \tag{2.45}$$

$$\delta P''' = R_\psi \, \delta P'' \, R_\psi^{-1} \tag{2.46}$$

As the sample of Weissman et al. constrains the current along two of the three dimensions, one may attempt to reproduce their results using $\langle(\delta\rho_{11}''')^2\rangle_{t,\phi,\theta,\psi}$ and $\langle(\delta\rho_{12}''')^2\rangle_{t,\phi,\theta,\psi}$ as reference quantities, where $\langle x\rangle_{t,\phi,\theta,\psi}$ denote averaging over time and all orientations. Other second order quantities will be linear combinations of these. As they assume that the sample is isotropic on time average, the following relations, which simplify the above quantities, are expected to hold:

$$\langle\delta\rho_{11}^2\rangle_t = \langle\delta\rho_{22}^2\rangle_t = \langle\delta\rho_{33}^2\rangle_t \tag{2.47}$$

$$\langle\delta\rho_{11}\delta\rho_{22}\rangle_t = \langle\delta\rho_{11}\delta\rho_{33}\rangle_t = \langle\delta\rho_{33}\delta\rho_{22}\rangle_t \tag{2.48}$$

$$\langle\delta\rho_{12}\delta\rho_{21}\rangle_t = \langle\delta\rho_{13}\delta\rho_{31}\rangle_t = \langle\delta\rho_{32}\delta\rho_{23}\rangle_t \tag{2.49}$$

$$\langle\delta\rho_{12}^2\rangle_t = \langle\delta\rho_{13}^2\rangle_t = \langle\delta\rho_{21}^2\rangle_t = \langle\delta\rho_{23}^2\rangle_t = \langle\delta\rho_{31}^2\rangle_t = \langle\delta\rho_{32}^2\rangle_t \tag{2.50}$$

Using the above identities, one finds that

$$\langle\delta(\rho_{11}''')^2\rangle_{t,\phi,\theta,\psi} = 0.2(3\langle\delta\rho_{11}^2\rangle_t + 2\langle\delta\rho_{11}\delta\rho_{22}\rangle_t + 2\langle\delta\rho_{12}^2\rangle_t + 2\langle\delta\rho_{12}\delta\rho_{21}\rangle_t) \tag{2.51}$$

$$\langle\delta(\rho_{12}''')^2\rangle_{t,\phi,\theta,\psi} = 0.2(\langle\delta\rho_{11}^2\rangle_t - \langle\delta\rho_{11}\delta\rho_{22}\rangle_t + 4\langle\delta\rho_{12}^2\rangle_t - \langle\delta\rho_{12}\delta\rho_{21}\rangle_t) \tag{2.52}$$

Next, Weissman et al. define their resistivity tensor fluctuation parameter as

$$S = \frac{2\langle \det\{\delta P\}\rangle_t}{\langle \mathrm{Sp}\{(\delta P)^2\}\rangle_t} \tag{2.53}$$

They give their rotation averaging result equations 8a-c respectively as

$$\text{(8a)} \quad \langle \delta\rho_{11}^2\rangle_t = \gamma(S+3)/4 \tag{2.54}$$

$$\text{(8b)} \quad \langle \delta\rho_{11}\delta\rho_{22}\rangle_t = \gamma(1+3S)/4 \tag{2.55}$$

$$\text{(8c)} \quad \langle \delta\rho_{12}^2\rangle_t = \gamma(1-S)/4 \tag{2.56}$$

$$\text{(8d)} \quad \langle \delta\rho_{11}\delta\rho_{12}\rangle_t = 0 \tag{2.57}$$

Substitution of their equations 8a-c into equation 2.53 for a 2x2 tensor suggests that they used a 2x2 tensor to define S, with the assumption that

$$\langle \delta\rho_{12}^2\rangle_t = \langle \delta\rho_{12}\delta\rho_{21}\rangle_t \tag{2.58}$$

as a 3x3 tensor would have terms like $\langle \delta\rho_{11}^2\rangle_t$ in the denominator, and terms like $\langle \delta\rho_{11}\delta\rho_{22}\delta\rho_{33}\rangle_t$ in the numerator. For a 2x2 resistivity fluctuation tensor,

$$S = \frac{\langle \delta\rho_{11}\delta\rho_{22}\rangle_t - \langle \delta\rho_{12}\delta\rho_{21}\rangle_t}{\langle \delta\rho_{11}^2\rangle_t + \langle \delta\rho_{12}\delta\rho_{21}\rangle_t} \tag{2.59}$$

One may rotate the 2D resistivity tensor in the plane,

$$R_\phi = \begin{pmatrix} \cos\phi & \sin\phi \\ -\sin\phi & \cos\phi \end{pmatrix} \tag{2.60}$$

$$R_\phi^{-1} = R_{-\phi} \tag{2.61}$$

$$\delta P' = R_\phi \, \delta P \, R_\phi^{-1} \tag{2.62}$$

$$\forall\phi[S(\delta P') = S(\delta P)] \tag{2.63}$$

The last result, namely that S_{2x2} is insensitive to rotation, makes S a generally descriptive parameter of the resistivity fluctuation tensor. One may rewrite the S-relationship as

$$S\langle \delta\rho_{11}^2\rangle_t + (S+1)\langle \delta\rho_{12}\delta\rho_{21}\rangle_t - \langle \delta\rho_{11}\delta\rho_{22}\rangle_t = 0 \tag{2.64}$$

One might wonder whether their calculations are based on a 2x2 tensor; a simple check may suffice: one takes the dependence of $\langle(\delta\rho'_{11})^2\rangle_{t,\phi}$ and $\langle(\delta\rho'_{12})^2\rangle_{t,\phi}$, or any other

such pair, on $\langle \delta\rho_{11}^2 \rangle_t$, $\langle \delta\rho_{11}\delta\rho_{22} \rangle_t$ and $\langle \delta\rho_{12}\delta\rho_{21} \rangle_t$, and combine the resulting equations with the S-relationship in equation 2.64; they are invariably underdetermined. Hence one may conclude that Weissman et al. used 3D rotations in combination with the 2D S-relationship.

Using equations 2.51 and 2.52 with the S-relationship, one may solve for $\langle \delta\rho_{11}^2 \rangle_t$, $\langle \delta\rho_{11}\delta\rho_{22} \rangle_t$ and $\langle \delta\rho_{12}\delta\rho_{21} \rangle_t$ in terms of $\langle (\delta\rho_{11}''')^2 \rangle_{t,\phi,\theta,\psi}$ and $\langle (\delta\rho_{12}''')^2 \rangle_{t,\phi,\theta,\psi}$. Substituting equations 8a-c of Weissman et alinto equations 2.51 and 2.52, one may solve for their parameter γ in each case. One obtains different results for γ for each pair of the three equations used. Solving any pair of the three resulting equations, with substitution of their equations 8a–c as necessary, yields $S = 1$, namely the scalar fluctuation case, though with $S = 0$ (dyadic - see below) or $S = -1$ (traceless) as possible alternate solutions. $S = 0$ might be a special case, as the resulting equations involve division by S.

Their equation 8d cannot be justified at all—nothing in the rotation results depends on terms like $\langle \delta\rho_{11}\delta\rho_{12} \rangle_t$! As such, nothing can be said about them on the basis of the rotation averages. A further problem with their work is that only 'dyadic' tensors, namely those that are proporsional to $\hat{k}\hat{k}^T$ [83], where $\hat{k}$ is a random direction, can have $S = 0$. If another type of fluctuator exists that also has $S = 0$, then one cannot derive general equations such as their equations 8a-c. One also suspects that similarly linear relationships of $\langle \delta\rho_{11}^2 \rangle_t$ et cetera in S, could be used to make $S = -1$ a general solution, to find the traceless fluctuators which were not found - the closest found was an apparent S of -0.48 [84]. It is not at all clear why $\langle \delta\rho_{11}^2 \rangle_t$ et cetera should be related to each other by the ratios of polynomials that are order one in S.

Weissman's insight as to the tensor nature of the fluctuations might be fruitfully adapted to future research, but his equations seem problematic.

2.4 Conclusion

Several materials and devices add 1/f noise to a practical detector setup. The science of the dependence of their 1/f noise levels S_0 and exponents α has been discussed in this chapter, and sufficient references have been given for the interested reader to initiate further study. In the next chapter, I derive relationships for the variance from $1/f$ noise

that is contributed to a detected quantity in a practical detector circuit. The results in chapter 3 depend on S_0 and α; they are assumed to be largely independent of frequency, over a sufficient range of frequencies.

Chapter 3

Noise Analysis of Imaging Detectors and Sample Sequences

This chapter contains the main results of my research. I determine a formula for the variance that is added to a typical x-ray image by $1/f$ noise and white noise, considering that the integrated dark current of a detector element (see chapter 1) is subtracted from the integrated photocurrent of said detector element. This subtraction of integrations is equivalent to a band-pass filter, which limits the noise variance contribution. The mathematical description that I use to calculate the noise variance contribution to the detected radiation, namely a bandpass filter, is insensitive to whether the dark-current integration precedes or follows the photocurrent integration, although in a practical detector, there will be different outcomes in the two scenarios, due to e.g. trapping of carriers and structural changes in the semiconductor element due to the exposure to x-ray radiation. Next I calculate the variance that white and $1/f$ noise contribute to sample sequences. These calculations of the contributed variance of the noise depend on the filtration of noise; I first show an outline of a derivation of the power-spectral density of a noise signal that is produced by filtering second-order stationary noise with a linear time-invariant filter. This is needed to calculate the above noise variance contributions.

3.1 Noise Filtration

A noise signal $x(t)$, with power-spectral density (PSD) $S_x(\omega)$, is filtered with a linear time-invariant filter of finite length, that has an impulse response $h(t)$, to produce $y(t)$ i.e.

$$y(t) = x(t) * h(t) \tag{3.1}$$

where '$*$' is the convolution operator. If the filter impulse response $h(t)$ is non-zero only within the window $\tau_{min} < t < \tau_{max}$, one may show, along the lines that I use below, that

$$S_y(\omega) = S_x(\omega) \cdot |H(\omega)|^2 \tag{3.2}$$

where $H(\omega)$ is the Fourier transform of the impulse response $h(t)$.

The Wiener-Khintchine theorem, introduced in chapter 1, states that the PSD is the Fourier transform of the autocovariance function,

$$S_y(\omega) = \int_{-\infty}^{\infty} \Phi_y(\tau^*) e^{-j\omega\tau^*} \, d\tau^* \tag{3.3}$$

When the autocorrelation function $R_y(\tau^*)$ of a wide-sense stationary (WSS, introduced in chapter 1) noise signal is measured over a sufficient period, it becomes equal to the autocovariance function $\Phi_y(\tau^*)$; it is then called 'ergodic'.

If one measures y(t) over a finite period, e.g. from T_1 to T_2, one may calculate a 'measured' PSD from the resulting autocorrelation function; the integral should be symmetric, to avoid an imaginary component in the PSD. Moreover, the Fourier transform should not exhaust the available measurement, i.e. the range of τ^* should remain a fraction of the data range of $y(t)$, to avoid a potentially unrepresentative autocovariance at the extremes of the integral. Let

$$S_y^{meas}(\omega) = \int_{(T_1-T_2)/M}^{(T_2-T_1)/M} R_y(\tau^*) e^{-j\omega\tau^*} \, d\tau^* \tag{3.4}$$

where M is a natural number.

For a given frequency ω, at which one seeks to measure $S_y(\omega)$, one needs

$$\omega(T_2 - T_1) \gg 2\pi M \tag{3.5}$$

to obtain an ergodic measurement of $S_y(\omega)$, i.e. the measurement period should be several multiples of the inverse frequency. To minimize spurious pickup of nearby spectral content, $\omega(T_2 - T_1)/(2\pi)$ should be an integer. One may partition the autocorrelation function into component functions that are limited each to narrow frequency bands, for the purpose of calculating the PSD, as the autocovariance function of ideal $1/f$ noise is infinite over an infinite range. As one measures the autocorrelation function over a longer period, lower-frequency components add more variance, because the measurement period becomes more than the period of a given component, whereas over a shorter period, a

lower frequency component merely contributes an apparent mean to the noise signal. To measure a spectrally limited component of the autocorrelation function ergodically, one may measure for a shorter time,

$$t_{meas} \sim 2\pi N/\omega \tag{3.6}$$

than one might for the entire autocorrelation function. The PSD may then be written in terms of a partial autocorrelation function in equation 3.4. The autocorrelation function is measured roughly from T_1 to T_2, i.e.

$$R_y^{meas}(\tau) = \int_{T_1-\tau/2}^{T_2-\tau/2} \frac{y(t^*) \cdot y(t^*+\tau^*)}{T_2 - T_1}\, dt^* \tag{3.7}$$

The limits are chosen to ensure that the autocorrelation function is even, i.e.

$$R_y(\tau^*) = R_y(-\tau^*) \tag{3.8}$$

This condition guarantees that any PSD calculated on the basis of a measured $R_y(\tau)$ will have a zero imaginary component. It is also structured to avoid having τ^* in the denominator, which could make constant limits in the integral possible, while making free changing of integration order problematic. Proving the filtration relationship, equation 3.2, using the autocorrelation function in equation 3.7, is beyond the scope of this thesis — only an outline is presented here. For that reason, a simplified autocorrelation function is used, namely

$$R_y(\tau) = \int_{T_1}^{T_2} \frac{y(t) \cdot y(t+\tau)}{T_2 - T_1}\, dt \tag{3.9}$$

Substituting, we find

$$S_y^{meas}(\omega) = \int_{(T_1-T_2)/M}^{(T_2-T_1)/M} e^{-j\omega\tau^*} \int_{T_1}^{T_2} \frac{y(t^*) \cdot y(t^*+\tau^*)}{T_2 - T_1}\, dt^*\, d\tau^* \tag{3.10}$$

The filtered noise signal $y(t)$ is related to the input noise signal $x(t)$ by the convolution integral,

$$y(t) = \int_{-\infty}^{\infty} x(\tau') \cdot h(t-\tau')\, d\tau' \tag{3.11}$$

Earlier, I stated that $h(t)$ is non-zero only from τ_{min} to τ_{max} — this allows a simplification of the convolution integral to

$$y(t) = \int_{\tau_{min}+t}^{\tau_{max}+t} x(\tau') \cdot h(t-\tau')\, d\tau' \tag{3.12}$$

My purpose here is to show an outline of a proof for equation 3.2, and as such, I simplify the convolution further, to ease reversals of orders of integration, to

$$y(t) = \int_{T_1}^{T_2} x(\tau') \cdot h(t - \tau')\, d\tau' \tag{3.13}$$

Then one may write the PSD as

$$\begin{aligned} S_y^{meas}(\omega) = \int_{(T_1-T_2)/M}^{(T_2-T_1)/M} e^{-j\omega\tau^*} \int_{T_1}^{T_2} \frac{1}{T_2 - T_1} \left[\int_{T_1}^{T_2} x(\tau') \cdot h(t^* - \tau')\, d\tau'\right] \cdot \\ \left[\int_{T_1}^{T_2} x(\tau'') \cdot h(t^* + \tau^* - \tau'')\, d\tau''\right] dt^*\, d\tau^* \end{aligned} \tag{3.14}$$

Next, one must substitute $\tau = -\tau^*$, to get

$$\begin{aligned} S_y^{meas}(\omega) = \int_{(T_1-T_2)/M}^{(T_2-T_1)/M} e^{j\omega\tau} \int_{T_1}^{T_2} \frac{1}{T_2 - T_1} \left[\int_{T_1}^{T_2} x(\tau') \cdot h(t^* - \tau')\, d\tau'\right] \cdot \\ \left[\int_{T_1}^{T_2} x(\tau'') \cdot h(t^* - \tau - \tau'')\, d\tau''\right] dt^*\, d\tau \end{aligned} \tag{3.15}$$

Then one must substitute $t = t^* - \tau$, to get

$$\begin{aligned} S_y^{meas}(\omega) = \int_{(T_1-T_2)/M}^{(T_2-T_1)/M} e^{j\omega\tau} \int_{T_1-\tau}^{T_2-\tau} \frac{1}{T_2 - T_1} \left[\int_{T_1}^{T_2} x(\tau') \cdot h(t + \tau - \tau')\, d\tau'\right] \cdot \\ \left[\int_{T_1}^{T_2} x(\tau'') \cdot h(t - \tau'')\, d\tau''\right] dt\, d\tau \end{aligned} \tag{3.16}$$

As the purpose here is to show an outline of a proof, and as that proof involves multiple rearrangements of integrals, I neglect the $-\tau$ in the integral over t, i.e.

$$\begin{aligned} S_y^{meas}(\omega) = \int_{(T_1-T_2)/M}^{(T_2-T_1)/M} e^{j\omega\tau} \int_{T_1}^{T_2} \frac{1}{T_2 - T_1} \left[\int_{T_1}^{T_2} x(\tau') \cdot h(t + \tau - \tau')\, d\tau'\right] \cdot \\ \left[\int_{T_1}^{T_2} x(\tau'') \cdot h(t - \tau'')\, d\tau''\right] dt\, d\tau \end{aligned} \tag{3.17}$$

Rearranging equation 3.17 multiple times yields

$$S_y^{meas}(\omega) = \int_{T_1}^{T_2} \int_{T_1}^{T_2} \int_{T_1}^{T_2} \frac{x(\tau') \cdot x(\tau'') \cdot h(t - \tau'')}{T_2 - T_1} \int_{(T_1-T_2)/M}^{(T_2-T_1)/M} e^{j\omega\tau} h(t + \tau - \tau')\, d\tau\, d\tau''\, d\tau'\, dt \tag{3.18}$$

Substituting $\tau_\alpha = \tau + t - \tau'$, where $d\tau_\alpha = d\tau$, one obtains

$$\begin{aligned} S_y^{meas}(\omega) = \int_{T_1}^{T_2} \int_{T_1}^{T_2} \int_{T_1}^{T_2} \frac{x(\tau') \cdot x(\tau'') \cdot h(t - \tau'')}{T_2 - T_1} \int_{(T_1-T_2)/M+t-\tau'}^{(T_2-T_1)/M+t-\tau'} e^{j\omega\tau_\alpha} h(\tau_\alpha)\, d\tau_\alpha \cdot \\ e^{j\omega(\tau'-t)}\, d\tau''\, d\tau'\, dt \end{aligned} \tag{3.19}$$

To simplify this equation, one may treat the inner integral as simply $H^*(\omega)$, that is, as the conjugate transfer function of the filter,

$$S_y^{meas}(\omega) = \int_{T_1}^{T_2}\int_{T_1}^{T_2}\int_{T_1}^{T_2} \frac{x(\tau')\cdot x(\tau'')\cdot h(t-\tau'')}{T_2-T_1} H^*(\omega) e^{j\omega(\tau'-t)}\, d\tau''\, d\tau'\, dt \tag{3.20}$$

if one specifies τ_{min} and τ_{max} of the filter as being within the limits of the inner integral generally. In a rigorous derivation, I expect that fragments of the autocorrelation integral will be integrated over portions of the impulse response, summing to an equivalent transfer function-autocorrelation product. Substituting $\tau_\beta = \tau'' - \tau'$, where $d\tau_\beta = d\tau''$, one obtains

$$S_y^{meas}(\omega) = \int_{T_1}^{T_2}\int_{T_1}^{T_2}\int_{T_1-\tau'}^{T_2-\tau'} \frac{x(\tau')\cdot x(\tau_\beta+\tau')\cdot h(t-\tau'-\tau_\beta)}{T_2-T_1} H^*(\omega) e^{j\omega(\tau'-t)}\, d\tau_\beta\, d\tau'\, dt \tag{3.21}$$

Rearranging, one finds

$$S_y^{meas}(\omega) = \int_{T_1}^{T_2}\int_{T_1-\tau'}^{T_2-\tau'} \frac{x(\tau')\cdot x(\tau_\beta+\tau')}{T_2-T_1} \int_{T_1}^{T_2} h(t-\tau'-\tau_\beta) e^{j\omega(\tau'-t)}\, dt H^*(\omega)\, d\tau_\beta\, d\tau' \tag{3.22}$$

Substituting $t' = t - \tau_\beta - \tau'$, where $dt' = dt$, one obtains

$$S_y^{meas}(\omega) = \int_{T_1}^{T_2}\int_{T_1-\tau'}^{T_2-\tau'} \frac{x(\tau')\cdot x(\tau_\beta+\tau')}{T_2-T_1} \int_{T_1-\tau_\beta-\tau'}^{T_2-\tau_\beta-\tau'} h(t') e^{-j\omega(t'+\tau_\beta)}\, dt' H^*(\omega)\, d\tau_\beta\, d\tau' \tag{3.23}$$

To simplify this equation, one may treat the inner integral as simply $H(\omega)$, i.e. as the transfer function of the filter, to obtain

$$S_y^{meas}(\omega) = \int_{T_1}^{T_2}\int_{T_1-\tau'}^{T_2-\tau'} \frac{x(\tau')\cdot x(\tau_\beta+\tau')}{T_2-T_1} H(\omega)H^*(\omega) e^{-j\omega\tau_\beta}\, d\tau_\beta\, d\tau' \tag{3.24}$$

where $H(\omega)H^*(\omega) = |H(\omega)|^2$. Rearranging, one finds

$$\begin{aligned} S_y^{meas}(\omega) = &\int_{T_1-T_2}^{0}\int_{T_1-\tau_\beta}^{T_2} \frac{x(\tau')\cdot x(\tau_\beta+\tau')}{T_2-T_1} |H(\omega)|^2 e^{-j\omega\tau_\beta}\, d\tau'\, d\tau_\beta \\ &+ \int_{0}^{T_2-T_1}\int_{T_1}^{T_2-\tau_\beta} \frac{x(\tau')\cdot x(\tau_\beta+\tau')}{T_2-T_1} |H(\omega)|^2 e^{-j\omega\tau_\beta}\, d\tau'\, d\tau_\beta \end{aligned} \tag{3.25}$$

One may simplify the inner integrals to obtain

$$\begin{aligned} S_y^{meas}(\omega) = &\int_{T_1-T_2}^{0} \frac{T_2-T_1+\tau_\beta}{T_2-T_1} R_x(\tau_\beta) |H(\omega)|^2 e^{-j\omega\tau_\beta}\, d\tau_\beta \\ &+ \int_{0}^{T_2-T_1} \frac{T_2-T_1-\tau_\beta}{T_2-T_1} R_x(\tau_\beta) |H(\omega)|^2 e^{-j\omega\tau_\beta}\, d\tau_\beta \end{aligned} \tag{3.26}$$

as the inner integrals in equation 3.25 are longer and shorter than $T_2 - T_1$, respectively. One may simplify further to obtain

$$\begin{aligned} S_y(\omega) = &\int_{T_1-T_2}^{T_2-T_1} R_x(\tau_\beta) e^{-j\omega\tau_\beta} \left|H(\omega)\right|^2 \, d\tau_\beta \\ &+ \int_{T_1-T_2}^{0} \frac{\tau_\beta}{T_2 - T_1} R_x(\tau_\beta) e^{-j\omega\tau_\beta} \left|H(\omega)\right|^2 \, d\tau_\beta \\ &- \int_{0}^{T_2-T_1} \frac{\tau_\beta}{T_2 - T_1} R_x(\tau_\beta) e^{-j\omega\tau_\beta} \left|H(\omega)\right|^2 \, d\tau_\beta \end{aligned} \tag{3.27}$$

The first integral simplifies to $S_x(\omega)\left|H(\omega)\right|^2$, and using the even property of the autocorrelation function, one finds

$$S_y(\omega) = S_x(\omega)\left|H(\omega)\right|^2 - \int_0^{T_2-T_1} \frac{2\tau_\beta \cdot R_x(\tau_\beta)}{T_2 - T_1} cos(\omega\tau_\beta) \left|H(\omega)\right|^2 \, d\tau_\beta \tag{3.28}$$

For white noise, the integral in equation 3.28 is zero, as the autocorrelation function is a constant-scaled Dirac delta function. For $1/f$ noise, at the lower frequencies, we have an $x \ln x$ dependence multiplied by a slow-changing cosine, which may render the integral modest; at the frequency of interest, one might expect the integral to grow with observation i.e. as $T_2 - T_1$; this does not seem to be the case, based on the experiments reported in chapter 4, and the integral may be an artifact of the rather imprecise derivation above. In the remainder of this chapter, equation 3.2 is used unmodified.

3.2 Transfer Functions and Variances

X-ray detectors' operation involves a photo-current measurement, which is preceded or followed by a dark-current measurement that is used as a reference; this procedure is repeated for each image taken. Several configurations of the detector are possible: 1. an integration of the dark-current, taken before or after an integration of the photo-current, may be subtracted from the integration of the photo-current; 2. an average of the integrations of the dark-current before and after the integration of the photo-current may be subtracted from the photo-current integration; 3. where the currents are averaged rather than integrated, an average of the dark-current may be subtracted from the photo-current average, though the averaging period of the photo-current may be different from the averaging period of the dark current.

I generate transfer functions in the following sections, to represent the above configurations of the detector, to develop a formula for the variance contribution of noise to the x-ray detector under the different configurations. The operation of these filters is that if equation 3.1 holds then $y(t_0)$ is the signal collected by the system after the subtraction of the integrated dark current, at time t_0. The ensemble variance that the noise contributes is

$$var = \frac{2}{2\pi} \int_0^\infty S(\omega) \ |H(\omega)|^2 \ d\omega \tag{3.29}$$

This variance may be measured by repeatedly measuring the unexposed reading of a detector, and taking the variance of the readings. The transfer functions $H(\omega)$ used in the following subsection is essentially the Correlated Double Sampling (CDS) transfer function of [54, 55, 56, 57, 58, 59].

3.2.1 Simple dark-current subtraction

The operation of a CDS-based detector is to subtract a 'dark' reading from an 'exposure' reading. Stated differently, a background reading is subtracted from the measurement. This is illustrated in figure 3.1. The dark current integral (on the left) in the figure is subtracted from the exposure current integral (on the right). In the sequence graphed, no photocurrent is apparent. The integrals have length T, and are separated, middle-to-middle by ΔT.

I represent the subtraction of the integrals by a frequency-domain transfer function, $H_{sub\,and\,int}$, which I construct from two integrators separated in time. A single integration over time T is given by the transfer function,

$$H_{int}(\omega) = T\text{sinc}(\omega T/2) \tag{3.30}$$

which is a low-pass filter. The transfer function for subtraction of values separated by ΔT is

$$H_{sub}(\omega) = 1 - e^{j\omega\Delta T} \tag{3.31}$$

which is a high-pass filter. The total transfer function for the subtraction of a delayed integration from another integration is thus

$$H_{sub\,and\,int}(\omega) = T\text{sinc}(\omega T/2) - e^{-j\omega\Delta T} T\text{sinc}(\omega T/2) \tag{3.32}$$

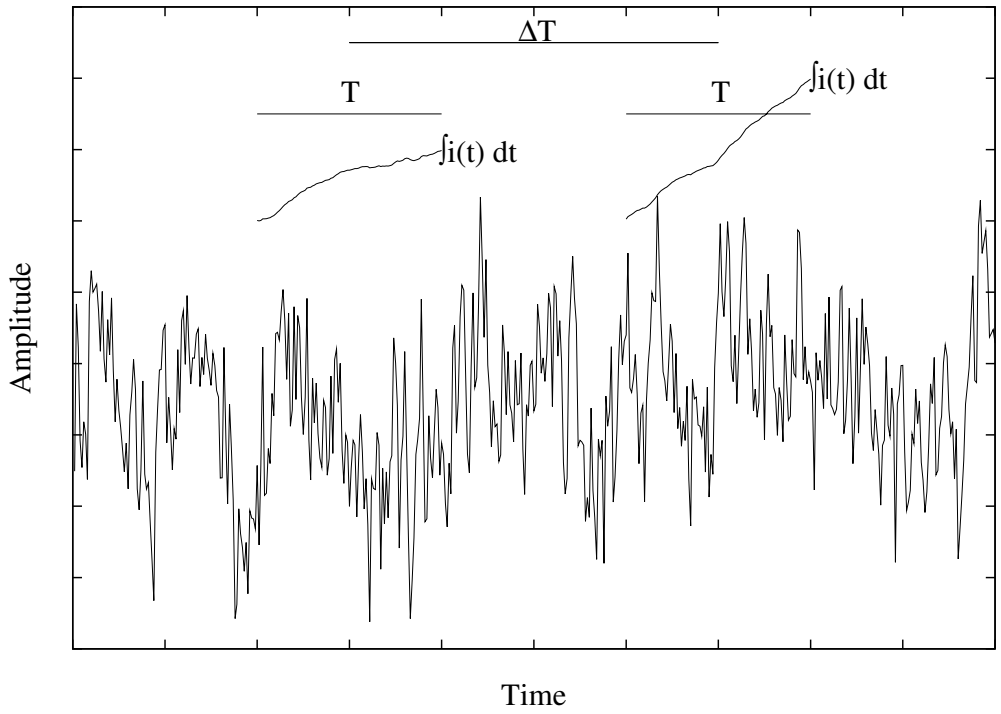

Figure 3.1: An example of $1/f$ noise versus time and correlated double sampling. Above, the bars indicate the integration time T and the integral separation ΔT. Lines marked with $\int i(t)\,dt$ are the cumulative integrals over the periods marked T, which are then subtracted; left axis not shown.

which is a band-pass filter. Notice that the above transfer function is not causal; with noise, causality does not impact the PSD in principle. The variance added to a pixel reading is

$$var = \frac{2}{2\pi}\int_0^\infty S(\omega)|H_{\text{sub and int}}(\omega)|^2\,d\omega \tag{3.33}$$

where the two in the numerator corrects the integral for a two-sided spectrum, which would otherwise go from $-\infty \rightarrow \infty$, and the 2π normalizes the angular frequency.

For subtraction of the dark current integration before or after the exposure integration, the variance for a $1/f^\alpha$ noise input with $\alpha = 1$ is

$$var \simeq 4S_0T^2\left[\zeta^2 \ln\frac{\sqrt{|\zeta^2-1|}}{\zeta} + \ln\sqrt{|\zeta^2-1|} + \zeta\ln\frac{\zeta+1}{|\zeta-1|}\right] \tag{3.34}$$

where $\zeta = \Delta T/T$, and S_0 is the factor that produces the PSD in

$$S(f) = \frac{S_0}{f^\alpha} \tag{3.35}$$

The more general expression of the variance for $\alpha \neq 1$ is

$$var = 8S_0(2\pi)^{\alpha-1}\Gamma(-\alpha-1)\sin\frac{\alpha\pi}{2}T^{\alpha+1}\left(1+\zeta^{\alpha+1}-\frac{|\zeta-1|^{\alpha+1}}{2}-\frac{(\zeta+1)^{\alpha+1}}{2}\right) \quad (3.36)$$

and for white noise, one obtains

$$var = 2S_W T \quad (3.37)$$

where S_W is the white PSD and $\Delta T \geq T$, i.e. that the dark-current and photo-current integrals do not overlap, which cannot happen in a real system.

Practical detectors suffer both $1/f$ and white noise; to see which noise type is more significant in a given detector, equations 3.34 or 3.36 must be compared to equation 3.37. I consider two cases, namely when the dark current integration is immediately followed by the exposure current integration, i.e. when $\zeta = 1$, and when the integrations are well separated, i.e. $\zeta \gg 1$. In the limit that ζ tends to 1, the variance in equation 3.34 becomes

$$var = 8S_0T^2\ln 2 \quad (3.38)$$

$1/f$ noise dominates a detector's SNR if

$$4S_0T\ln 2 > S_w \quad (3.39)$$

The SNR of a detector dominated by $1/f$ noise scales as

$$SNR \propto \frac{1}{8S_0\ln 2} \quad (3.40)$$

Notice that the $1/f$ noise SNR does not improve with longer integration time; increasing the integration time is a standard method used by engineers to improve SNR and fails for $1/f$ noise. If the integrations are well separated, the variance in equation 3.34 is approximately

$$var \simeq 4S_0T^2\ln(\Delta T/T) \quad (3.41)$$

If the integrations are well separated, $1/f$ noise dominates the detector when

$$2S_0T\ln(\Delta T/T) > S_w \quad (3.42)$$

The SNR of a detector dominated by $1/f$ noise weakens with the logarithm of the separation of the integrations,

$$SNR \propto \frac{1}{4S_0\ln(\Delta T/T)} \quad (3.43)$$

3.2.2 Double measurement of dark current

One may use the average of the dark current integrations prior to and after the photocurrent integration to correct, or subtract from, the photocurrent integration in a practical detector. When this is done, the resulting subtraction is represented by

$$H_{\text{sub}}(\omega) = 1 - e^{j\omega\Delta T} - e^{-j\omega\Delta T} \tag{3.44}$$

The variance is again calculated through equation 3.33. In this scenario, $1/f^{\alpha}$ noise with $\alpha = 1$ contributes a variance of

$$var = \frac{S_0 T^2}{2}\left[4\zeta \ln\frac{(\zeta+1)^2\cdot(2\zeta-1)}{(\zeta-1)^2\cdot(2\zeta+1)} + 4\zeta^2 \ln\left(4\frac{|\zeta^2-1|}{|4\zeta^2-1|}\right) + \ln\frac{|\zeta^2-1|^4}{|4\zeta^2-1|}\right] \tag{3.45}$$

where $\zeta = \Delta T/T$ as before. In the more general case where $\alpha \neq 1$, the $1/f$ noise contributes a variance of

$$\begin{aligned} var = (2\pi)^{\alpha-1} S_0 \sin\frac{\pi\alpha}{2}\Gamma(-\alpha-1)T^{\alpha+1}\left[8\zeta^{\alpha+1} - 2^{\alpha+2}\zeta^{\alpha+1} + 6\right. \\ \left. -4|\zeta-1|^{\alpha+1} - 4(\zeta+1)^{\alpha+1} + |2\zeta-1|^{\alpha+1} + (2\zeta+1)^{\alpha+1}\right] \end{aligned} \tag{3.46}$$

White noise contributes

$$var = 1.5 S_W T \tag{3.47}$$

If the integrals are unseparated, $\alpha = 1$ $1/f$ noise contributes

$$var = \frac{S_0 T^2}{2}\ln\frac{2^{24}}{3^9} \tag{3.48}$$

$1/f$ noise dominates when

$$3 S_0 T \ln\frac{2^{24}}{3^9} > S_w \tag{3.49}$$

in which case the SNR of the measured signal is proportional to

$$\frac{2}{S_0 \ln\frac{2^{24}}{3^9}} \tag{3.50}$$

Increasing the integration time again does not improve the SNR if $1/f$ noise is dominant. If the integrals are well separated, i.e. $\zeta \gg 1$,

$$var \simeq S_0 T^2\left(3\ln\frac{\Delta T}{T} - \ln 2\right) \tag{3.51}$$

$1/f$ noise dominates when

$$\frac{2}{3}S_0T\left(3\ln\frac{\Delta T}{T}-\ln 2\right)>S_w \tag{3.52}$$

in which case the SNR of the measured signal is proportional to

$$SNR\propto\frac{1}{S_0\left(3\ln\frac{\Delta T}{T}-\ln 2\right)} \tag{3.53}$$

3.2.3 Unequal subtractions

If one uses averages instead of integrals in the subtraction then one may use different averaging times for the dark and photo-current averages. Let the averaging times be T and γT where γ is simply a scaling factor, then the transfer function for averaging followed by subtraction is

$$H_{\text{sub and avg}}=\text{sinc}(\omega T)-e^{j\omega\Delta T}\text{sinc}(\omega\gamma T) \tag{3.54}$$

where ΔT is the time between the centers of the averaging periods. Notice that the effects of subtraction and of averaging are no longer separable. The variances obtained are, for $1/f^\alpha$ noise with $\alpha=1$,

$$\begin{aligned}var=&S_0\left[2\ln\frac{\sqrt{|4\zeta^2-(1+\gamma)^2|}}{2}\cdot\frac{\sqrt{|4\zeta^2-(1-\gamma)^2|}}{2\gamma}+2\zeta\ln\left|\frac{(2\zeta+1)^2-\gamma^2}{(2\zeta-1)^2-\gamma^2}\right|\right.\\&\left.+\frac{1}{2\gamma}\left[4\zeta^2+1+\gamma^2\right]\ln\left|\frac{4\zeta^2-(1+\gamma)^2}{4\zeta-(1-\gamma)^2}\right|+2\frac{\zeta}{\gamma}\ln\left|\frac{(2\zeta+\gamma)^2-1}{(2\zeta-\gamma)^2-1}\right|\right]\end{aligned} \tag{3.55}$$

For the more general case of $\alpha\neq 1$, the variance contributed is

$$\begin{aligned}var=&2S_0(2\pi T)^{\alpha-1}\Gamma(-1-\alpha)\sin\frac{\pi\alpha}{2}\left(2+2\gamma^{\alpha-1}+2^{-\alpha}\gamma^{-1}\cdot\left[|2\zeta-\gamma+1|^{\alpha+1}\right.\right.\\&\left.\left.+|2\zeta+\gamma-1|^{\alpha+1}-(2\zeta+\gamma+1)^{\alpha+1}-|2\zeta-\gamma-1|^{\alpha+1}\right]\right)\end{aligned} \tag{3.56}$$

The SNR scales as the inverse of the variance, and in both equations 3.55 and 3.56 the dependence on the averaging periods is weak.

3.3 Sample Sequences

As with x-ray detectors, sampling systems are affected by noise and the contribution to the variance from $1/f$ noise may become a concern. I calculate the $1/f$ noise variance contribution next.

3.3.1 N Samples

I next calculate the variance that $1/f$ noise adds to a sample sequence, where the noise might be internal to the sampler—a distraction from the signal, or actual noise being sampled for the purpose of studying the noise. This sampling of noise is illustrated in figure 3.2, and the variance is that of the N samples. The noise is sampled by way of each integration. Each integral has length T and is separated from the next integral by ΔT. The sample is generated by a potentially weighted averaging,

$$x_n = \frac{1}{T}\int_{n\Delta T - T/2}^{n\Delta T + T/2} x(t')w(n\Delta T - t')\,dt' \tag{3.57}$$

where $w(t)$ is the weighting function. A transfer function H_{avg} is determined by a scaled Fourier transform of the weighting function,

$$H_{\text{avg}}(\omega) = \frac{1}{T}\int_{T/2}^{T/2} w(t)e^{-j\omega t}\,dt \tag{3.58}$$

Once H_{avg} is known, the various samples x_n are generated by shifts of H_{avg}.

$$H_x(n;\omega) = e^{j\omega n\Delta T}H_{\text{avg}}(\omega) \tag{3.59}$$

In order to calculate the variance of the N samples that define the sample sequence, their average is needed. The averaging may also be represented as a transfer function, which contains the sum of the transfer functions for each of the samples.

$$H_{\overline{x}}(\omega) = H_{\text{avg}}(\omega)\frac{1}{N}\sum_{n=1}^{N} e^{j\omega n\Delta T} \tag{3.60}$$

Note that there are now two averages at issue: firstly, the integral averaging that produces a sample, and secondly, the summation averaging of the separate samples.

The noise variance of the sample sequence may be calculated as

$$var = \frac{1}{N}\sum_{n=1}^{N}(x_n - \overline{x})^2 \tag{3.61}$$

However, the quantity of interest is the ensemble expectation of the noise variance,

$$\overline{var} = E\left\{\frac{1}{N}\sum_{n=1}^{N}(x_n - \overline{x})^2\right\} \tag{3.62}$$

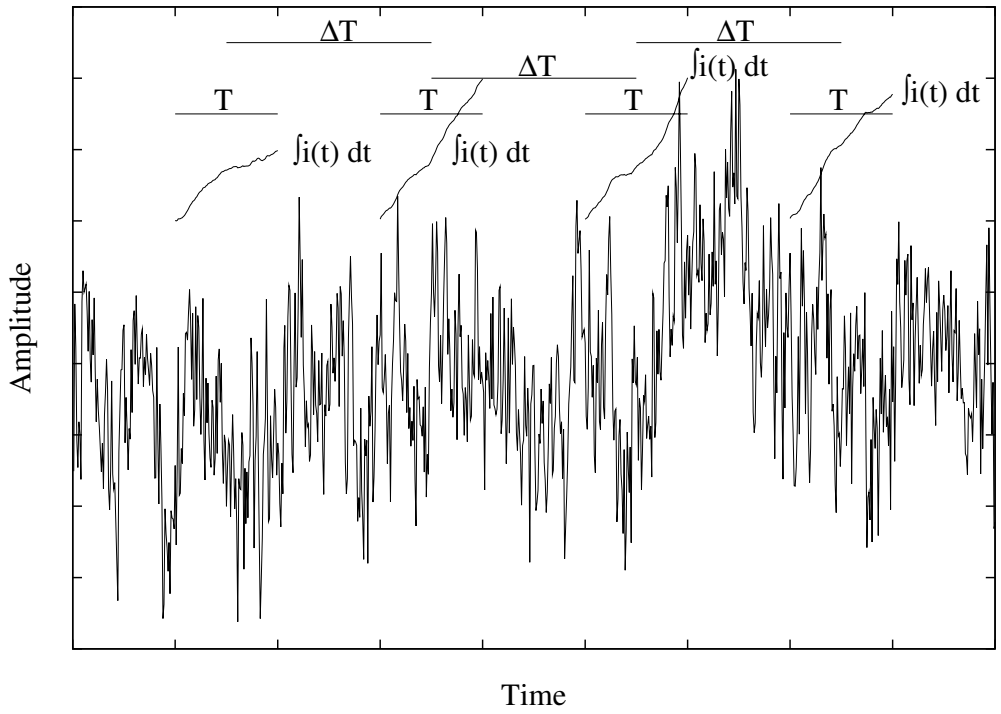

Figure 3.2: An example of $1/f$ noise versus time and sampling of the $1/f$ noise signal. Above, the bars indicate the integration time for each sample, T, and the sample separation ΔT. Lines marked with $\int i(t)\,dt$ are the cumulative integrals over the periods marked T; left axis not shown.

One may exchange the summation and ensemble expectation as follows,

$$\overline{var} = \frac{1}{N}\sum_{n=1}^{N} E\left\{(x_n - \overline{x})^2\right\} \tag{3.63}$$

As the ensemble expectation of $(x_n - \overline{x})$ is zero, the ensemble expectation of $(x_n - \overline{x})^2$ is simply the variance of $(x_n - \overline{x})$, which may be calculated in the frequency domain, as

$$E\left\{(x_n - \overline{x})^2\right\} = \frac{2}{2\pi}\int_0^{\infty} S(\omega)\left|H_{\Delta}(n;\omega)\right|^2\,d\omega \tag{3.64}$$

where

$$H_{\Delta}(n;\omega) = H_{\text{avg}}(\omega)e^{j\omega n\Delta T} - H_{\overline{x}}(\omega) \tag{3.65}$$

Then the ensemble expectation of the noise variance contribution is

$$\overline{var} = \frac{1}{N}\sum_{n=1}^{N}\frac{2}{2\pi}\int_0^{\infty} S(\omega)\left|H_{\Delta}(n;\omega)\right|^2\,d\omega \tag{3.66}$$

One may reverse the order of summation and integration,

$$\overline{var} = \frac{2}{2\pi}\int_0^{\infty} S(\omega)\frac{1}{N}\sum_{n=1}^{N}\left|H_{\Delta}(n;\omega)\right|^2\,d\omega \tag{3.67}$$

One may define a sample sequence transfer function

$$|H_{\text{seq}}(\omega; N)|^2 = \frac{1}{N}\sum_{n=1}^{N} |H_{\Delta}(n;\omega)|^2 \tag{3.68}$$

$$= |H_{\text{avg}}(\omega)|^2 \frac{4}{N^2}\sum_{n=1}^{N}(N-n)\sin^2(n\omega\Delta T/2) \tag{3.69}$$

The total variance of a length N noise sample sequence is then

$$var = \frac{2}{2\pi}\int_0^{\infty} S(\omega)|H_{\text{seq}}|^2\, d\omega \tag{3.70}$$

As an example, consider unweighted averaging, i.e.

$$H_{avg}(\omega; N) = \text{sinc}(\omega T/2) \tag{3.71}$$

For a sample sequence of $1/f^{\alpha}$ noise with $\alpha = 1$, the variance contributed is

$$\overline{var} = 2S_0\sum_{n=1}^{N}\frac{(N-n)}{N^2} \times \left[\ln\left|n^2\zeta^2 - 1\right| + n^2\zeta^2 \ln\frac{|n^2\zeta^2 - 1|}{n^2\zeta^2} + 2n\zeta\ln\frac{n\zeta+1}{|n\zeta-1|}\right] \tag{3.72}$$

where $\zeta = \Delta T/T$. For the more general case of $\alpha \neq 1$, the noise contributes a variance of

$$\overline{var} = 4(2\pi T)^{\alpha-1} S_0 \Gamma(-\alpha-1)\sin\frac{\alpha\pi}{2}\sum_{n=1}^{N}\frac{(N-n)}{N^2}\left[2(n\zeta)^{\alpha+1} + 2 - |n\zeta-1|^{\alpha+1} - (n\zeta+1)^{\alpha+1}\right] \tag{3.73}$$

For a sample sequence of white noise,

$$\overline{var} = \frac{N-1}{N}\frac{S_W}{T} \tag{3.74}$$

corresponding to the usual biased estimator of the variance.

The normalized variance of a length-N sample-sequence of $1/f^{\alpha}$ noise with $\alpha = 1$ is graphed in figure 3.3 for different N; unweighted averaging is used.

3.3.2 Infinite Number of Samples, or Apparent Variance

If one allows the number of samples to become infinite, while constraining the total time that the samples occupy to be constant, the averaging integrals must overlap; this case is a useful and simple limit, corresponding to the variance of a moving average over a finite period. The variance is calculated in a manner similar to that for the finite sampling case.

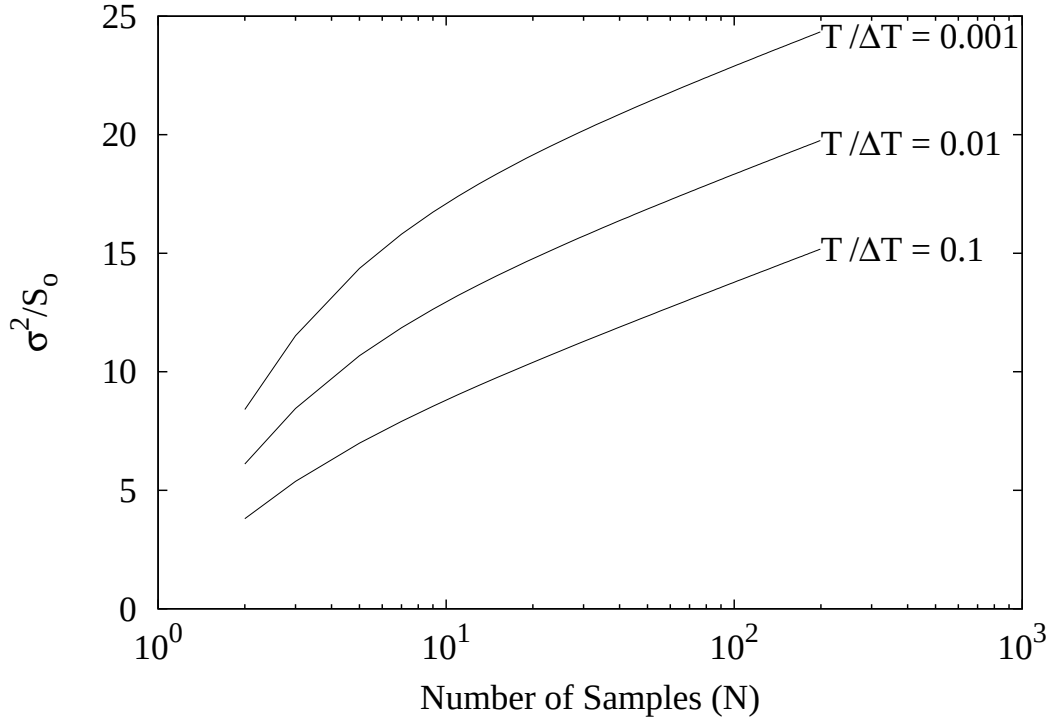

Figure 3.3: Normalized variance of N samples at different $1/\zeta$ for $\alpha = 1$

Variance is the expectation of the square of the difference of a random variable from its mean,

$$var\{x\} = E\left[(x - E[x])^2\right] \tag{3.75}$$

In a practical noise measurement, one can only find an approximate (measured) mean, and an approximate (measured) variance,

$$\widetilde{x}(t_1, t_2) = \frac{1}{t_2 - t_1} \int_{t_1}^{t_2} x(t')\, dt' \tag{3.76}$$

$$\widetilde{var}(x; t_1, t_2) = \frac{1}{t_2 - t_1} \int_{t_1}^{t_2} \left[x(t') - \tilde{x}(t_1, t_2)\right]^2 \, dt' \tag{3.77}$$

One may calculate an ensemble expectation of the approximate variance,

$$E\left[\widetilde{var}(x; t_1, t_2)\right] = E\left\{\frac{1}{t_2 - t_1} \int_{t_1}^{t_2} \left[x(t') - \tilde{x}(t_1, t_2)\right]^2 \, dt'\right\} \tag{3.78}$$

By reversing the order of the averaging integral and ensemble expectation, one obtains

$$E\left[\widetilde{var}(x; t_1, t_2)\right] = \frac{1}{t_2 - t_1} \int_{t_1}^{t_2} E\left\{\left[x(t') - \tilde{x}(t_1, t_2)\right]^2\right\} \, dt' \tag{3.79}$$

As $E\left[x(t') - \tilde{x}(t_1, t_2)\right]$ is expected to be zero, $E\left\{\left[x(t') - \tilde{x}(t_1, t_2)\right]^2\right\}$ is simply the ensemble variance of $[x(t') - \tilde{x}(t_1, t_2)]$, which is

$$E\left\{\left[x(t') - \tilde{x}(t_1, t_2)\right]^2\right\} = \frac{2}{2\pi}\int_0^\infty S(\omega)\left|e^{j\omega t'} - \mathrm{sinc}(\omega T_o/2)\right|^2 d\omega \tag{3.80}$$

where $T_o = t_2 - t_1$, as the noise is assumed to be second order stationary, and hence statistically invariant upon a time shift. Consequently,

$$E\left[\widetilde{var}(x; T_o)\right] = \frac{1}{T_o}\int_{-T_o/2}^{T_o/2}\frac{2}{2\pi}\int_0^\infty S(\omega)\left|e^{j\omega t'} - \mathrm{sinc}(\omega T_o/2)\right|^2 d\omega\, dt' \tag{3.81}$$

One may reverse the integrations to obtain

$$E\left[\widetilde{var}(x; T_o)\right] = \frac{2}{2\pi}\int_0^\infty S(\omega)\frac{1}{T_o}\int_{-T_o/2}^{T_o/2}\left|e^{j\omega t'} - \mathrm{sinc}(\omega T_o/2)\right|^2 dt'\, d\omega \tag{3.82}$$

$$= \frac{2}{2\pi}\int_0^\infty S(\omega)\left[1 - \mathrm{sinc}^2(\omega T_o/2)\right] d\omega \tag{3.83}$$

One may define an apparent variance transfer function

$$|H_{\mathrm{app}}(\omega; T_o)|^2 = 1 - \mathrm{sinc}^2(\omega T_o/2) \tag{3.84}$$

The ensemble expectation of the variance of a sample sequence with an infinite number of overlapping samples over a finite period is

$$E[\widetilde{var}(\omega; T_0)] = \frac{2}{2\pi}\int_0^\infty S(\omega)|H_{\mathrm{app}}(\omega; T_0)|^2\, d\omega \tag{3.85}$$

Most noise sources have an apparent PSD that diverges in the high frequency limit of the variance integral (e.g. 3.83), so one may wish to restrict the high–frequency content, e.g. by having samples of some finite length, which would then overlap,

$$E\left[\widetilde{var}(x_{\mathrm{sample}}; T_o)\right] = \frac{2}{2\pi}\int_0^\infty S(\omega)\left|H_{\mathrm{app}}(\omega; T_o)\right|^2 \cdot \left|H_{\mathrm{avg}}(\omega)\right|^2 d\omega \tag{3.86}$$

$H_{\mathrm{app}}(\omega; T_o)$ may also be derived as the limit as $N \to \infty$ of (3.69), with $N\Delta T = T_o$, in which the transfer function becomes a Riemann sum,

$$\lim_{N\to\infty} H_{\mathrm{seq}}(\omega; N) = \left|H_{\mathrm{avg}}(\omega)\right|^2 \frac{4}{T_o^2}\int_0^{T_o}(T_o - t')\sin^2(\omega t'/2)\, dt' \tag{3.87}$$

$$= \left|H_{\mathrm{avg}}(\omega)\right|^2\left[1 - \mathrm{sinc}^2(\omega T_o/2)\right] \tag{3.88}$$

Finally, a more flippant, though still correct derivation can also be made. Let the 'universe' of interest be the noise sequence in the window T_o; the transfer function that will pass all the noise power in the window is

$$H_{\text{all}}(\omega; T_o) = 1 \tag{3.89}$$

The transfer function that will pass only the average (apparent DC) power in the window T_o is

$$H_{\text{DC}}(\omega; T_o) = \text{sinc}(\omega T_o/2) \tag{3.90}$$

But the variance and the power of the DC must sum to the total power, including in the window T_0,

$$|H_{\text{var}}(\omega; T_o)|^2 + |H_{\text{DC}}(\omega; T_o)|^2 = |H_{\text{all}}(\omega; T_o)|^2 \tag{3.91}$$

Solving for the variance transfer function for the T_o window,

$$|H_{\text{var}}(\omega; T_o)|^2 = 1 - \text{sinc}^2(\omega T_o/2) \tag{3.92}$$

The variance that $1/f^\alpha$ noise with $\alpha = 1$ contributes to an infinite sample sequence of finite length with unweighted averaging in equation 3.86 is

$$var = S_0 \left[\frac{-7}{6} + \ln\left|\zeta^2 - 1\right| + \frac{1}{6}\zeta^{-2} \ln\left|\zeta^2 - 1\right| - \frac{1}{6}\zeta^2 \ln\frac{\zeta^2}{|\zeta^2 - 1|} - \frac{2}{3}\left(\zeta + \zeta^{-1}\right) \ln\frac{|\zeta - 1|}{\zeta + 1} \right] \tag{3.93}$$

where $\zeta = T_0/T$. In the more general case of $\alpha \neq 1$, the noise contributes

$$\begin{aligned} var = \frac{4(2\pi T)^{\alpha-1} S_0 \Gamma\left(-1-\alpha\right) \sin\frac{\alpha\pi}{2}}{\left[\zeta^2\left(3+\alpha\right)\left(2+\alpha\right)\right]} & \left[2 - \left(\zeta+1\right)^{3+\alpha} - \left|\zeta - 1\right|^{3+\alpha} + 2\zeta^{3+\alpha}\right. \\ & \left. + \left(2+\alpha\right)\left(3+\alpha\right)\zeta^2\right] \end{aligned} \tag{3.94}$$

For white noise, when the samples overlap, if $T_o > T$, the variance is

$$var = S_W T^{-1}\left(1 + \zeta^{-2} - \zeta^{-1}\right) \tag{3.95}$$

The variance of infinitely sampled noise is graphed in figure 3.4; unweighted averaging is used.

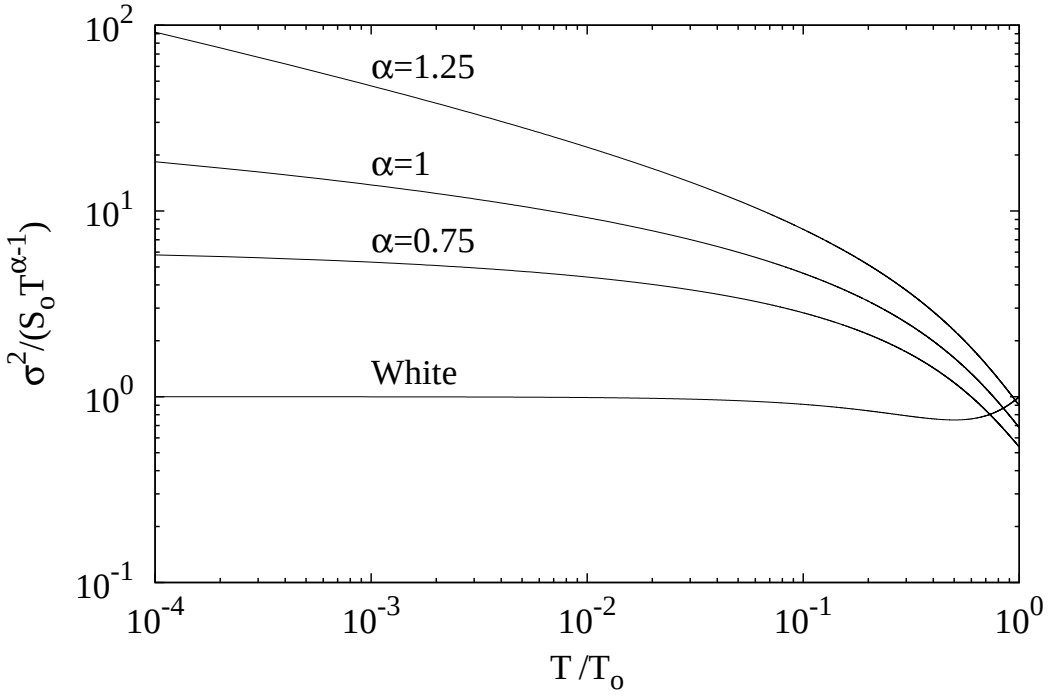

Figure 3.4: Normalized variance of infinite sampling at different α

3.4 Discussion

I derived in outline a proof for the noise filtration relationship stated in equation 3.2. I have ignored the integral term for the remaining work, as it is always omitted, and may be an artifact of the simplistic derivation; a more detailed proof, in progress at the time of writing, suggests a heavy reliance on the second-order stationarity of noise, as fragments of the autocorrelation integrals together sum to create the transfer functions, suggesting that further reorderings of the integrations may be necessary.

I have derived transfer functions for various practical detectors, including samplers and I have calculated the associated variances for various types of noise signals input to each detector. All the transfer functions that I derived have the properties

$$\frac{\partial}{\partial\omega}|H_{cor}(\omega)|^2\Big|_{\omega=0} = 0 \tag{3.96}$$

and

$$|H_{cor}(0)|^2 = 0 \tag{3.97}$$

which suppress the low-frequency variance divergence of $1/f$ noise. In order to calculate

these variances, I assumed that the noise is wide-sense stationary (WSS).

Each of the $\alpha = 1$ variances had to be calculated indirectly. Two methods were used for each calculation, namely imposing a low-frequency cut-off that restricts the variance, i.e.

$$S(f) = \frac{S_0}{\sqrt{f^2 + f_0^2}} \tag{3.98}$$

and then taking the limit $f_0 \to 0$, and calculating the variance where $\alpha \neq 1$ taking the limit $\alpha \to 1$. The two methods produce identical results.

A more generally useful result is that when $1/f$ noise dominates, SNR does not improve with longer integration times, unlike when white noise dominates, where the SNR does improve with longer integration times.

Chapter 4

Measuring Noise Variance

I performed experiments to test the analysis of the variance contribution of noise to detectors in chapter 3. I experimentally obtained noise sequences with white-like and $1/f$-like power-spectral densities. I used the N-sample and infinite sample contributions of variance transfer functions, and applied them to the measured power-spectral densities of the white-like and $1/f$-like noise sequences obtained, to calculate their variance contributions under different N, ΔT and T as per chapter 3.

4.1 Numerical Noise

One needs a noise source that produces a noise signal, that may be sampled readily, to test the theoretical results of chapter 3. One may generate numerical noise, which may be numerically integrated and subtracted, to simulate the operations whose variance contributions are calculated in chapter 3. Similarly, one may numerically integrate N times, with the integrations spread—start-to-start—by ΔT, and the integrations have a period of T. The latter method was used in this chapter. This requires noise with 7-9 decades of white or $1/f$ tendency, in order to meaningfully test the relationships derived in chapter 3: approximately 3 decades may be sacrificed to integration, which is a low-pass filtration and thus producing realistic integration effects, and at least 2 decades could be sacrificed to the subtraction, while leaving several decades of representative tendency in the noise to generate the variance of interest.

To generate the noise numerically, one may either generate an appropriate frequency domain random sequence, and convert it to the time domain, i.e. Rice's method [85], or one may generate a time domain signal directly by using an appropriate algorithm. The noise output must be generated at equally spaced intervals, as variation in the sampling rate

affects the PSD of the sample sequence for non-white (e.g. $1/f$) noise. Sum-of-Markovian type $1/f$ noise generation algorithms (that rely on Surdin, cited in [61]) generate a sequence of transition times, that do not generally align with sampling edges; simply forcing transition times to sample edges may modify the PSD, and additional processing may be required to maintain a $1/f$ spectrum - white spectrum will remain white, due to the statistical independence of any two white noise samples.

Rice's method involves the generation of 'Gaussian' noise, such that the orthogonal components a_n and b_n of the Fourier transform of a finite sequence of the noise are each statistically independent Gaussian random variables, i.e. if $x(t)$ is the noise signal,

$$x(t) = \sum_{n=1}^{N} a_n \cos n\omega_0 t + b_n \sin n\omega_0 t \tag{4.1}$$

the variables a_n and b_n are statistically independent, equal variance random variables,

$$a_n,\, b_n \sim \mathrm{N}(0, \sigma_n^2/2) \tag{4.2}$$

and ω_0 is the fundamental frequency, such that if one has N samples, and one generates a sample sequence of sampling rate f_s, then

$$\omega_0 = \frac{2\pi f_s}{N} \tag{4.3}$$

The variance is related to the PSD by

$$\sigma_n^2 = \frac{1}{2\pi} \int_{(n-0.5)\omega_0}^{(n+0.5)\omega_0} S(\omega) d\omega \tag{4.4}$$

To generate seven or more decades of $1/f$ noise using this method, one needs to compute an inverse (fast) Fourier transform (IFFT) of 10^7 or more points, as well as a random number generator that can produce such a number of roughly independent pseudo-random numbers. Greater accuracy is also needed—the information that is lost by adding 10^7 or more 64-bit (IEEE754 binary64 "double") floating point numbers, e.g. in the course of an IFFT, may become significant, and one often needs an additional decade of noise to avoid the correlations caused by the 'circularity' of the Rice method noise. Rice's method produces 'circular' noise, in that by making the sequence 'circular'—such that the last sample precedes the first. 'Breaking' the sequence at another sample pair into a new linear sequence gives the same PSD as the original sample sequence. This may be seen

as follows. In equation 4.2, as a_n and b_n are independent, they may be resolved into r_n and ϕ_n, where a_n, b_n are cartesian coordinates corresponding to the polar coordinates r_n and ϕ_n. By breaking the (circular) sequence at a different sample pair, ϕ_n is rotated—corresponding to a delay or advance, with

$$H(\omega) = e^{j\omega\,\Delta T_{delay}} \tag{4.5}$$

but r_n remains unchanged, so at the new phase angle, the components are a'_n and b'_n, with

$$a_n^2 + b_n^2 = a_n'^2 + b_n'^2 \tag{4.6}$$

thus leaving the PSD unchanged. A deeper problem emerges - a real noise sequence is not circular, thus one may only use a fraction of a circular noise sequence to simulate real noise.

If one seeks to generate 9 decade noise using 128-bit floating point numbers, to avoid accuracy losses arising from addition steps, one would need 16 gigabytes of Random Access Memory (RAM) for the inverse Fourier transform step alone, assuming an in-place inverse fast Fourier transform (iFFT) algorithm. Hence it is not presently practical to test the relationships of chapter 3 by Rice's method.

With Rice's method, one takes the desired Power Spectral Density (PSD), and calculates a time sequence - both the time domain signal and the PSD are required to test the results of chapter 3. If a time-domain algorithm is used to generate the noise, somewhat less memory is needed, as the PSD may be calculated based on an autocorrelation function that is substantially shorter than the total sequence, depending on how low a frequency one wishes to calculate the PSD to. Thus, if implemented, a Surdin-type noise generator may prove less demanding to implement than an equivalent Rice's method generator, including when PSD verification is included.

4.2 Electronic Noise

An obvious alternative to numerical noise generation is to sample amplified electronic noise. In our laboratory, the general practice, aimed at measuring the PSD over a finite frequency band, was to bandpass the noise and amplify it. The immediate problem with

this approach is that it is hard to get more than six decades of noise (0.1Hz to 100kHz), as a $1/f$ noise signal that is filtered by a high-pass filter with a cut-off frequency below 0.1Hz tends to swamp the noise amplifier, and it is hard to get $1/f$ noise at or beyond relatively low frequencies such as 100kHz. Another problem is that a huge sampling rate (at least 200kHz) would be required to obtain these six decades.

To obtain more decades of noise with the desired PSD, at a lower sampling rate, mixing methods were used. The mixing methods may be understood as follows. If one multiplies two signals $x(t)$ and $y(t)$, with Fourier transforms $X(f)$ and $Y(f)$, their product

$$z(t) = x(t) \times y(t) \tag{4.7}$$

has a Fourier transform that is the convolution of the individual Fourier transforms,

$$Z(f) = X(f) * Y(f) \tag{4.8}$$

If $y(t)$ is a complex exponential,

$$y(t) = e^{j\omega_m T} \tag{4.9}$$

then the Fourier transform of $z(t)$ is a sum of shifted Fourier transforms of $x(t)$,

$$Z(f) = X(f - \omega_m/(2\pi)) \tag{4.10}$$

As I work with real-valued functions, I use (co)sines,

$$y(t) = \cos(\omega_m t) \tag{4.11}$$

one obtains

$$Z(f) = \frac{1}{2}X\left(f - \omega_m/(2\pi)\right) + \frac{1}{2}X\left(f + \omega_m/(2\pi)\right) \tag{4.12}$$

Likewise, if

$$w(t) = z(t) \cdot y(t) \tag{4.13}$$

then the Fourier transform of $w(t)$ is also a sum of shifted Fourier transforms of $x(t)$,

$$W(f) = \frac{1}{2}X(f) + \frac{1}{4}X\left(f - \omega_m/(2\pi)\right) + \frac{1}{4}X\left(f + \omega_m/(2\pi)\right) \tag{4.14}$$

The PSD is not the Fourier transform of the noise signal, and thus a more careful derivation is needed.

To calculate the PSD that results from mixing noise, the effect of mixing may be accounted for in the autocorrelation function. By the Wiener-Khintchine theorem (introduced in chapter 1), the PSD of a noise signal may be related to its auto-covariance function by

$$S(\omega) = \int_{-\infty}^{\infty} e^{-j\omega\tau}\,\phi(\tau)\,d\tau \tag{4.15}$$

For a finite measurement, one may take the measured PSD as

$$S^{meas}(\omega) = \int_{-T}^{T} e^{-j\omega\tau}\,\phi(\tau)\,d\tau \tag{4.16}$$

If the autocorrelation function (or some component of it, as per chapter 3) is measured to ergativity in some period $2MT$ (where $M > 2$), then one may use the auto-correlation function,

$$R(\tau) = \int_{-(M-1)T-\tau/2}^{(M-1)T-\tau/2} \frac{x(t)\cdot x(t+\tau)}{2(M-1)T}\,dt \tag{4.17}$$

to calculate the PSD,

$$S_x^{meas}(\omega) = \int_{-T}^{T} e^{-j\omega\tau} \int_{-(M-1)T-\tau/2}^{(M-1)T-\tau/2} \frac{x(t)\cdot x(t+\tau)}{2(M-1)T}\,dt\,d\tau \tag{4.18}$$

The PSD of $z(t)$ may be calculated as

$$S_z^{meas}(\omega) = \int_{-T}^{T} e^{-j\omega\tau} \int_{-(M-1)T-\tau/2}^{(M-1)T-\tau/2} \frac{z(t)\cdot z(t+\tau)}{2(M-1)T}\,dt\,d\tau \tag{4.19}$$

$$= \int_{-T}^{T} e^{-j\omega\tau} \int_{-(M-1)T-\tau/2}^{(M-1)T-\tau/2} \frac{x(t)\cdot x(t+\tau)}{2(M-1)T} \left[\frac{1}{2}\cos\omega_m(2t+\tau) + \frac{1}{2}\cos\omega_m\tau\right] dt\,d\tau \tag{4.20}$$

Rearranging the above, one finds

$$\begin{aligned} S_z^{meas}(\omega) = &\int_{-T}^{T} e^{-j\omega\tau}\frac{e^{j\omega_m\tau}+e^{-j\omega_m\tau}}{4} \int_{-(M-1)T-\tau/2}^{(M-1)T-\tau/2} \frac{x(t)\cdot x(t+\tau)}{2(M-1)T}\,dt\,d\tau \\ &+ \int_{-T}^{T} e^{-j\omega\tau}\frac{e^{j\omega_m\tau}}{4} \int_{-(M-1)T-\tau/2}^{(M-1)T-\tau/2} \frac{x(t)\cdot x(t+\tau)}{2(M-1)T}\,e^{j\omega_m 2t}\,dt\,d\tau \\ &+ \int_{-T}^{T} e^{-j\omega\tau}\frac{e^{-j\omega_m\tau}}{4} \int_{-(M-1)T-\tau/2}^{(M-1)T-\tau/2} \frac{x(t)\cdot x(t+\tau)}{2(M-1)T}\,e^{-j\omega_m 2t}\,dt\,d\tau \end{aligned} \tag{4.21}$$

The last two terms are expected to be zero, as the $x(t)\cdot x(t+\tau)$ is expected to be fairly consistent over time, such as to make the integral over its product with a sinusoid be of order $1/M$. Letting the last two terms go to zero, one is left with

$$S_z^{meas}(\omega) = \frac{1}{4}S_x^{meas}(\omega-\omega_m) + \frac{1}{4}S_x^{meas}(\omega+\omega_m) \tag{4.22}$$

which is the original PSD shifted up and down by ω_m.

The PSD of the twice mixed signal $w(t)$ may be calculated as

$$S_w^{meas}(\omega) = \int_{-T}^{T} e^{-j\omega\tau} \int_{-(M-1)T-\tau/2}^{(M-1)T-\tau/2} \frac{w(t)\cdot w(t+\tau)}{2(M-1)T}\, dt\, d\tau \tag{4.23}$$

Substituting for $w(t)$ one finds

$$\begin{aligned} S_w^{meas} = \int_{-T}^{T} \frac{e^{-j\omega\tau}}{4} \int_{-(M-1)T-\tau/2}^{(M-1)T-\tau/2} \frac{x(t)\cdot x(t+\tau)}{2(M-1)T} \Big[1 + \cos 2\omega_m(t+\tau) + \cos 2\omega_m t + \\ \frac{1}{2}\cos 2\omega_m\tau + \frac{1}{2}\cos 2\omega_m(2t+\tau)\Big]\, dt\, d\tau \end{aligned} \tag{4.24}$$

Rearranging the above, one finds

$$\begin{aligned} S_w^{meas}(\omega) = &\int_{-T}^{T} \frac{e^{-j\omega\tau}}{4} \int_{-(M-1)T-\tau/2}^{(M-1)T-\tau/2} \frac{x(t)\cdot x(t+\tau)}{2(M-1)T} \left[1 + \frac{1}{2}\cos 2\omega_m t\right] dt\, d\tau \\ &+ \int_{-T}^{T} \frac{e^{-j\omega\tau}}{4} \int_{-(M-1)T-\tau/2}^{(M-1)T-\tau/2} \frac{x(t)\cdot x(t+\tau)}{2(M-1)T} \Big[\cos 2\omega_m t\cos 2\omega_m\tau + \cos 2\omega_m t - \\ &\sin 2\omega_m t \sin 2\omega_m\tau + \frac{1}{2}\cos 4\omega_m t\cos 2\omega_m\tau - \frac{1}{2}\sin 4\omega_m t \sin 2\omega_m\tau\Big]\, dt\, d\tau \end{aligned} \tag{4.25}$$

The last term is expected to be zero, as the $x(t)\cdot x(t+\tau)$ is again expected to be fairly consistent over time, such as to make the integral over its product with a sinusoid be of order $1/M$. Letting the last term go to zero, one is left with

$$S_w^{meas}(\omega) = \frac{1}{4}S_x^{meas}(\omega) + \frac{1}{16}S_x^{meas}(\omega + 2\omega_m) + \frac{1}{16}S_x^{meas}(\omega - 2\omega_m) \tag{4.26}$$

which is the original PSD plus the original PSD shifted up and down by $2\omega_m$.

White noise, that was flat at very low frequencies, was generated using a single mixing step. White noise from a resistor was high-pass filtered by a capacitor, amplified and bandpassed from 3Hz to 300kHz, then multiplied by a sinusoid of 150kHz, to bring the noise down around DC with the circuitry of figure 4.1, to generate a noise signal with the PSD in figure 4.2. Spectral peaks corresponding to true sinusoids, presumably due to biases in the mixer and amplifier, corresponding to peaks in the PSD of the original spectrum in figure 4.2, were suppressed with an infinite impulse response (IIR) filter. The IIR filter has the poles and zeros as illustrated in figure 4.3; the poles and zeros have angles that correspond to the spectral peaks of the unfiltered white noise, given the sampling rate;

the zeros lie on the unit circle, and the poles have a radius of 0.995. Three closely spaced pole-zero pairs were used to suppress each spectral peak in the white noise, to produce a noise signal with the spectrum in figure 4.4.

As $1/f$ noise is usually a variation in resistance, one may mix the $1/f$ noise to $1/|f \pm f_m|$ bilateral noise by applying a sinusoidal voltage or current to a carbon composition resistor, which has a high level of $1/f$ noise, that serves as the noise source. By doing this, I also generated a problematically large sinusoid, which I cancelled as follows. A voltage divider was set up, including the noise source resistor and a low noise, wirewound potentiometer, and 180° out-of-phase sinusoids were applied to the ends of the voltage divider, as per figure 4.5. Let the difference between the resistances of the nominal 1MΩ resistors be ΔR. Then the voltage in the middle of the divider at the input of the amplifier is

$$V(t) = \frac{V_{IN}(t)}{2\text{M}\Omega}\Delta R(t) \tag{4.27}$$

which has the $1/|f \pm f_m|$ spectrum. The remaining sinusoid was suppressed by adjusting the variable resistor to approximately the resistance of the noise source, thus leaving the $1/|f - f_0|$ noise. Upon amplification, the signal was band-passed and mixed down to DC. $1/f$ noise was generated in this manner. $1/f$ noise has a tendency to 'wander' (i.e. the short-term average varies over time—see e.g. Keshner [21]), so that after adjusting the variable resistor at the beginning of a noise recording, a day's worth of 1/f noise is available before the dynamic range of the amplifier (that amplifies the $1/|f - f_0|$ noise) is reached.

White noise was recorded for 12 hours at a sampling rate of 2kHz, and $1/f$ noise for 24 hours at 1kHz, to generate 86.4M samples, using Labview. Two problems with Labview are that the program can only record batches of up to 1 million samples at a time, and that the time elapsed between one batch of samples and another is not consistent.

Figure 4.6 had several problematic features around 30-100 mHz. A simulation, where 20 to 26 samples were randomly skipped after every 1000 samples of $1/f$ noise, failed to reproduce the problematic spectral features in figure 4.6. Another possible source of these errors is possible drift-correcting circuitry in the mixer chip used. Such circuitry would treat the shift in the short term average as a drift to correct, and will as such, suppress this shift. By suppressing this shift at semi-regular intervals (e.g. 10-30s), the natural progression of the 1/f noise is semi-systematically disturbed by a relatively large

amount; my suspicion is that this gives rise to the features in the spectrum. These features do not occur in the white noise, presumably as non-overlapping samples of white noise are statistically independent, and thus as long as subsequent samples remain statistically independent, one expects that the spectrum will remain white, irrespective of variations in the sampling rate.

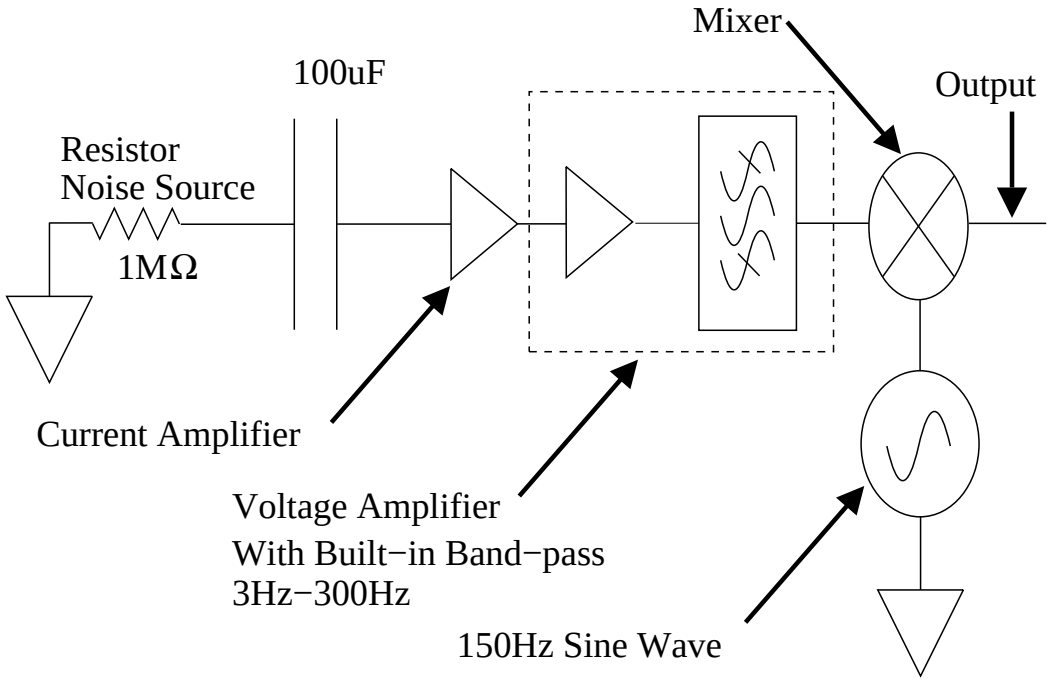

Figure 4.1: White Noise Generator

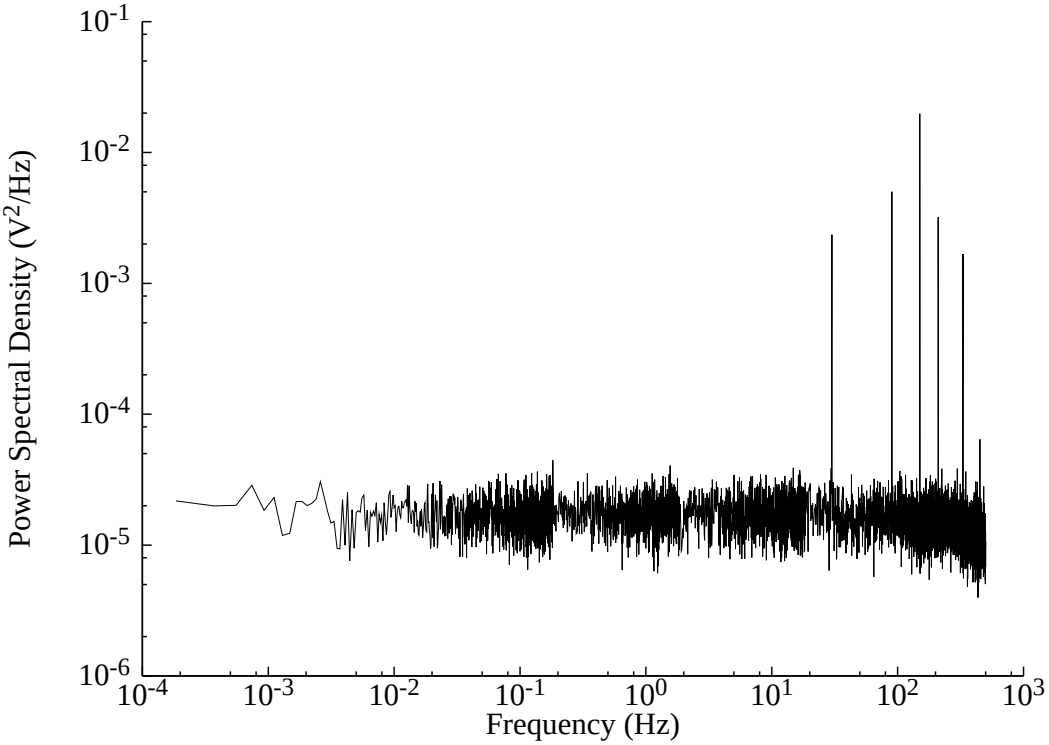

Figure 4.2: The Power-Spectral Density of the Unfiltered White Noise Signal

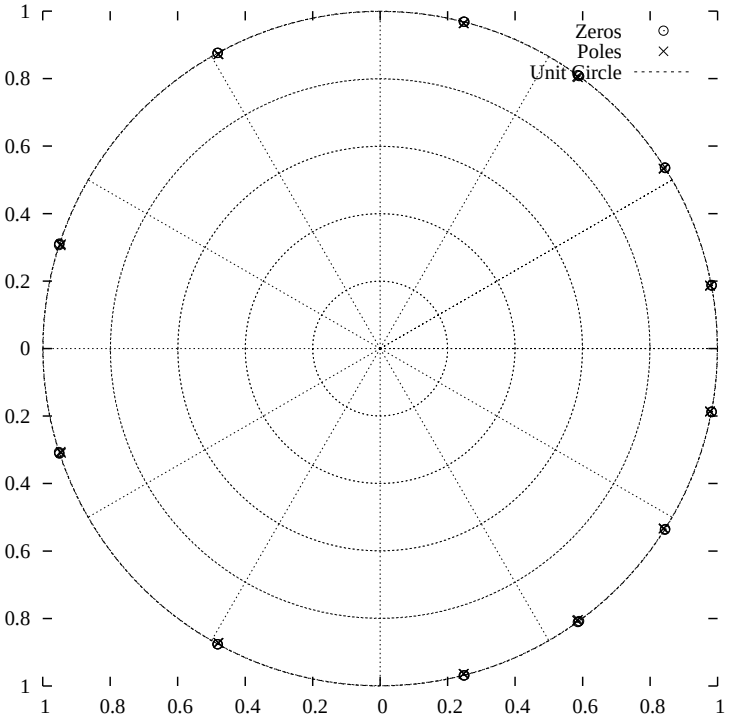

Figure 4.3: Each apparent pole-zero pair on this graph is actually three closely spaced pole-zero pairs. This filter was used to suppress the spikes in figure 4.2 to produce noise with the spectrum in figure 4.4.

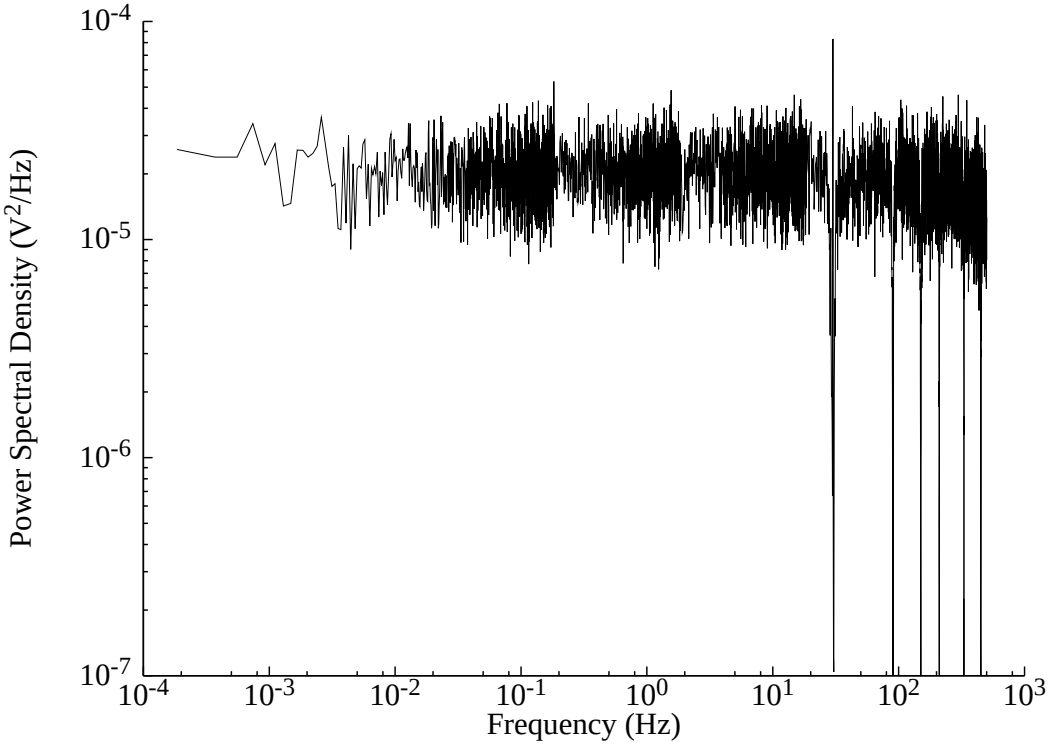

Figure 4.4: The Power-Spectral Density of the Filtered White Noise Signal

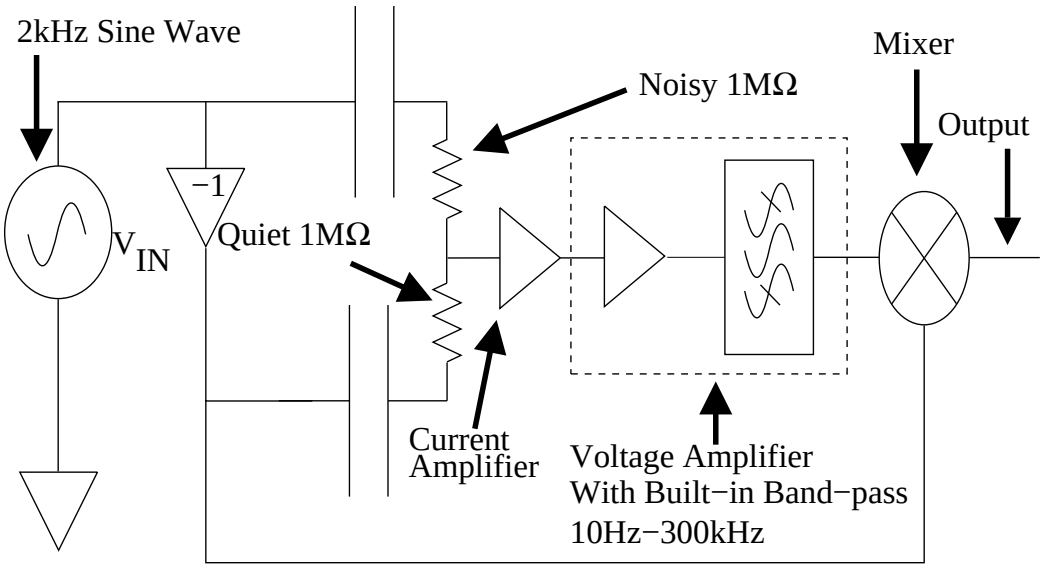

Figure 4.5: 1/f Noise Generator

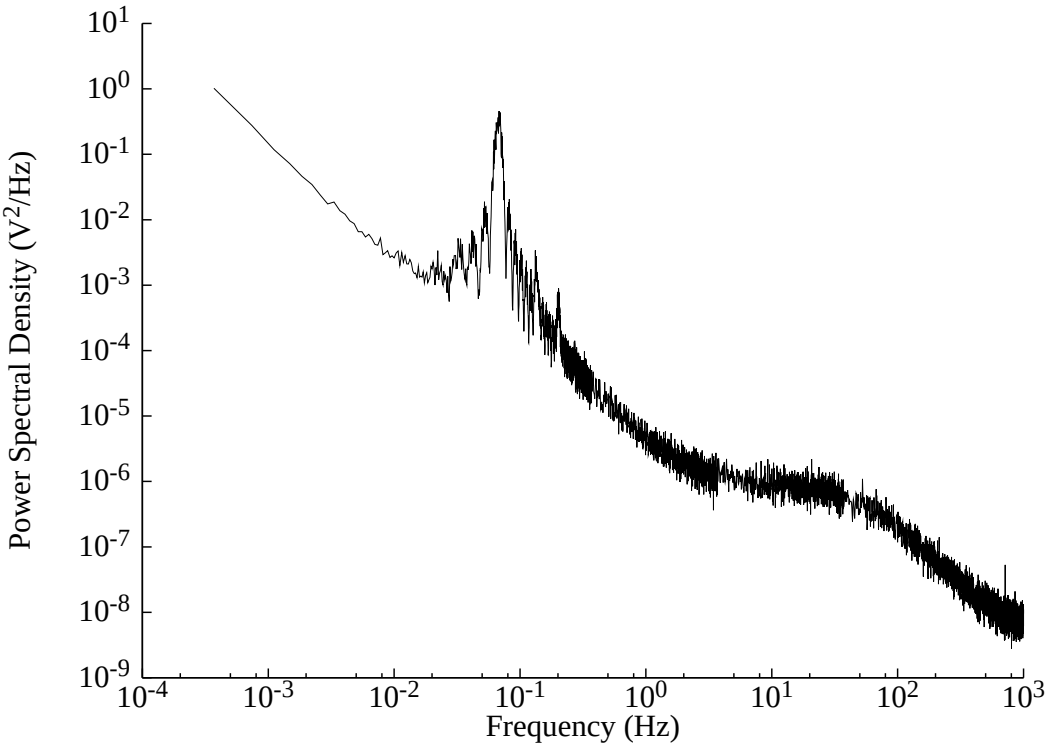

Figure 4.6: The Power-Spectral Density of the $1/f$, Structured Signal

4.3 Results

In the following section, I discuss each configuration of measurement, as specified by ΔT and T, for the white and $1/f$-like noise sequences' variance at different N.

The results of chapter 3 were tested by using odd-N sample sequences, by integrating the generated noises' PSD in equations 3.70 and 3.86, but using an integrating rather than an averaging transfer function, and by calculating an equivalent variance in the work of McDowell et al., according to the equation

$$var_{\text{McDowell}} = \frac{2}{2\pi} \int_{1/(N\Delta T+T)}^{\infty} S_x(\omega) \left|H_{int}(\omega)\right| \, d\omega \tag{4.28}$$

In the following graphs, white and $1/f$ noise sample sequences' average variances are graphed. Also graphed are the predictions of these average variances, calculated by integrating the product of the N-sample and infinite sample transfer functions with the PSD of the noise signal over frequency. The prediction of McDowell et al. of these average variances in equation 4.28 are also graphed.

Figure 4.7 represents the variance of a sample sequence of white noise, with $\Delta T = 10$s and $T = 0.01s$. The dependent axis has the units of the square of the voltage integration with time, as may be expected for a variance of the integral. The independent axis has units of the number of samples, and is a logarthmically scaled axis. The 'measured' variance is that calculated by numerically integrating portions of the noise sequence, and by then taking the variance of N such ΔT spaced integrations. The N-sample, infinite-sample and McDowell projections were calculated by integrating the product of the 'white' noise sequence PSD's product with the appropriate transfer functions for N or infinite number of samples, or by performing McDowell's integral in equation 4.28. For a smaller number of samples ($N < 35$), the N-sample projection yields a truer variance estimate than that of the infinite sample and McDowell projections, whereas for $N > 35$ the reverse holds. All three methods converge in their estimate of the variance as the number of samples grow, and they underestimate in the large sample limit by about 1.5%. The truer estimates of the McDowell and infinite sample methods at larger numbers of samples may be due to this estimate. At all numbers of samples, the McDowell and infinite sample projections provide identical results. The following graphs also have a linear dependent axis for variance, and

a logarithmic independent axis for the number of samples.

Figure 4.8 represents the variance of a sample sequence of white noise, with $\Delta T = 10$s and $T = 0.02s$. For a smaller number of samples ($N < 45$), the N-sample projection yields a truer variance estimate than provided by the infinite sample and McDowell projections, whereas for $N > 45$ the reverse holds. All three methods of calculating the expected variance converge in their estimate of the variance as the number of samples grow, and they underestimate in the large sample limit by about 1%.

Figure 4.9 represents the variance of a sample sequence of white noise, with $\Delta T = 1$s and $T = 0.01s$. For a smaller number of samples ($N < 25$), the N-sample projection yields a truer variance estimate than provided by the infinite sample and McDowell projections, whereas for $N > 25$ the reverse holds. All three methods of calculating the expected variance converge in their estimate of the variance as the number of samples grow, and they underestimate in the large sample limit by about 1.5%.

Figure 4.10 represents the variance of a sample sequence of white noise, with $\Delta T = 1$s and $T = 0.02$. For a smaller number of samples ($N < 45$), the N-sample projection yields a truer variance estimate than provided by the infinite sample and McDowell projections, whereas for $N > 45$ the reverse holds. All three methods of calculating the expected variance converge in their estimate of the variance as the number of samples grow, and they underestimate in the large sample limit by about 1%.

Figure 4.11 represents the variance of a sample sequence of white noise, with $\Delta T = 0.1$s and $T = 0.01s$. For a smaller number of samples ($N < 31$), the N-sample projection yields a truer variance estimate than provided by the infinite sample and McDowell projections, whereas for $N > 31$ the reverse holds. All three methods of calculating the expected variance converge in their estimate of the variance as the number of samples grow, and they underestimate in the large sample limit by about 1.5%.

Figure 4.12 represents the variance of a sample sequence of white noise, with $\Delta T = 0.1$s and $T = 0.02s$. For a smaller number of samples ($N < 51$), the N-sample projection yields a truer variance estimate than provided by the McDowell projection, and for $N < 67$ the N-sample projection provides a truer estimate of the variance than provided by the infinite sample projection. All three methods of calculating the expected variance converge in their estimate of the variance as the number of samples grow, and they underestimate

in the large sample limit by about 1%. Above 100 samples, the McDowell and infinite sample projections provide identical results; at the smaller numbers of samples, McDowell's projection is truer than the infinite sample projection.

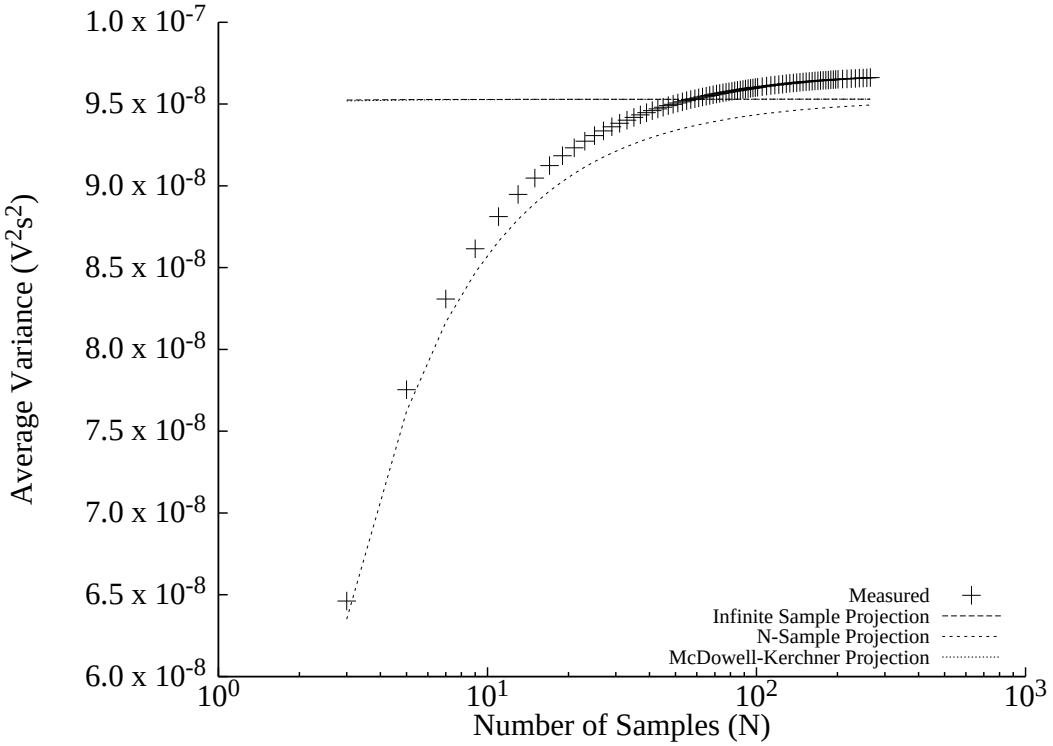

Figure 4.7: White Noise Sample Sequence Variance, $\Delta T = 10\text{s}$, $T = 0.01\text{s}$

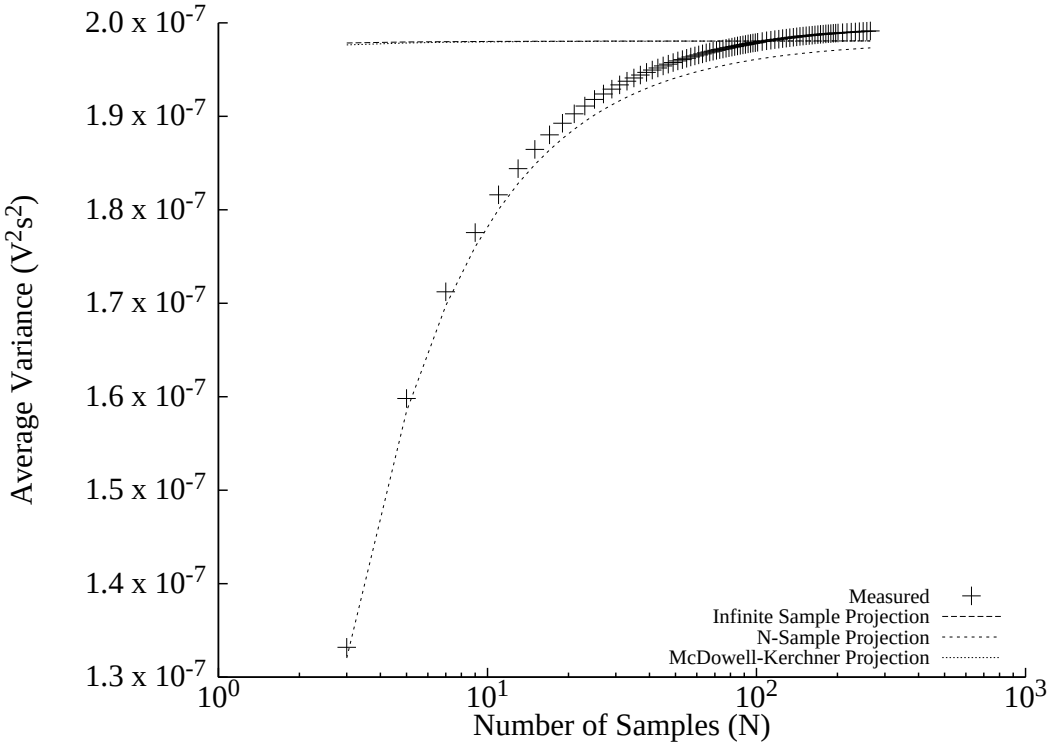

Figure 4.8: White Noise Sample Sequence Variance, $\Delta T = 10$s, $T = 0.02$s

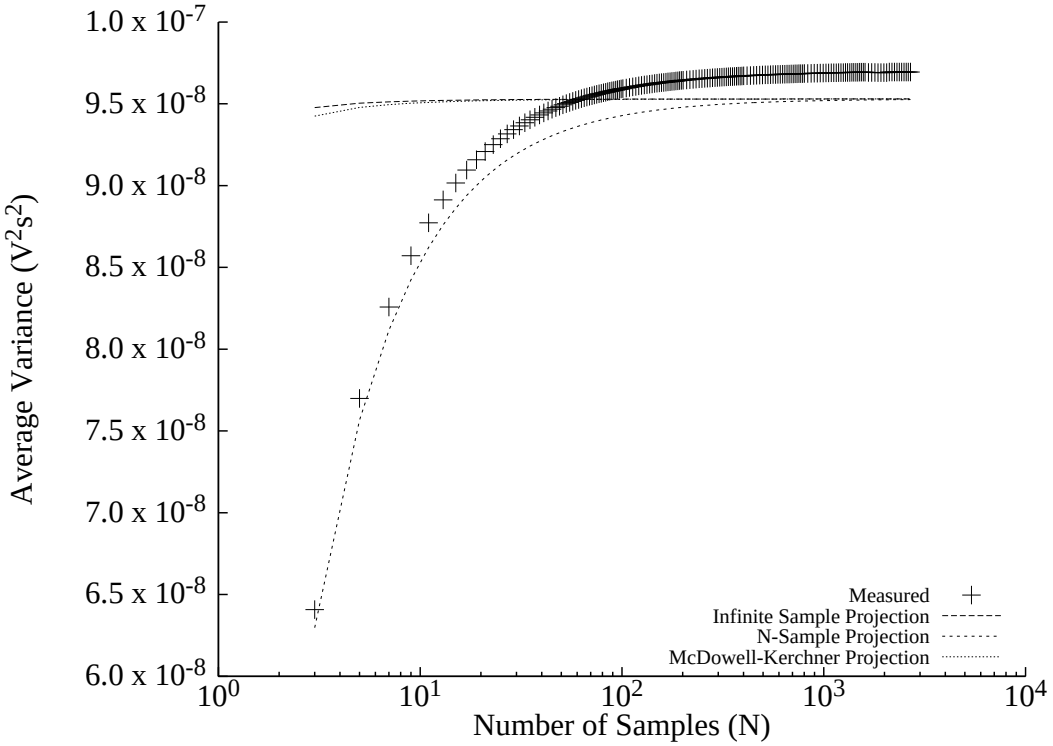

Figure 4.9: White Noise Sample Sequence Variance, $\Delta T = 1$s, $T = 0.01$s

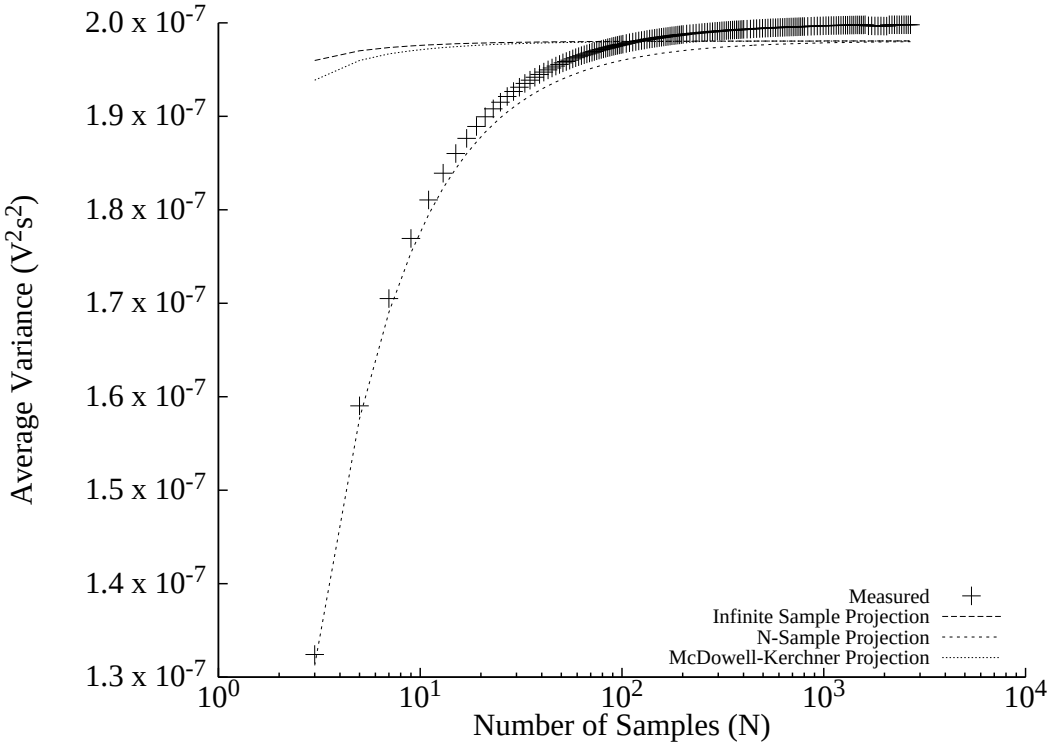

Figure 4.10: White Noise Sample Sequence Variance, $\Delta T = 1\text{s}$, $T = 0.02\text{s}$

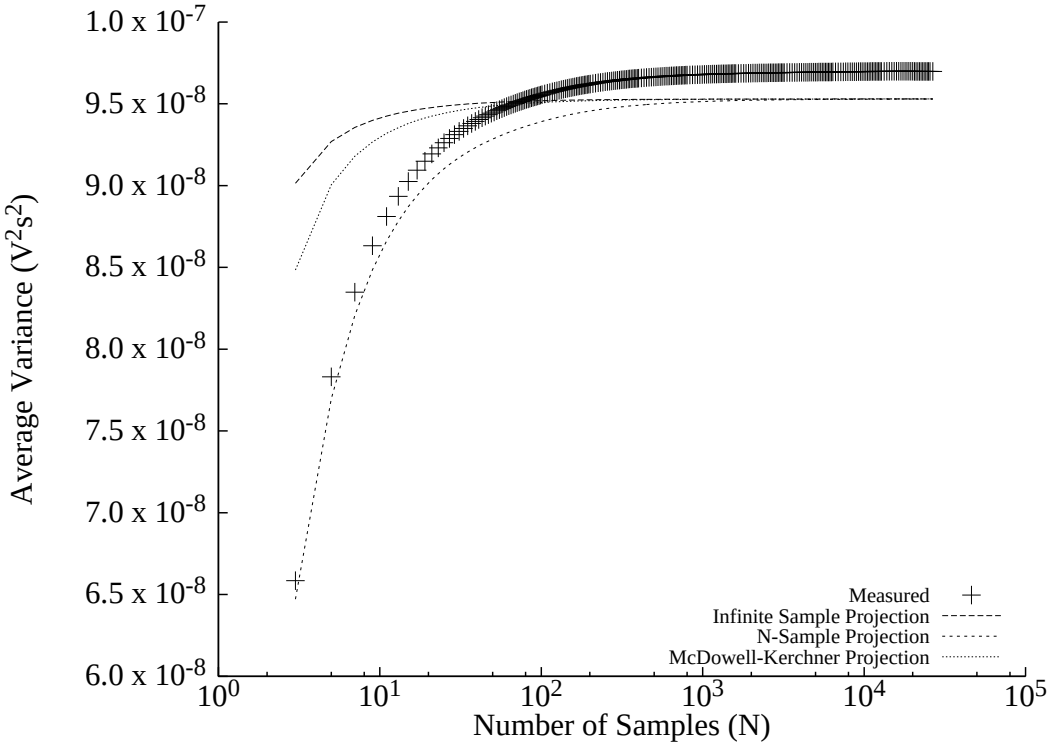

Figure 4.11: White Noise Sample Sequence Variance, $\Delta T = 0.1\text{s}$, $T = 0.01\text{s}$

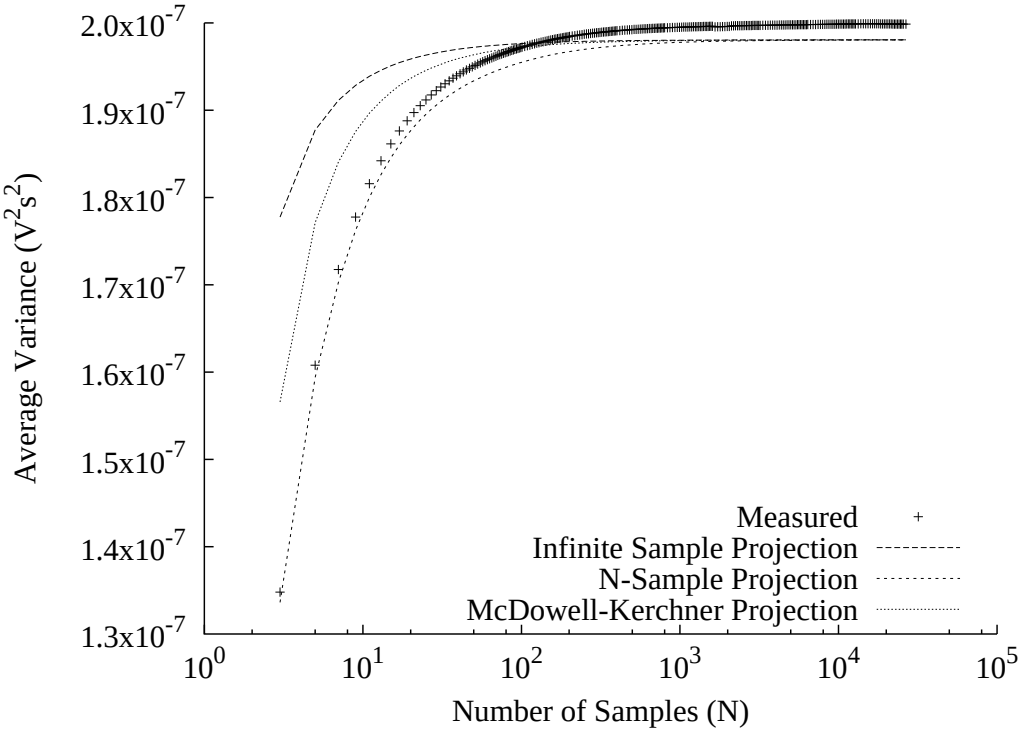

Figure 4.12: White Noise Sample Sequence Variance, $\Delta T = 0.1$s, $T = 0.02$s

The above variance graphs show excellent agreement (error on the order of 1%) of the PSD-based N-sample variance prediction with the measured variance of the white noise. The number of samples at which the variances were measured and calculated were spaced logarithmically, to illustrate the broad consistency of the agreement. The small but consistent error might arise from the averagings and numerical integrations that are required for calculating the 'measured' variances, and from a finite precision used in calculating the PSD. This error is not a source of concern.

Figure 4.13 represents the variance of a sample sequence of $1/f$-like noise, with $\Delta T =$ 10s and $T = 0.01s$. The dependent axis has the units of the square of the voltage integration with time, as may be expected for a variance of the integral. The independent axis has units of the number of samples, and is a logarthmically scaled axis. The 'measured' variance is that calculated by numerically integrating portions of the noise sequence, and by then taking the variance of N such ΔT spaced integrations. The N-sample, infinite-sample and McDowell projections were calculated by integrating the product of the '$1/f$' noise sequence PSD's product with the appropriate transfer functions for N or infinite number of samples, or by performing McDowell's integral in equation 4.28. For a smaller number of samples and for very large numbers of samples (exausting the data-set), the N-sample and infinite sample projections yield a truer variance estimate than provided by the McDowell projection. At an intermediate number of samples, McDowell's projection provides a truer estimate of the contributed variance. At higher numbers of samples, the N-sample and infinite sample projections converge in their estimate of the variance as the number of samples grow, and they first overestimate then underestimate the variance as the number of samples grow; the maximum error between the N-sample and measured variance is about 9%. The staircase shape of the McDowell projection is an artifact of the discretized PSD that is calculated from the sequence data.

Figure 4.14 represents the variance of a sample sequence of $1/f$-like noise, with $\Delta T =$ 10s and $T = 0.02s$. Again, for a smaller number of samples and for very large numbers of samples (exausting the data-set), the N-sample and infinite sample projections yield a truer variance estimate than provided by the McDowell projection, and at an intermediate number of samples, McDowell's projection provides a truer estimate of the contributed variance. Also, at higher numbers of samples, the N-sample and infinite sample projections converge in their estimate of the variance as the number of samples grow, and they first overestimate then underestimate the variance as the number of samples grow; this remains true for subsequent graphs. The maximum error between the N-sample projection and actual variance is about 8%. The staircase shape of the McDowell projection is an artifact of the discretized PSD that is calculated from the sequence data; this is also true for subsequent graphs.

Figure 4.15 represents the variance of a sample sequence of $1/f$-like noise, with $\Delta T =$ 1s

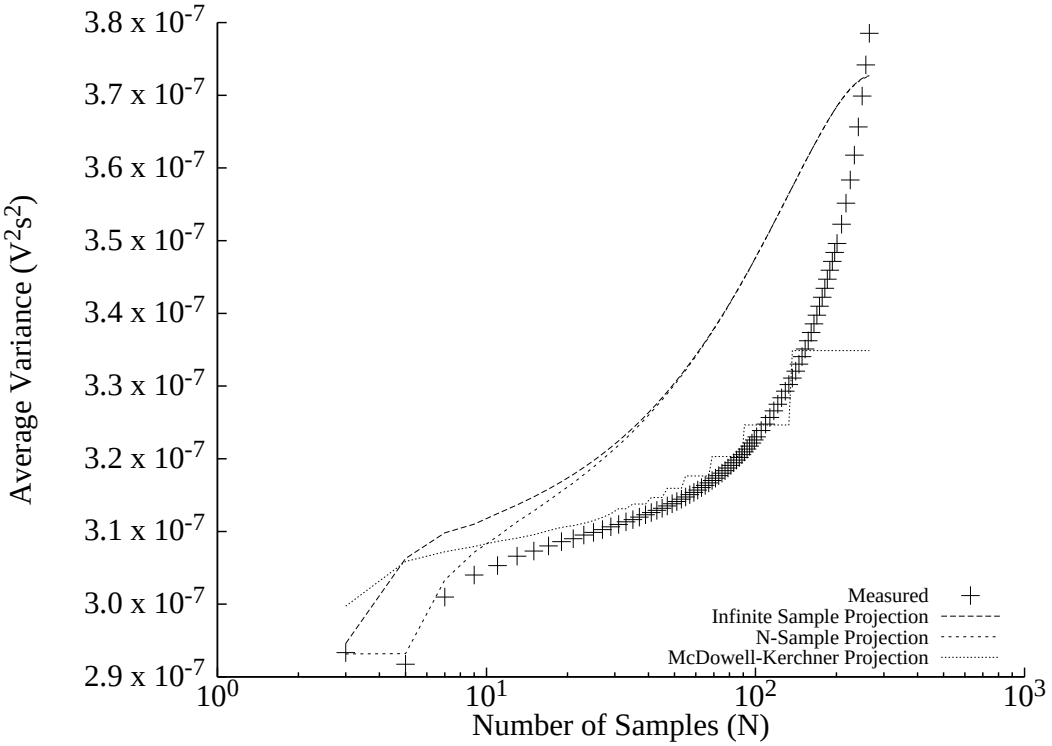

Figure 4.13: $1/f$ Noise Sample Sequence Variance, $\Delta T = 10$s, $T = 0.01$s

and $T = 0.01s$. The maximum error between the N-sample projection and the actual variance is about 8%. The sudden increase in the variance around 15 samples in this graph and the following graph, and around 150 samples in the next two graphs, is due to the spikes in the PSD around 30–100 mHz, in figure 4.6.

Figure 4.16 represents the variance of a sample sequence of $1/f$-like noise, with $\Delta T = 1$s and $T = 0.02s$. The maximum error between the N-sample projection and actual variance is about 8%.

Figure 4.17 represents the variance of a sample sequence of $1/f$-like noise, with $\Delta T = 0.1$s and $T = 0.01s$. The maximum error between the N-sample projection and actual variance is about 8%.

Figure 4.18 represents the variance of a sample sequence of $1/f$-like noise, with $\Delta T = 0.1$s and $T = 0.02s$. The maximum error between the N-sample projection and the actual variance is about 10%.

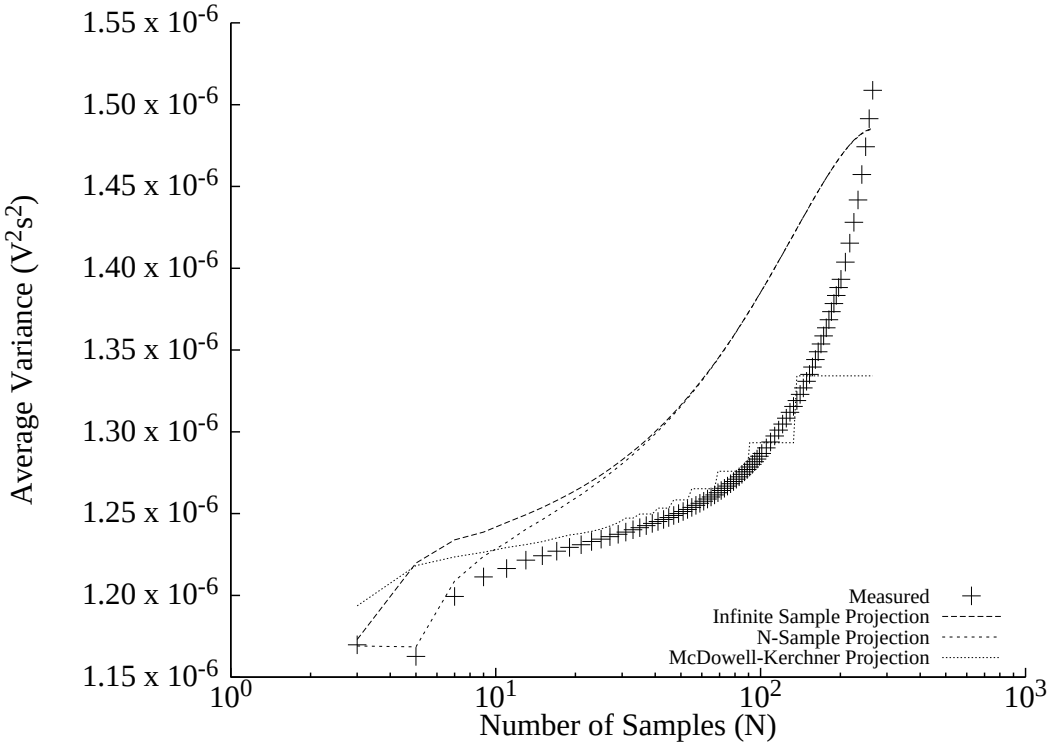

Figure 4.14: $1/f$ Noise Sample Sequence Variance, $\Delta T = 10\text{s}$, $T = 0.02\text{s}$

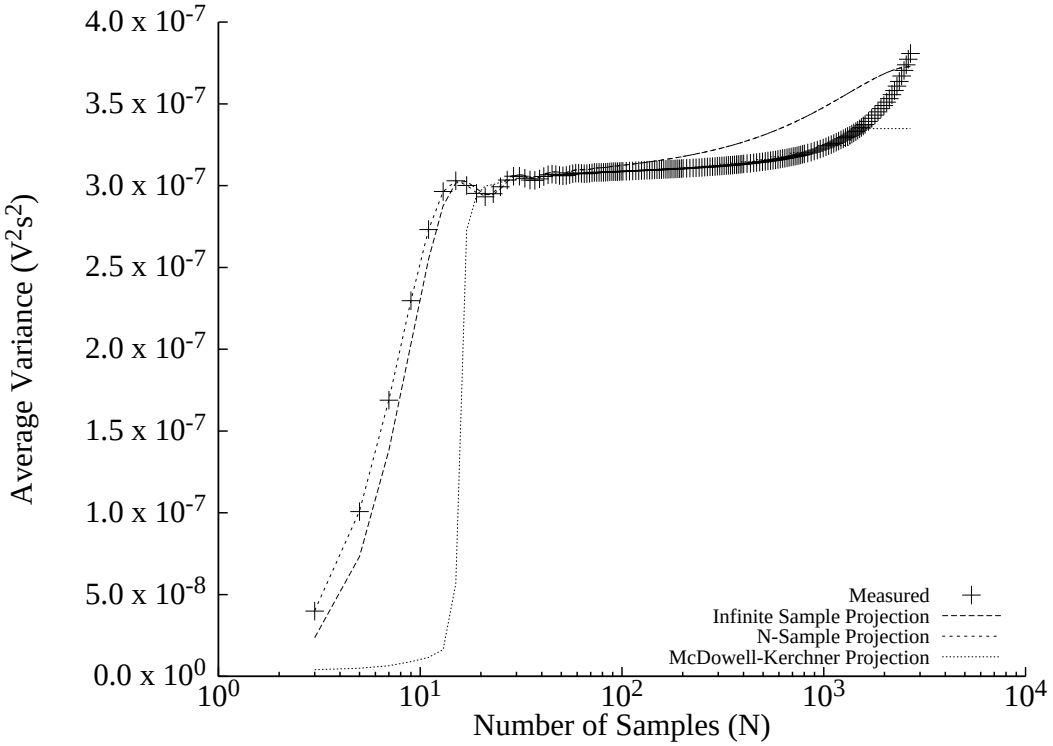

Figure 4.15: $1/f$ Noise Sample Sequence Variance, $\Delta T = 1\text{s}$, $T = 0.01\text{s}$

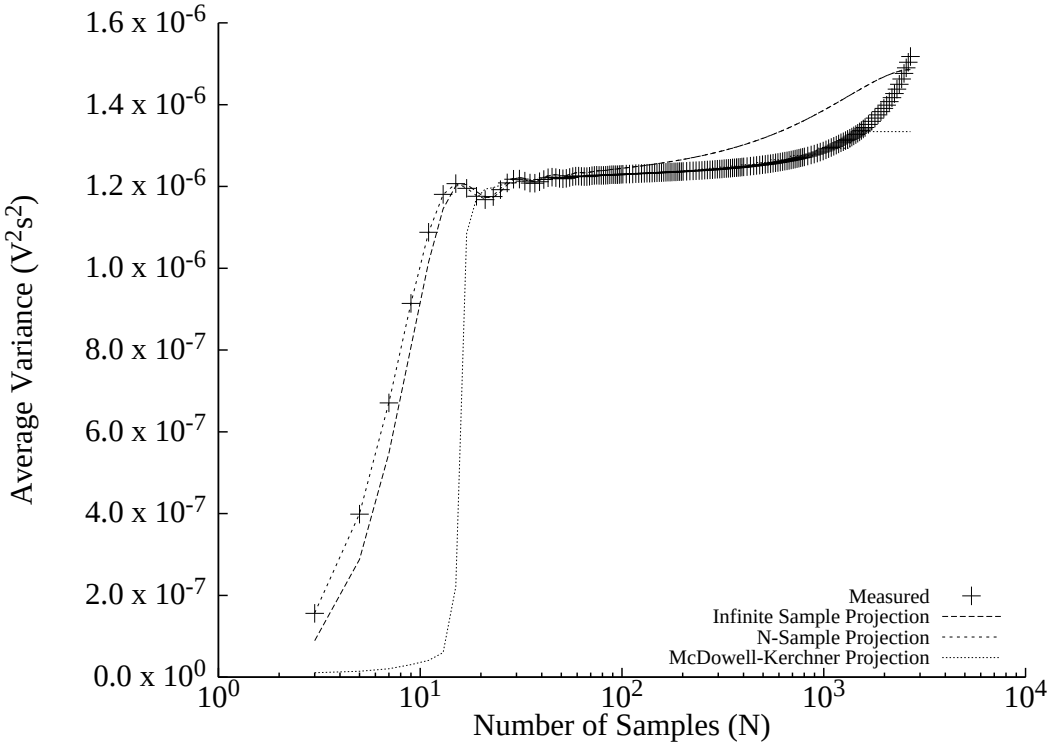

Figure 4.16: $1/f$ Noise Sample Sequence Variance, $\Delta T = 1$s, $T = 0.02$s

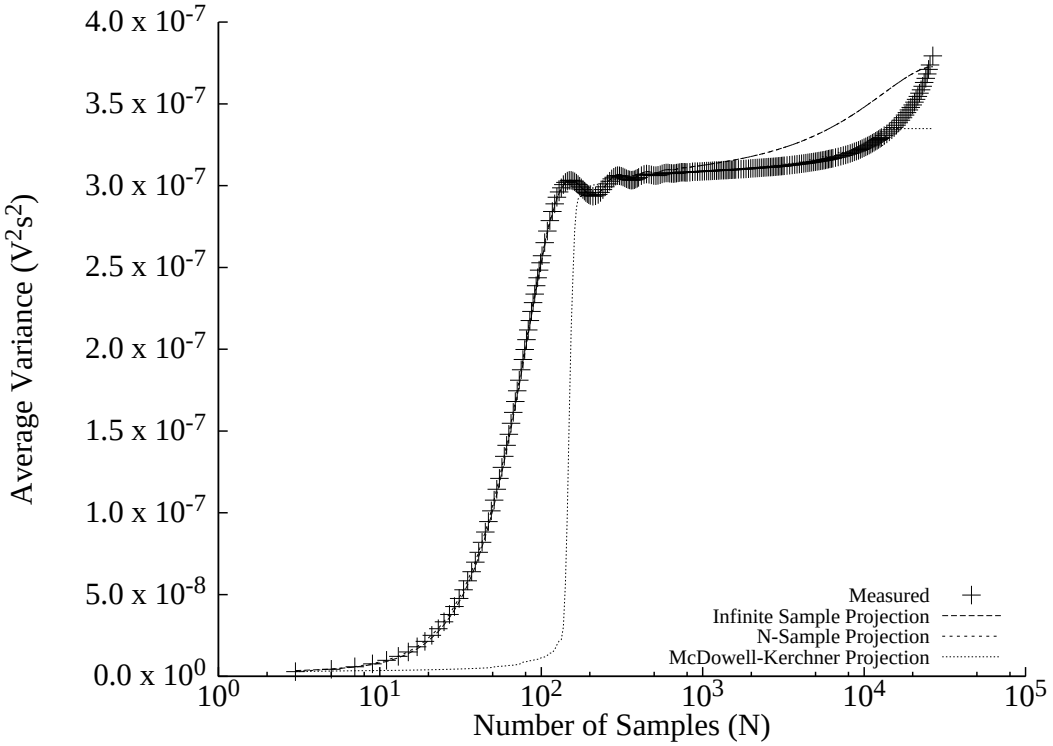

Figure 4.17: $1/f$ Noise Sample Sequence Variance, $\Delta T = 0.1$s, $T = 0.01$s

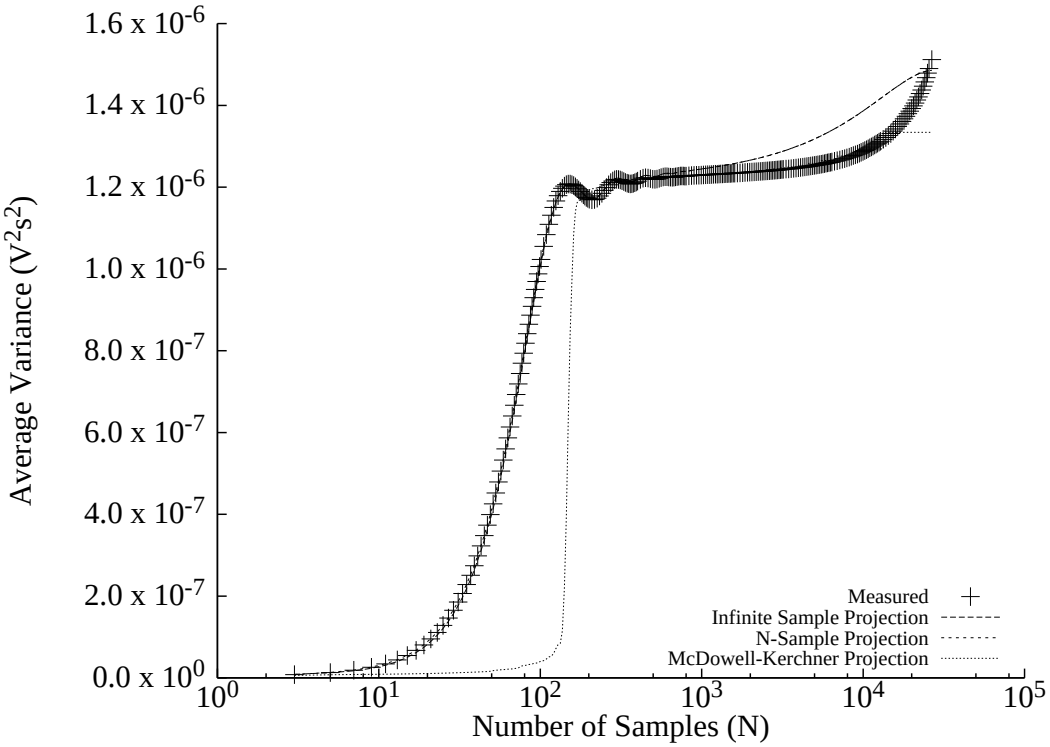

Figure 4.18: $1/f$ Noise Sample Sequence Variance, $\Delta T = 0.1$s, $T = 0.02$s

The above variance graphs show good agreement (maximum error on the order of 10%) of the PSD-based N-sample variance prediction, with the measured variance of the noise samples. The number of samples at which the variances were measured and calculated were spaced logarithmically, to illustrate the broad tendency of the agreement—at lower numbers of samples, the agreement between the N-sample, PSD-based calculation and the measured variance is excellent, but as $N \cdot \Delta T$ approaches the length of the $1/f$ noise sequence, the error grows. This error may be ascribed to the incomplete ergodicity of the $1/f$ noise signal at low frequencies included by so long a measurement, or equivalently, that the PSD of such a short signal—compared to the frequencies included by the measurement—is not representative of the sequence variance, given the length of the sequence.

The above measurements agree with the expectation developed in chapter 3, and may as such be considered as evidence of the validity of chapter 3's results.

Chapter 5

Summary and Future Research

Ionizing radiation was shown to be a general hazard. Gofman [86] showed that the differential harm per unit radiation increased at lower doses. Early X-ray workers found that erythemas, cancers and other ills resulted from repeated x-ray exposure. Gofman and O'Connor [8] suggested that radiation exposure be minimized to the minimum needed for an image, and that patients be informed of the additional risk of cancer for each exposure. X-ray imaging does provide medically useful information, so exposing a patient to insufficient radiation to form a useful image is to expose the patient unnecessarily; to minimize radiation exposure in the process of producing a medically useful image, sufficient radiation must be used during the first exposure, thus avoiding further exposures. A technological challenge is then to reduce the exposure necessary to achieve a given quality of image.

For a given exposure, higher quality, or higher signal-to-noise ratio (SNR) images, i.e. images that have lower pixel-to-pixel variance (mottle) for a given irradiation and resolution, may in principle be obtained using electronic imaging detectors, especially of the direct-conversion type, than with film or film with an intensifying screen. Indirect conversion detectors also exist, but use intensifying screens, often with a similar loss of resolution, and invariably with increased mottle, due to interpixel interference, as the intensifying screens cause radiation that would be incident on one pixel to give rise to radiation that is incident on nearby pixels. Mottle in electronic detectors arises from electronic noise, such as white, $1/f$ and kTC noise [87]. The mottle added by white and kTC noise is finite, but the mottle added by $1/f$ noise may in principle be limited only by the analog-to-digital converter, as the noise variance diverges in the low frequency limit.

To reduce the mottle added by white noise, the signal from each detector element may

by averaged over a longer period. To reduce the mottle from $1/f$ noise, a measurement of the detector dark current may be subtracted from the exposure photocurrent. In chapter 3, it was shown that no SNR improvement is to be had by increasing the averaging time, for idealized $1/f$ noise. For $1/f^{\alpha}$ noise, with $\alpha > 1$, the SNR may worsen somewhat with longer integration times, and for $\alpha < 1$, an often negligible improvement in SNR may be had.

The method of calculating variance developed in chapter 3 calculates the ensemble variance of various noise sources (e.g. white, $1/f$) in the frequency domain, through the use of linear, time-invariant (LTI) moving model-filters, such that if $h(t)$ is the constructed filter's impulse response and $H(\omega)$ is its Fourier transform, if $x(t)$ is the noise source of interest, and is second-order stationary, if $S_x(\omega)$ is the power-spectral density (PSD) of $x(t)$, if

$$y(t) = x(t) * h(t) \tag{5.1}$$

is the noise signal produced by the filtration, and if $y(t_0)$ is the noise output of the detector after a detection at time t_0, then the ensemble variance contributed by the noise to the detector, is the ensemble variance of $y(t_0)$,

$$var\{y(t_0\} = \frac{1}{\pi} \int_0^{\infty} S_x(\omega) \left|H(\omega)\right|^2 \, d\omega \tag{5.2}$$

A side project was also undertaken to calculate the variance of sample sequences of noise. Composite filters were generated for the variance of sample sequences, by averaging over power-transfer functions for individual samples, e.g. averaging over $|H(\omega, n)|^2$ or $|H(\omega, t)|^2$.

The general technique of chapter 3 was verified in chapter 4. Sample sequence results were used, as their functioning presupposed the functioning of the subtraction transfer functions, while being more adaptable. White and $1/f$-like noise were sampled at $1-2$kHz for about a day; the PSD of each was calculated, and the average variance of sample sequences of various lengths were calculated for the noise sample sequences taken, both directly from the noise sample sequences and on the basis of their PSDs. Only where the ergodicity of the variance was weak, i.e. where the sample sequence length was within one order of magnitude of the length of the data set, did the PSD-calculated variance of the $1/f$-like noise diverge substantially from the directly calculated variance. As such, the variance calculation method of chapter 3 may be considered verified.

5.1 Future Research

In chapter 2, it was shown that $1/f$ noise is still poorly understood. One avenue of future research into $1/f$ noise is to measure the frequency exponent of the PSD at multiple frequencies, to properly evaluate the Dutta et alia [62] relationships, as a check on their validity, and to calculate realistic distributions of fluctuators. Another avenue considers the tensor nature of $1/f$ noise—one may devise a formulation for Weissman et al.'s Q parameter (in [81]), selected for traceless fluctuations, instead of their scalar-fluctuator selected Q; this way, it might be found that some noise sources do indeed have traceless fluctuations.

Material research, especially into suppressing 1/f noise in the frequency decades passed by the detection process, is another potentially profitable avenue, involving the material origin of $1/f$ noise. A calculation of the expected variance, possibly within error bounds, of non-white second spectra $1/f$ noise would also be valuable, as the relationships derived in chapter 3 are for second-order stationary $1/f$ noise, i.e. noise that has a memory-less variation of power per unit frequency at any given frequency.

As detectors' semiconductor elements need not have second-order stationary noise, it may also be useful to sample their dark current repeatedly over long periods, to measure the resulting variance contribution, without relying on a power-spectral density formalism.

The $1/f$-induced variance of multiple types of detectors, not all limited to x-ray detectors, can be described by the mathematical relationships and methods of chapter 3. As such, faulty variance calculations and engineering approaches may be avoided in future.

References

[1] R. Brecher, *The Rays.* Baltimore: Williams and Wilkins, 1969, p. 62.

[2] R. Brecher, *The Rays.* Baltimore: Williams and Wilkins, 1969, p. 118.

[3] F. H. Attix, *Radiation Dosimetry volume I 2nd Edition.* New York: Academic Press, 1966, pp. 5–6.

[4] R. F. Mould, *A Century of X-rays and Radioactivity in Medicine.* Philadelphia: Institute of Physics Publishing, 1993, pp. 186–187.

[5] R. Brecher, *The Rays.* Baltimore: Williams and Wilkins, 1969, pp. 82–85.

[6] J. S. Benseler, *The Radiology Handbook: A Pocket Guide to Medical Imaging.* Athens, Ohio: Ohio University Press, 2006, pp. 26–27.

[7] J. Gofman, *Radiation Induced Cancer from Low-Dose Exposure: An Independent Analysis.* San Fransisco: Comittee for Nuclear Responsibility, inc, 1990, pp. 35_9–35_11.

[8] J. Gofman and E. O'Connor, *Cancer Risk from X-rays.* San Fransisco: Sierra Club Books, 1985.

[9] H. E. Johns, *The Physics of Radiology 2nd Edition.* Springfield, Illinois: Charles C Thomas, 1961, p. 618.

[10] R. Brecher, *The Rays.* Baltimore: Williams and Wilkins, 1969, p. 127.

[11] R. Brecher, *The Rays.* Baltimore: Williams and Wilkins, 1969, p. 117.

[12] R. F. Mould, *A Century of X-rays and Radioactivity in Medicine.* Philadelphia: Institute of Physics Publishing, 1993, p. 75.

[13] R. Brecher, *The Rays.* Baltimore: Williams and Wilkins, 1969, p. 176.

[14] S. C. White and M. J. Pharoah, *Oral Radiology: Principles and Interpretation.* St. Louis, Missouri: Mosby Elsevier, 2009, pp. 10–16.

[15] R. Brecher, *The Rays.* Baltimore: Williams and Wilkins, 1969, p. 73.

[16] R. Brecher, *The Rays.* Baltimore: Williams and Wilkins, 1969, p. 55.

[17] S. C. White and M. J. Pharoah, *Oral Radiology: Principles and Interpretation.* St. Louis, Missouri: Mosby Elsevier, 2009, pp. 56–57.

[18] R. Mason and S. Bourne, *A Guide to Dental Radiography.* Oxford: Oxford University Press, 1998, p. 34.

[19] S. O. Kasap and J. A. Rowlands, "Direct-conversion flat-panel x-ray image sensors for digital radiography," *Proceedings of the IEEE*, vol. 90, no. 4, pp. 591–604, 2002.

[20] R. Mason and S. Bourne, *A Guide to Dental Radiography.* Oxford: Oxford University Press, 1998, p. 48.

[21] M. S. Keshner, "1/f noise," *Journal IEEE*, vol. 70, no. 3, pp. 212–218, 1982.

[22] E. J. McDowell, X. Cui, Z. Yaqoob, and C. Yang, "A generalized noise variance analysis model and its application to the characterization of 1/f noise," *OPTICS EXPRESS*, vol. 15, no. 7, pp. 3833–3848, 2007.

[23] S. C. White and M. J. Pharoah, *Oral Radiology: Principles and Interpretation.* St. Louis, Missouri: Mosby Elsevier, 2009, p. 46.

[24] S. C. White and M. J. Pharoah, *Oral Radiology: Principles and Interpretation.* St. Louis, Missouri: Mosby Elsevier, 2009, p. 62.

[25] J. S. Benseler, *The Radiology Handbook: A Pocket Guide to Medical Imaging.* Athens, Ohio: Ohio University Press, 2006.

[26] J. R. D. Murray, E. J. Holmes, and R. R. Misra, *A-Z of Musculoskeletal and Trauma Radiology.* Cambridge: Cambridge University Press, 2008.

[27] W. Herring, *Learning Radiology: Recognizing the Basics.* Philadelphia, Pennsylvania: Mosby Elsevier, 2007.

[28] W. Herring, *Learning Radiology: Recognizing the Basics.* Philadelphia, Pennsylvania: Mosby Elsevier, 2007, p. 243.

[29] A. Papoulis and S. U. Pillai, *Probability, Random Variables and Stochastic Processes.* McGraw-Hill, 2002, p. 95.

[30] A. Papoulis and S. U. Pillai, *Probability, Random Variables and Stochastic Processes.* McGraw-Hill, 2002, pp. 145–146.

[31] F. H. Attix and W. C. Roesch, *Radiation Dosimetry volume II 2nd Edition.* New York: Academic Press, 1966, p. 74.

[32] F. H. Attix and W. C. Roesch, *Radiation Dosimetry volume II 2nd Edition.* New York: Academic Press, 1966, p. 75.

[33] F. H. Attix and W. C. Roesch, *Radiation Dosimetry volume II 2nd Edition.* New York: Academic Press, 1966, pp. 79–81.

[34] F. H. Attix and W. C. Roesch, *Radiation Dosimetry volume II 2nd Edition.* New York: Academic Press, 1966, pp. 75–77.

[35] F. H. Attix and W. C. Roesch, *Radiation Dosimetry volume II 2nd Edition.* New York: Academic Press, 1966, p. 82.

[36] M. J. Buckingham, *Noise in Electronic Devices and Systems.* Ellis Horwood Limited, 1985, p. 18.

[37] S. O. Kasap, *Optoelectronics and Photonics.* Prentice Hall, 2001, p. 246.

[38] M. J. Buckingham, *Noise in Electronic Devices and Systems.* Ellis Horwood Limited, 1985, pp. 180–200.

[39] S. Kogan, *Electronic Noise and Fluctuations in Solids.* Cambridge University Press, 1996, p. 31.

[40] S. Kogan, *Electronic Noise and Fluctuations in Solids.* Cambridge University Press, 1996, p. 33.

[41] S. Kogan, *Electronic Noise and Fluctuations in Solids.* Cambridge University Press, 1996, p. 43.

[42] S. Kogan, *Electronic Noise and Fluctuations in Solids.* Cambridge University Press, 1996, pp. 227–229.

[43] S. Kogan, *Electronic Noise and Fluctuations in Solids.* Cambridge University Press, 1996, pp. 208–209.

[44] L. K. J. Vandamme, X. Li, and D. Rigaud, "1/f noise in mos devices, mobility or number fluctuations?" *IEEE transactions on Electron Devices*, vol. 41, no. 11, pp. 1936–1945, 1994.

[45] S. Kogan, *Electronic Noise and Fluctuations in Solids.* Cambridge University Press, 1996, p. 205.

[46] M. J. Buckingham, *Noise in Electronic Devices and Systems.* Ellis Horwood Limited, 1985, pp. 15–16.

[47] M. J. Buckingham, *Noise in Electronic Devices and Systems.* Ellis Horwood Limited, 1985, p. 21.

[48] M. J. Buckingham, *Noise in Electronic Devices and Systems.* Ellis Horwood Limited, 1985, p. 29.

[49] S. Kogan, *Electronic Noise and Fluctuations in Solids.* Cambridge University Press, 1996, p. 6.

[50] A. Papoulis and S. U. Pillai, *Probability, Random Variables and Stochastic Processes.* McGraw-Hill, 2002, p. 376.

[51] M. J. Buckingham, *Noise in Electronic Devices and Systems.* Ellis Horwood Limited, 1985, p. 50.

[52] M. J. Buckingham, *Noise in Electronic Devices and Systems.* Ellis Horwood Limited, 1985, p. 50.

[53] E. J. McDowell, J. Ren, and C. Yang, "Fundamental sensitivity limit imposed by dark 1/f noise in the low optical signal detection regime," *OPTICS EXPRESS*, vol. 16, no. 10, pp. 6822–6832, 2008.

[54] Y. Değerli, F. Lavernhe, P. Magnan, and J. A. Farré, "Analysis and reduction of signal readout circuitry temporal noise in cmos image sensors for low-light levels," *IEEE TRANSACTIONS ON ELECTRON DEVICES*, vol. 47, no. 5, pp. 949–962, 2000.

[55] J. Cheon and G. Han, "Noise analysis and simulation method for a single-slope adc with cds in a cmos image sensor," *IEEE TRANSACTIONS ON CIRCUITS AND SYSTEMS*, vol. 55, no. 10, pp. 2980–2987, 2008.

[56] N. Kawai and S. Kawahito, "Noise analysis of high-gain, low-noise column readout circuits for cmos image sensors," *IEEE TRANSACTIONS ON ELECTRON DEVICES*, vol. 51, no. 2, p. 185, 2004.

[57] B. C. Kim, J. Jeon, , and H. Shin, "Temporal noise analysis and reduction method in cmos image sensor readout circuit," *IEEE TRANSACTIONS ON ELECTRON DEVICES*, vol. 56, no. 11, pp. 2489–2495, 2009.

[58] J. Ulrici, "Bildgebung mit depfet-pixelmatrizen für autoradiographische anwendungen," Ph.D. dissertation, Rheinischen Friedrich–Wilhelms–Universität, Bonn, 2003.

[59] R. J. Kansy, "Response of a correlated double-sampling circuit to 1/f noise," *IEEE Journal of Solid-State Circuits*, vol. SC-15, no. 3, pp. 373–375, 1980.

[60] S. Kogan, *Electronic Noise and Fluctuations in Solids.* Cambridge University Press, 1996, pp. 24–47.

[61] F. N. Hooge, "On the additivity of generation–recombination spectra. part 2: 1/f noise," *Physica B*, vol. 336, pp. 236–251, 2003.

[62] P. Dutta, P. Dimon, and P. M. Horn, "Energy scales for noise processes in metals," *Physical Review Letters*, vol. 43, no. 9, pp. 646–649, 1979.

[63] D. M. Fleetwood and N. Giordano, "Direct link between 1/f noise and defects in metal films," *Physical Review B*, vol. 31, no. 2, pp. 1157–1160, 1985.

[64] E. Borovitskaya and M. S. Shur, "On theory of 1/f noise in semiconductors," *Solid-State Electronics*, vol. 45, pp. 1067–1069, 2001.

[65] C. Pfeiffer, "Semiconductor 1/f noise from dynamic coupling of charge carriers and lattice," *Journal of Applied Physics*, vol. 90, no. 7, pp. 3653–3655, 2001.

[66] B. I. Shklovskii, "1/f noise in variable range hopping," *Physical Review B*, vol. 67, p. 045201, 2003.

[67] B. Kaulakys, V. Gontis, and M. Alaburda, "Point process model of 1/f noise vs a sum of lorentzians," *Physical Review E*, vol. 71, pp. 1–11, 2005.

[68] B. Kaulakys, J. Ruseckas, V. Gontis, and M. Alaburda, "Nonlinear stochastic models of 1/f noise and power-law distributions," *Physica A*, vol. 365, pp. 217–221, 2006.

[69] S. Kogan, *Electronic Noise and Fluctuations in Solids.* Cambridge University Press, 1996, pp. 217–219.

[70] G. A. Garfunkel, G. B. Alers, and M. B. Weissman, "Mesoscopic noise studies of atomic motions in cold amorphous conductors," *Physical Review B*, vol. 41, no. 8, pp. 4901–4919, 1990.

[71] R. D. Black, M. B. Weissman, and F. M. Fliegel, "1/f noise in metal films lacks spatial correlation," *Physical review B*, vol. 24, no. 12, pp. 7454–7456, 1981.

[72] A. Bora and A. K. Raychaudhuri, "Evolution of 1/f noise during electromigration stressing of metal film: Spectral signature of electromigration process," *Journal of Applied Physics*, vol. 99, pp. 1–7, 2006.

[73] D. M. Fleetwood and N. Giordano, "Effect of strain on the 1/f noise of metal films," *Physical Review B*, vol. 28, no. 6, pp. 3625–3627, 1983.

[74] J. Pelz and J. Clarke, "Dependence of 1/f noise on defects induced in copper films by electron irradiation," *Physical Review Letters*, vol. 55, no. 7, pp. 738–741, 1985.

[75] C. E. Parman, N. E. Israeloff, and J. Kakalios, "Conductance-noise power fluctuations in hydrogenated amorphous silicon," *Physical Review Letters*, vol. 69, no. 7, pp. 1097–1100, 1992.

[76] J. P. R. Bakker, "Noise and degradation of amorphous silicon devices," Ph.D. dissertation, Universiteit Utrecht, 2003, see chapters four and five.

[77] P. Fantini, A. Pirovano, D. Ventrice, and A. Redaelli, "Experimental investigation of transport poperties in chalcogenide materials through 1/f noise measurements," *Applied Physics Letters*, vol. 88, p. 263506, 2006.

[78] E. P. Vandamme and L. K. J. Vandamme, "Critical discussion on unified 1/f noise models for mosfets," *IEEE transactions on Electron Devices*, vol. 47, no. 11, pp. 2146–2152, 2000.

[79] M. Aoki and M. Kato, "Hole-induced 1/f noise increase in mos transistors," *IEEE Electron Device Letters*, vol. 17, no. 3, pp. 118–120, 1996.

[80] S. M. Kogan and K. E. Nagaev, "On the low–frequency current 1/f noise in metals," *phys*, vol. 49, no. 4, pp. 387–389, 1984.

[81] M. B. Weissman, R. D. Black, and W. M. Snow, "Calculations of experimental implications of tensor properties of resistance fluctuations," *Journal of Applied Physics*, vol. 53, no. 9, pp. 6276–6279, 1982.

[82] S. Kogan, *Electronic Noise and Fluctuations in Solids.* Cambridge University Press, 1996, p. 224.

[83] M. B. Weissman, "Relations between geometrical factors for noise magnitudes in resistors," *Journal of Applied Physics*, vol. 51, no. 11, pp. 5872–5875, 1980.

[84] R. D. Black, P. J. Restle, and M. B. Weissman, "Nearly traceless 1/f noise in bismuth," *Physical Review Letters*, vol. 51, no. 16, pp. 1476–1479, 1983.

[85] M. C. Wang and G. E. Uhlenbeck, "On the theory of the brownian motion ii," *Reviews of Modern Physics*, vol. 17, no. 2–3, pp. 323–342, 1945.

[86] J. Gofman, *Radiation Induced Cancer from Low-Dose Exposure: An Independent Analysis.* San Fransisco: Comittee for Nuclear Responsibility, inc, 1990.

[87] S. O. Kasap and J. A. Rowlands, "Direct-conversion flat-panel x-ray image detectors," *IEE proceedings. Circuits, devices, and systems*, vol. 149, no. 2, pp. 85–96, 2002.